ABSTRACT

KARAM, AMANDA LOUISE. Developing and Validating Novel On-line Methods for Quantifying Microalgal Growth in Photobioreactors. (Under the direction of Dr. Joel Ducoste & Dr. Francis de los Reyes III).

Microalgae have long been recognized as a potential biofuel feedstock with interests for this purpose exploding in recent decades alongside the rising concerns of global warming. Overall, microalgal cultivation still lacks the volumetric productivity and efficiency necessary to make the algae-to-biofuel production process economically attractive. Further investigation and validation of on-line methods for quantifying microalgal growth in bench-scale experiments could lead to more strategic and insightful experiments that will help optimize algal bioreactors. This research describes the validation of two novel *in-situ* methods for quantifying microalgal growth using custom constructed photobioreactor (PBR) equipped with on-line data acquisition and controls.

The first part of the dissertation describes the assembly and operation of this bench-scale PBR that continuously monitors pH, light, and temperature. This system was constructed for precise pH control using custom-programmable scripts that controlled CO_2 into the system based on chemical equilibrium models.

The second part of this work describes an approach for estimating biomass using light sensor measurements. This work first involved the characterization of light in microalgal cultivation vessels, then rigorously evaluated which biocomponents (total biomass, cells, and chl a etc.) served as the best predictors for light attenuation. Results showed that Beer-Lambert's law predicted photosynthetic light attenuation well when both biomass and chlorophyll a were considered as distinct attenuating components, providing light and biomass estimates with around 6% and 12% average error, respectively, compared to those from experimentally measured data.

Finally, a novel on-line approach developed using continuous pH measurements within a pH-controlled PBR provided relatively simple experimental assay for obtaining high-resolution data on the microalgae's organic carbon growth based on inorganic carbon flows. This approach showed qualitative agreement to lab-based grab sample measurement assays for total organic carbon and cell counts across various nitrogen (2.5 – 5.0 mM KNO_3) and bicarbonate conditions (5.0 to 40 HCO_3^-mM). Furthermore, this carbon-tracking approach showed a strong linear relationship (R^2= 0.98) when compared to the lab-measured total organic carbon of the suspended microalgae. More specifically, the TOC measured in suspended solids portion of algal culture was consistently around 60% of the sensor-based estimates.

Advancing microalgal-based biofuels towards sustainability requires a delicate understanding of the biological, physical, and chemical reaction mechanisms during cultivation. These novel on-line methods give relatively simple, yet powerful, tools for better assessing microalgal growth in real time in a custom-built photobioreactor, and they can aid researchers in improving our understanding of algae mechanisms to optimize bioproducts.

Developing and Validating Novel On-line Methods for Quantifying Microalgal Growth in Photobioreactors

by
Amanda Louise Karam

A dissertation submitted to the Graduate Faculty of
North Carolina State University
in partial fulfillment of the
requirements for the degree of
Doctor of Philosophy

Civil Engineering

Raleigh, North Carolina
2022

APPROVED BY:

_____	_____
Dr. Joel Ducoste Committee Co-Chair	Dr. Francis de los Reyes III. Committee Co-Chair
_____	_____
Dr. Heike Winter Sederoff	Dr. Andrew Grieshop

DEDICATION

I would like to dedicate this dissertation to Dr. William Gray, who taught me as an undergraduate student at UNC-Chapel Hill in a course for environmental modeling.

This PhD dissertation process has highlighted many of my inherent struggles with focus and the subsequent pitfalls that often follow when I 'get lost' within the mycelium of my thought network. Dr. Gray celebrated me as a 'thinker', while also encouraging balance and discipline. He encouraged an unbiased search for the truth and always encouraged his students '*to take some time to think!'* His belief in me gave me hope at time when I needed it the most.

As part of this dissertation dedication, I would like to include a quote from Dr. Gray along with a cartoon he included in his coursework notes—notes that I often revisited during this PhD process when problem solving or when I was grappling to balance 'focus' with a search for understanding after observing something 'weird' during the research process….

"When observing some phenomenon that we do not understand, how will we go about gaining understanding? One approach is to just label the phenomenon as "weird." That is easy and requires no thought. However, if we are going to make inroads to understanding, we need some sort of protocol to follow, some set of basic principles to fall back on, and some approach to discovery. Of course, it is easy to just stick on a label and move on. Take some time to think!"
– Dr. William Gray, 2010

Thank you, Dr. Gray.

BIOGRAPHY

Amanda Karam completed her Bachelor of Science with honors in environmental science and a minor in computer science from the University of North Carolina at Chapel Hill. With pursuit to continue her passion for science, engineering, and research, she started graduate school at North Carolina State University under the advising of Dr. Ducoste and Dr. de los Reyes in the Department of Civil, Construction, and Environmental Engineering. She is thankful for the colleagues she has gotten to learn and grow from, and the invaluable training opportunities she has had at NC State.

ACKNOWLEDGMENTS

Funding & Education:
National Science Foundation (NSF), Emerging Frontiers in Research and Innovation (EFRI)
NCSU Department of Civil, Construction, and Environmental Engineering Department (CCEE)
NCSU Graduate School & College of Engineering
NCSSM, UNC-Chapel Hill, Public funding to education

Advisors, Committee, Mentors:
Dr. Joel Ducoste, advisor, NCSU Department of CCEE
Dr. Francis de los Reyes, advisor, NCSU Department of CCEE
Dr. Heike Sederoff, Committee member, NCSU Department of Plant and Microbial Biology
Dr. Andrew Grieshop, Committee member, NCSU Department of CCEE

Greg Gangi, mentor professor, UNC-Chapel Hill
Dr. William Gray, mentor professor, UNC-Chapel Hill

Colleagues & Collaborators:
Dr. James 'Jim' Levis, NCSU Department of CCEE
Dr. Ranji Ranjithan, NCSU Department of CCEE
Dr. Amy Grunden, Professor, NCSU Department of Plant and Microbial Biology

Dr. Yi-Chun Lai, faithful and steadfast *Dunaliella* collaborator and friend, CCEE
Dr. Arpit Sardana, dungeon lab mate and friend, CCEE
Dr. Jacob Dums, collaborator, NCSU Department of Plant and Molecular Biology
Dr. Colin Murphree, collaborator, NCSU Department of Plant and Molecular Biology

Christopher Stanford, NCSU Machine Shop Supervisor, College of Engineering
Jake Rhodes, Machine Shop Supervisor, NCSU Department of CCEE
Dr. Lisa Castellano, Environmental engineering lab manager
Jodie Gregoritsch, NCSU CCEE Graduate student coordinator

Neighbors, Friends, Family:
Dr. Dylan Horne
Danielle Kelly Riegel
Gabe Yip
Ashutosh Pande
Derrick Lammers
Talisha Burt
Roland Wimberly
My family

TABLE OF CONTENTS

LIST OF TABLES

LIST OF FIGURES

CHAPTER 1: MOTIVATION & BACKGROUND

1.1 Motivation

Microalgae have long been recognized as a potential biofuel feedstock, and interest in them for this purpose has exploded in recent decades alongside the rising concerns of global warming[1]. Unlike first-generation biofuels based on land plants (e.g., corn and soybeans), algae-based biofuels divert fewer resources away from the food, land, and water supply since the algae can be cultivated year-round on barren land using *saltwater* or wastewater as the liquid media[2,3]. Microalgae are also known for their high growth rates – surpassing the productivity of even the fastest growing terrestrial crops – and their ability to accumulate high levels of neutral lipid energy storage compounds[4–6].

Overall, microalgal cultivation still lacks the volumetric productivity and efficiency necessary to make the algae-to-biofuel production process economically attractive[7]. Thus, a major research focus has been on optimizing this cultivation process, which requires collaborative efforts that combine knowledge and modeling of microalgal growth and lipid production as well as environmental process engineering and life cycle assessment. Accurately modeling microalgal growth is crucial for developing economical full-scale operations and requires a fundamental understanding of the relevant biological processes, and how these processes interact with the culturing environment. Microalgae are incredibly adaptive and dynamic organisms that are able to grow and thrive in constantly fluctuating environments[8–12]. This fluctuating growth environment, and the microalgae's ability to quickly respond to such environment, makes both studying and modeling microalgae challenging. As the research in this area has advanced, methods for controlling algal cultures and modeling their growth have evolved; models have often become more complex as researchers attempt to refine traditional modeling approaches to more accurately capture microalgal growth [13,14]. However, despite increased research efforts, a unifying approach on best practices for modeling microalgal growth has yet to emerge. For example, a recent review by Darvehei (2018) listed 27 different approaches for describing the impact of light on algal growth and 17 different approaches for quantifying the impact of nutrients on algal growth[14]. While many of these models share overarching themes, e.g., many using Monod-type kinetic equations to describe how specific growth rates vary with substrate concentration, there is still a noteworthy lack of convergence between modeling approaches. Many challenges still faced with modeling should ***warrant reflection and a call for further collaboration between engineers and scientists to develop better methods for probing the underlying mechanisms that drive these primary producers.*** Crucial details necessary to grasp how microalgae operate, both as individual cells and as communities, could be overlooked due to the nature of the traditional approaches used when studying these highly dynamic organisms, *i.e.*, the large amount of time and volume needed for quantifying biomass reduces sampling frequency. On-line growth quantification can lead to more rapid and refined experimentations with less culture disturbances from sample collection and system perturbations that may follow.

Further investigation and validation of on-line experimental methods for quantifying microalgal growth in bench-scale setups could lead to novel strategic and illuminating experiments that help us understand these organisms more thoroughly. **This research dissertation highlights the development and validation of two novel *in-situ* methods for quantifying microalgal growth using a custom-built photobioreactor (PBR) equipped with live data acquisition and controls.** These methods are validated using the **marine halotolerant** microalga *Dunaliella viridis*.

1.2 Relevant Background

Microalgae absorb light energy and consume inorganic carbon, *e.g.*, CO_2, to synthesize glucose during photosynthesis (Equation 1-1). This process, in which dissolved CO_2 is removed from the liquid media, drives the pH upwards (Equation 1-2 - 1-3).

$$6\,CO_2 + 6H_2O + light \rightarrow C_6H_{12}O_6 + 6O_2 \quad \text{1-1}$$

$$pCO_{2(g)} \leftrightarrow CO_{2(aq)} \leftrightarrow \{\mathrm{H_2CO_3}\}_{(\mathrm{aq})} \leftrightarrow \{H\}^+ + \{HCO_3^{-1}\}_{(aq)} \leftrightarrow \{H^+\} + \{CO_3^{2-}\}_{(aq)} \quad \text{1-2}$$

$$pH = -\log[\{\mathrm{H}^+\}] \quad \text{1-3}$$

The pH increase rate will depend on not only the health and concentration of the microalgae, but also many abiotic factors including the composition of the water, specifically the carbonate buffering capacity, the CO_2 in the solution, and the associated rate and kinetic parameters that dictate the mass transport of carbon at the gas-liquid interface. Furthermore, microalgae absorb/scatter light, which leads to light attenuation and spatial distributions that affect their growth environment.

Light and carbon are two critical culture properties that change dynamically as microalgal grow to the densities required for full-scale biofuel-based cultivation. Advances in sensor technology that monitor and control these dynamic systems, along with an increase in sensor accessibility, have opened new potential pathways to discovery for scientists researching these oxygenic photosynthetic organisms.

1.2.1 Use of O_2, pH, CO_2 sensors for studying microalgae

Plant and micro- biologists have long used oxygen sensors as a tool for assessing photosynthetic and respiratory activity in algae. These types of measurements are often performed over relatively short time periods using closed-chambered apparatuses that can measure oxygen exchange, light, and absorbance in small sample volumes (< 5 mL)[15]. Much of the data collected from these types of experiments have formed the basis of many current photosynthetic models used in engineering applications that attempt to model and optimize algal growth[16–19]. Many of these same measuring principles can be applied to monitor microalgal growth over longer time scales in larger bench- and pilot-scale applications.

Measuring gas production or consumption in microalgal cultures over longer time scales and larger volumes as compared to the physiological studies described above, however, is complicated as the mass transfer of O_2 and CO_2 between the gas and liquid phases must be considered more rigorously, in addition to the chemical and biological processes that can potentially affect these transfer rates. Even still, using oxygen production measurements as a means for studying

microalgal growth has been used for decades. In fact, in open raceway pond experiments conducted in the late 1980s, dissolved oxygen (DO) electrodes were relatively successful at estimating bulk biomass within 15% on average by measuring the oxygen evolution rate[20]. This method involved periodically bubbling air into the algal ponds every few hours and monitoring the oxygen increase rates thereafter. After accounting for gaseous exchange with the atmosphere, these oxygen production rates were related to biomass production by assuming a constant conversion.[21]

More recently, oxygen probes have also been extensively used for growth modeling purposes in ways that range from calibrating models with raw DO concentrations data[22] to using these measurements as a means of estimating biomass[23]. These on-line DO sensors also allow for dynamic experiments and have been used in attempts to model the photosynthetic response of *Scenedesmus obtusiusculus* after experiencing abrupt changes in light intensity[24]. Headspace gas analyzers, for both O_2 and CO_2, are also employed in creative ways to quantify photosynthetic activity and growth in *airtight* culturing systems. For example, using a CO_2/O_2 gas analyzer, Kliphuis et al. (2010) estimated the photosynthetic quotient (PQ), *i.e.*, the molar ratio between the oxygen production rate (OPR) and carbon uptake rate (CUR) and assessed the overall' photosynthetic productivity of *Chlorella sorokiniana* algae under different light intensities and mixing regimes by measuring changes in the off-gas concentrations as compared to the continuously bubbled input gas concentration (2% CO_2 enriched N_2). Furthermore, in an attempt to quantify 'light' respiration rates, Kliphuis et al. (2011) modified their setup with the ability to remove small subsamples through a dark tube where an oxygen microsensor measured oxygen uptake rates[25]. This modification was needed since respiration rates will decline rapidly after algal cultures are subjected to darkness (on the order of minutes), and their current setup did not allow for this type of monitoring resolution. For example, *D. tertiolecta* 'light' respiration rates have been shown to decrease down to steady-state 'dark' baseline rates within an hour after exposure to darkness[26].

On-line gas measurements, both dissolved and gaseous, provide invaluable information for those studying and modeling these photosynthetic microbes. Historically DO measurements have been more commonly utilized in microalgal experiments as compared to gaseous O_2/CO_2 measurements or dissolved CO_2. Estimating the OPR or CUR of cultures directly via gas sensors requires a sophisticated airtight setup to allow for *quick* and reliable gas exchange measurements. Measuring the dissolved CO_2 has only recently been feasible with newer membrane technology, and still requires special consideration of the chemical reactions involved with carbonate species. While more commonly implemented in experimental setups, DO probes still have limitations. DO electrodes are still relatively expensive as compared to pH electrodes, which do not require special membranes. In addition, certain types of electrodes consume oxygen as part of the measuring process, limiting their measurement accuracy, response time, and applicability[27]. Moreover, since oxygen is a byproduct of photosynthesis, relating oxygen production to biomass production requires further assumptions about the photosynthetic quotient if the carbon uptake rates are not also measured. In experiments that have tracked both OPR and CUR, PQ is shown to vary between 1-1.5, and will depend on the nitrogen source and the oxidation state of the biomass produced (*i.e.*, lipids are more reduced than proteins)[28,29].

1.2.2 Use of pH electrodes in microalgal cultures

pH electrodes are arguably the most commonly used on-line sensor in bench-scale PBRs. These inexpensive probes can be used to monitor and control the pH, which is often done with CO_2 injection. And while dissolved oxygen electrodes are still more commonly used to estimate photosynthetic activity and growth with microalgae, there has been an increase interest in implementing pH data into growth models in ways to *help* define the carbon flows within an algal culturing environment[30,31].

To fully capture the state of the carbon within a system—including the total dissolved inorganic carbon (DIC) and the distribution of carbon species—more than just the pH must be considered. However, tracking the total carbon is possible using various approaches that combine lab-based measurements with chemical equilibrium models. If the pH and the activity of the dissolved CO_2, *i.e.* **{**$H_2CO_3^*$**}**, are known, then the DIC concentration, m_{DIC}, can be theoretically calculated using equilibrium constants for carbonic acid K_1, K_2 and knowledge of the relevant activity coefficients γ. These relations are shown by Equations 1-4 through 1-7. *Note, since carbonic acid is nearly indistinguishable from dissolved CO_2 in solution, they are often lumped together and referred to as $H_2CO_3^*$.*

$$\{H^+\} = 10^{-pH} \tag{1-4}$$

$$m_{DIC} = m_{H_2CO_3^*} + m_{HCO_3^-} + m_{CO_3^{2-}} \tag{1-5}$$

$$m_x = \frac{\{x\}}{\gamma_x} \tag{1-6}$$

$$DIC = \{H_2CO_3^*\}\left[\frac{1}{\gamma_{H_2CO_3^*}} + \frac{\frac{K_1}{\{H^+\}}}{\gamma_{HCO_3^-}} + \frac{\frac{K_1K_2}{\{H^+\}^2}}{\gamma_{CO_3^{2-}}}\right] \tag{1-7}$$

Filali et al. (2011) utilized this concept to experimentally measure DIC when performing growth experiments in an air-lift PBR used for modeling *Chlorella vulgaris.* Since *Chlorella* is a freshwater species, the largely salt-dependent activity coefficients are assumed to equal one, thus, simplifying this approach for estimating DIC from dissolved CO_2 measurements. DIC is then tracked as a state variable in this model (Equation 1-8), where it is dependent on 1) the microalgal growth rate μ, 2) microalgal biomass concentration X, 3) a carbon-to-biomass conversion coefficient M_x, and 4) the mass transfer rate of CO_2 into solution N_{CO2}, since CO_2 is continuously bubbled into the PBR.

$$\frac{d[DIC]}{dt} = -\mu\left(\frac{X}{M_x}\right) + N_{CO_2} \tag{1-8}$$

Using a similar concept as shown in Equation 1-8, Titica et al. (2014) formulates a dynamic pH model for autotrophic growth of the microalgae marine *Chlamydomonas reinhardtii*[30]. This approach is different, however, in that an algal growth model is combined with a chemical and thermodynamic model *to estimate pH*. In this salt-water system, since the *dissolved CO_2 is not measured*, additional constraints involving the mass and charge balance of the chemical system must be considered to fully define the DIC. As such, the activity coefficients also must be estimated.

To our knowledge, pH has not been used in a method for assessing growth directly by relating this property to the DIC outside a growth modeling context where microalgal growth parameters could impact carbon flow estimates. While the concepts behind these approaches are similar, the direct approach does not depend on any estimate of the microbial growth rate. This differentiation is key because it allows for many of the built-in assumptions used in the previous work when relating pH to DIC to be tested directly and rigorously validated. Thus overall, there is more of an emphasis on directly modeling the inorganic-to-organic carbon flows, and less on modeling microalgal growth with respect to light and nutrients, etc. as done in previous work as part of fitting growth parameters that affect DIC estimates.

This research uses pH as a tool for tracking carbon flows within a PBR and estimating the total carbon assimilated by microalgae by relating pH to the carbon removed from a marine microalgal culturing system. The pH in such a system, and the rate at which the pH in this system changes under various forcings, *i.e.*, microalgal growth, diffusion of CO_2 between the liquid and gaseous phases (Figure 1-1), will depend on many factors, such as salinity, buffering capacity, etc.

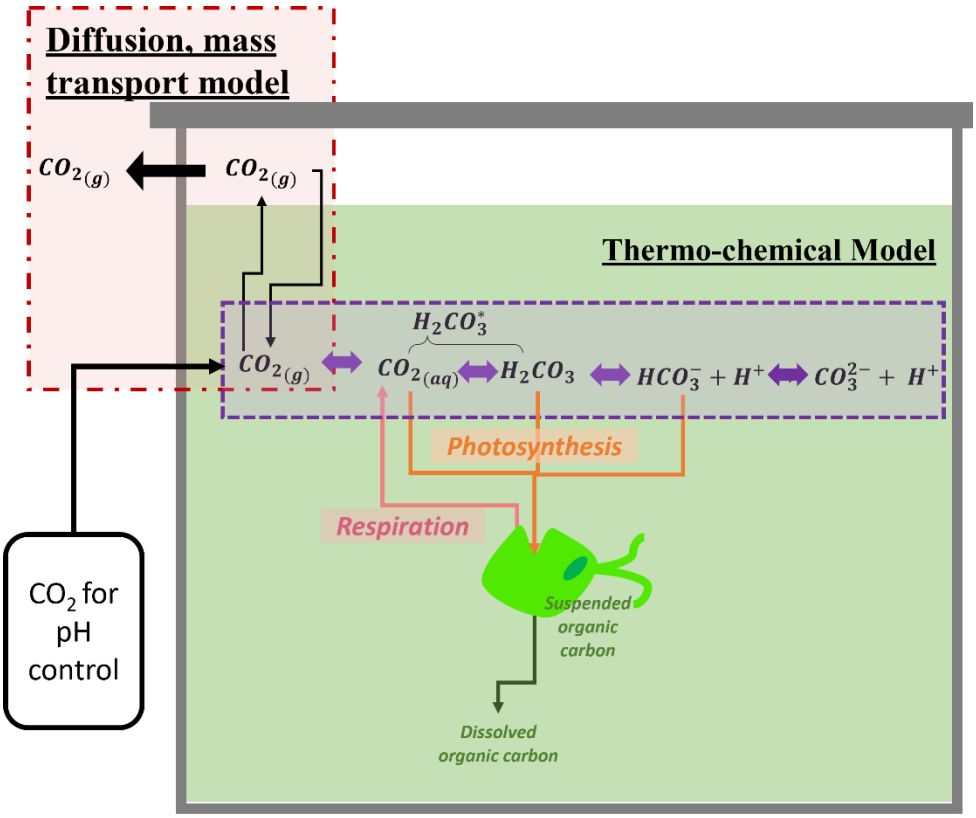

Figure 1-1. Simplified overview of the governing relations that dictate the inorganic-to-organic carbon flows within a typical bench scale microalgal photobioreactor with pH controlled via CO_2 injection.

This research seeks to answers whether the following: 1) pH data can be used with a thermochemical equilibrium to reliably estimate DIC within culturing mediums commonly used to grow marine algae, and 2) can this pH-to-DIC data, if combined with a diffusion model, led to accurate estimates of the inorganic-to-organic carbon flow within a bioreactor that is cultivating microalgae.

1.3 Research overview

The overall goal of this research was to develop and validate on-line methods to estimate biomass and carbon assimilation rates of the marine microalgae *Dunaliella viridis* during algae cultivation. These methods rest on the following hypotheses:

Key Hypothesis 1 (KH1): Chlorophyll and non-chlorophyll biomass are key light-absorbing biocomponents within an algal PBR, and concentrations of both are needed to accurately estimate light attenuation in a flat-plate PBR.

Key Hypothesis 2 (KH2): Microalgal biomass concentrations can be estimated, given the light attenuation absorption coefficients, and chlorophyll concentration.

Key Hypothesis 3 (KH3): pH combined with chemical equilibrium thermodynamic models are sufficient to assess the total dissolved inorganic carbon concentrations within a batch ~3-L, well-mixed and controlled microalgal PBR.

Key Hypothesis 4 (KH4): The combined pH measurement data and chemical equilibrium thermodynamic model can serve as an on-line growth assessment tool within a pH-controlled bioreactor.

These above hypotheses required the following task completions:

Task 1: Design and construct a bench-scale photobioreactor with pH control and live data acquisition and monitoring [*Chapter 2*].

Task 2: Perform experimental tests to evaluate important pigment and non-pigmented components in dynamic light characterization and biomass growth [*Chapter 3*].

Task 3A: Develop a model that includes both an equilibrium sub-model and carbon mass transfer by diffusion relationship to relate the pH to total dissolved inorganic carbon during microalgal cultivation. [*Chapter 4]*

Task 3B: Validate the proposed carbon estimation method by performing experiments over a range of salt, pH, dissolved CO_2 concentrations, and microalgal concentrations. [*Chapter 4]*

This dissertation showcases two sensor-based approaches for estimating microalgal growth in real time. On-line methods such as these could prove critical to unraveling some of the complex behavior observed in microalgae that has made studying and modeling their growth so challenging.

CHAPTER 2: CONSTRUCTION AND SETUP OF A BENCH-SCALE ALGAL PHOTOSYNTHETIC BIOREACTOR WITH TEMPERATURE, LIGHT, AND PH MONITORING FOR KINETIC GROWTH TESTS.

See the attached paper published in *The Journal of Visualized Experiments (JoVE)* in 2017.

Video Article

Construction and Setup of a Bench-scale Algal Photosynthetic Bioreactor with Temperature, Light, and pH Monitoring for Kinetic Growth Tests

Amanda L. Karam[1], Catherine C. McMillan[1], Yi-Chun Lai[1], Francis L. de los Reyes III[1], Heike W. Sederoff[2], Amy M. Grunden[2], Ranji S. Ranjithan[1], James W. Levis[1], Joel J. Ducoste[1]

[1]Department of Civil, Construction, and Environmental Engineering, North Carolina State University

[2]Department of Plant and Microbial Biology, North Carolina State University

Correspondence to: Francis L. de los Reyes III at fldelosr@ncsu.edu

URL: https://www.jove.com/video/55545
DOI: doi:10.3791/55545

Keywords: Bioengineering, Issue 124, Photosynthetic bioreactors, microalgae, growth kinetics, biofuel, temperature, light, pH, automated monitoring

Date Published: 6/14/2017

Citation: Karam, A.L., McMillan, C.C., Lai, Y.C., de los Reyes III, F.L., Sederoff, H.W., Grunden, A.M., Ranjithan, R.S., Levis, J.W., Ducoste, J.J. Construction and Setup of a Bench-scale Algal Photosynthetic Bioreactor with Temperature, Light, and pH Monitoring for Kinetic Growth Tests. *J. Vis. Exp.* (124), e55545, doi:10.3791/55545 (2017).

Abstract

The optimal design and operation of photosynthetic bioreactors (PBRs) for microalgal cultivation is essential for improving the environmental and economic performance of microalgae-based biofuel production. Models that estimate microalgal growth under different conditions can help to optimize PBR design and operation. To be effective, the growth parameters used in these models must be accurately determined. Algal growth experiments are often constrained by the dynamic nature of the culture environment, and control systems are needed to accurately determine the kinetic parameters. The first step in setting up a controlled batch experiment is live data acquisition and monitoring. This protocol outlines a process for the assembly and operation of a bench-scale photosynthetic bioreactor that can be used to conduct microalgal growth experiments. This protocol describes how to size and assemble a flat-plate, bench-scale PBR from acrylic. It also details how to configure a PBR with continuous pH, light, and temperature monitoring using a data acquisition and control unit, analog sensors, and open-source data acquisition software.

Video Link

The video component of this article can be found at https://www.jove.com/video/55545/

Introduction

Due to growing concerns about global climate change and finite fossil fuel resources, governments have been developing policies to reduce fossil fuel consumption and to encourage the development of new, sustainable transportation fuels. The United States Environmental Protection Agency has developed the Renewable Fuel Standard (RFS), which requires that 36 of the annual 140 billion gallons of U.S. transportation fuel mix come from renewable fuel sources by 2022. Innovative and transformational technologies will be necessary to meet these and future renewable energy standards[1].

The use of microalgae-based biofuels has the potential to help meet the national RFS while reducing greenhouse gas emissions[2]. Microalgae-based biofuels have several advantages compared to first-generation biofuels based on terrestrial food crops, such as corn and soybeans. Unlike first-generation biofuels, algae-based biofuels consume fewer land, water, and food-related resources, since algae can be cultivated year-round and on barren land using saltwater or wastewater. Microalgae have high growth rates compared terrestrial crops and can accumulate high levels of lipids, which can be readily converted to biodiesel[3]. Currently, no industrial-scale algae-to-biofuel plants exist due to the high costs of the energy-intensive production processes, which consist of algal cultivation, lipid separation, and lipid refining into biodiesel. More research is needed to make these processes more efficient and sustainable.

PBRs, which are optically clear, enclosed installations for the production of phototrophic microorganisms in an artificial environment, are considered one of the most promising cultivation methods[3]. However, current designs still lack the volumetric productivity necessary to make the algae-to-biofuel production process more efficient and economically attractive[4]. Powerful mathematical models that consider light irradiance and attenuation, the transport of nutrients and CO_2, and the growth of the microalgae can greatly facilitate the optimization of PBR design and operation. Bench-scale growth experiments are required to determine species-specific growth parameters for these optimization models.

Kinetic tests require the careful monitoring and control of experimental setups to prevent unintended inhibitors of growth. Given the photosynthetic nature of algae (*i.e.*, their consumption of CO_2 and absorption of light), maintaining controlled conditions is especially difficult in bench-scale PBRs. As depicted in *Equation 1*, the amount of dissolved CO_2 in the growth medium, commonly denoted as $H_2CO_3^*$ (*Equation 2*), will be, at minimum, a function of: 1) the CO_2 partial pressure and Henry's equilibrium constant, which dictates the amount of gas that will dissolve in solution (*Equation 3*); 2) the initial chemical composition of the growth medium, which impacts the speciation and activity of the carbonate ions and pH (*Equations 4 and 5*); and 3) the temperature, which impacts *Equations 3-5*[5].

$$pCO_{2(g)} \leftrightarrow CO_{2(aq)} \leftrightarrow \{H_2CO_3\}_{(aq)} \leftrightarrow \{H\}^+ + \{HCO_3^{-1}\}_{(aq)} \leftrightarrow \{H^+\} + \{CO_3^{2-}\}_{(aq)} \quad (Equation\ 1)$$

$$H_2CO_3^* = CO_{2(aq)} + \{H_2CO_3\}_{(aq)} \quad (Equation\ 2)$$

$$K_H(T) = \frac{pCO_{2(g)}}{\{H_2CO_3^*\}} \quad (Equation\ 3)$$

$$K_{a1}(T) = \frac{\{H^+\}\{HCO_3^-\}}{\{H_2CO_3^*\}} \quad (Equation\ 4)$$

$$K_{a2}(T) = \frac{\{H^+\}\{CO_3^{2-}\}}{\{HCO_3^-\}} \quad (Equation\ 5)$$

The various phases and the chemical speciation of carbon create a challenge for measuring and maintaining a consistent dissolved carbon concentration within a PBR while holding other conditions constant (*e.g.*, the pH increases as the algae consume CO_2, and increasing the dissolved CO_2 substrate can possibly lead to an acidic environment that inhibits growth)[6].

An additional layer of complexity for controlling conditions during algal kinetic tests involves the light intensity within the PBR. The average light intensity inside a PBR is a function of not only the incident light intensity, but also the design (*e.g.*, material, shape, depth, and mixing), the absorbance of algal biomass components (particularly chlorophyll), and the light-scattering properties of the algal cells. As the algae grow, the average light intensity will decrease. This change in light intensity, whether caused by an increase in total cells and biomass, an increase in chlorophyll content per cell, or both, can eventually induce a metabolic response, such as an increase in chlorophyll production per cell or the use of carbohydrate and lipid storage products for energy[7]. Continuous monitoring of the light intensity from within the reactor provides invaluable information. This data can help to ensure that conditions stay within a specified range and can be used to help estimate algal growth and absorbance parameters if combined with other measurements (*i.e.*, biomass, chlorophyll concentration, reactor depth, incident light, *etc.*).

Understanding how algae grow under a specified set of conditions requires that the pH, dissolved CO_2, light intensity, and temperature be monitored in bench-scale kinetic experiments. Many algal growth setups are not equipped to monitor conditions to the extent required for calibrating kinetic models, making the modeling process extremely challenging[8]. Although many companies offer bench-scale PBRs with automation and control, these bench-scale setups can be extremely expensive (~$20,000) and might not accommodate all experimental considerations of a given research question.

The first step in setting up a control-feedback system for a batch experiment is live data acquisition. This paper aims to demonstrate how to construct and set up a bench-scale PBR equipped with continuous light, pH, and temperature monitoring. This real-time monitoring setup can help to ensure that the experimental conditions stay within desired ranges, at the researcher's discretion. While this protocol does not detail specific control mechanisms, these step-by-step instructions provide a basic foundation for the data acquisition framework required before more sophisticated control feedbacks can be implemented.

Protocol

1. Construct the Bench-scale PBR Body and Lid

NOTE: For illustration purposes, *Dunaliella sp.*, a ~10 µm halotolerant microalgae lacking a cell wall, was used as the model organism for the construction of this PBR.

1. **Determine the PBR volume required for the research needs.**
    1. Determine the experimental objectives for this PBR.
    2. Decide which algal measurement assays, *M*, are necessary to characterize the growth of the algal species of interest, including the volume required per assay, *v*; the number of technical replicates, *n*; the sampling frequency, *f*; and the duration of experiments, *t*.
    NOTE: Project-specific research questions, algal species, and available equipment dictate the algal properties measured, the methods used for these measurements, and how frequently these measurements are taken. Biomass; cell counts; and total chlorophyll pigment, protein, lipid, carbohydrate, and external nitrate concentration measurements are common ways of assessing growth, and daily sampling over 5 - 14 days is a common approach for growth tests[9,10].
    3. Calculate the total culture volume, V_s, required for sampling throughout one experiment using *Equation 6*.

$$V_S = \left([M_0 \quad M_1 \quad M_{\dots} \quad M_m] \times \begin{bmatrix} v_0 \\ v_1 \\ v_{\dots} \\ v_m \end{bmatrix} \right) * n * f * t \quad Equation\ 6$$

    4. Use *Equation 7* to estimate a target PBR volume, V_p, using V_s from step 1.1.3 and a maximum volume removal fraction, *F*.

$$V_R = \frac{V_S}{F} \quad Equation\ 7$$

    NOTE: Removing less than a pre-specified fraction of the total culture volume (*e.g.*, ~20%) can help to ensure that the conditions within the PBR *i.e.*, (mixing power, light distribution, *etc.*) do not drastically vary over the course of the experiment as the culture volume is removed.
        1. Assuming a 10-day experiment where biomass; cell counts; and total chlorophyll, protein, lipid, carbohydrate, and nitrate concentrations are measured daily in triplicate, use a total sampling volume of ~600 mL. If aiming to remove no more than 18.75% of the total culture volume, use a total working reactor volume of at least 3.2 L.

2. **Select sensors and accessories for the PBR experiments.**

1. Select pH, light, and temperature probes to use for continuous monitoring.
   NOTE: Sensors should be compatible with the data acquisition unit and should withstand internal culture conditions (*i.e.*, pH range, light, heat, algal debris, salt, *etc.*). Stainless steel and salt-tolerant probes were selected here since *Dunaliella sp.* are marine microalgae.
2. Select an impeller design and motor to satisfy the experimental mixing requirements.
   NOTE: For example, a low-shear, axial impeller is a good choice for *Dunaliella* algae, as they lack a cell wall and can easily shear[11]. These algae have flagellar locomotion and do not need intense mixing[11]. Low mixing speeds can be attained using a 12 V mini-gear motor. The impeller and shaft can be 3D-printed (3D printing information can be found in the materials list).

3. **Assemble the PBR body and lid.**
   1. Determine the dimensions of the reactor, based on the volume calculations in step 1.1, keeping in mind the experimental objectives and potential constraints (*e.g.*, space).
      NOTE: A PBR design with a lower surface-to-volume ratio is preferred, as this shape minimizes light attenuation throughout the PBR, providing a more consistent light distribution throughout the experiment.
   2. Cut five pieces of optically clear cast acrylic sheets (~0.25-0.5 in thick) using a table saw, according to the PBR design and size established in step 1.3.1.
   3. Make sure that the joint edges are smoothed, but not rounded, using 200 to 400 grit sandpaper.
   4. Secure the edges of the acrylic pieces together with tape and/or clamps.
      NOTE: Acrylic cement is not a glue. If the acrylic bonding surfaces are rough or the acrylic pieces are not evenly aligned, this bonding cement will not be effective.
   5. In a well-ventilated area, apply acrylic cement along the joints using a needle dispenser. The plastic surfaces will immediately adhere together. Allow the pieces to sit for 24 h.
      WARNING: A mask and gloves should be worn to avoid inhalation and skin exposure when using acrylic cement.
   6. Apply viscous acrylic cement to the joints to ensure that the PBR is watertight. Leave the cement to dry for 24-48 h, according to the cement instructions; drying times may vary.
   7. Fill the reactor with water to check for visible leaks. If no leaks are apparent, place the reactor on paper towels and recheck for signs of leakage after 24-36 h.
      NOTE: Acrylic sheets no less than ~0.5 in thick should be used to assemble PBRs holding more than ~2 L; thinner sheets may bow under water pressure and cause leaks. Gaskets and re-enforcing screws can be used as a more robust alternative to acrylic cement (**Figure 1**). This type of assembly requires precision machinery and must be done extremely carefully, as acrylic can easily crack.
   8. Use a machine shop to design the PBR lid, with ports to accommodate sensors and other PBR accessories and needs (*i.e.*, impeller, gas lines, sampling ports, *etc.*). Make sure that the internal components do not interfere with each other.
      NOTE: The PBR and PBR lid configuration/design will depend upon reactor accessories and experimental objectives. See **Figure 1** for an example of a PBR reactor and lid design (further details can be found in the materials section). This PBR design will be referenced for the remainder of the protocol.

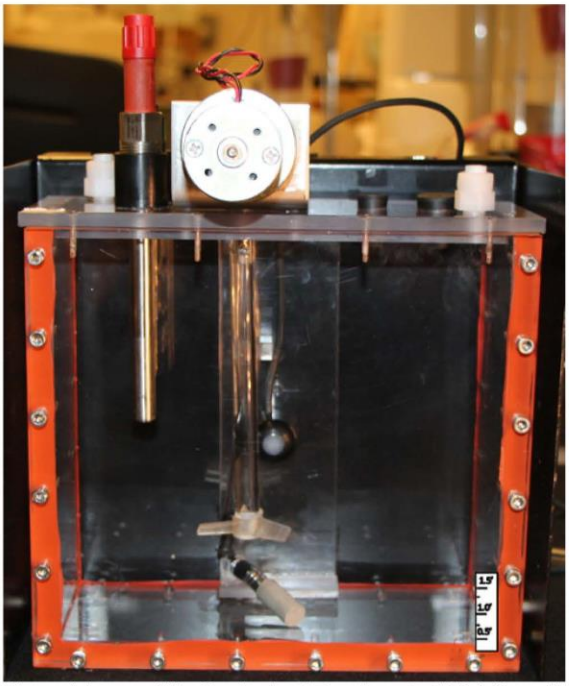

Figure 1: Image of the Customized Bench-scale PBR Setup with Sensors and a Mixer. This setup shows a mixer, an electrode secured to the lid through a threaded port in the lid, and a light sensor attached to a specially designed lid. This lid design also includes the attachment of a 12 V DC mini-gear motor. Please click here to view a larger version of this figure.

2. Set up and Configure Sensors with the Data Acquisition and Control Unit

NOTE: Sensors translate changes in the physical world into a measurable analog signal, often voltage. Data acquisition units serve as an interface between the digital and physical world and can be used to read these analog signals and convert them into discrete values, as instructed by a computer. The data-acquiring unit described herein has an analog input resolution of 16 bits, can read up to 14 analog signals (±10 V), and can supply the power required by some sensors (up to 5 V). These instructions provide an overview on how to set up this data acquisition and control unit to convert an analog signal into more meaningful values for light, pH, and temperature within a PBR. These instructions do not detail important concepts (*i.e.*, quantization, precision, response time, *etc.*) needed to fully interpret these measured values and to quantify uncertainty.

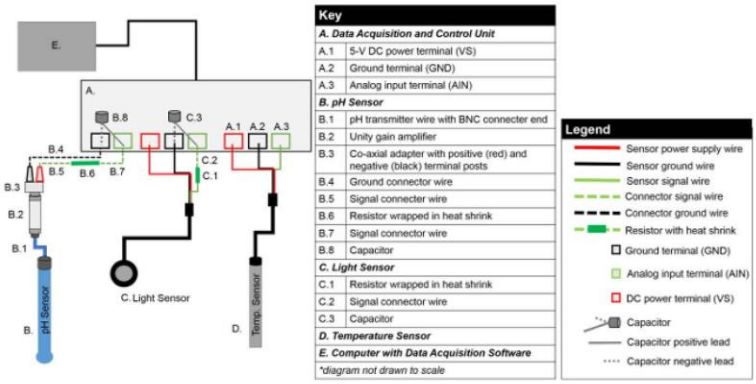

Figure 2: Sensor-to-data Acquisition and Control Unit Connection Diagram. This diagram shows how to set up pH, light, and temperature sensors to the data acquisition and control unit used for this protocol. Signal processing components for the pH and light sensor are shown. Please click here to view a larger version of this figure.

1. **Set up and configure the light sensor with the data acquisition and control unit using a low-pass filter.**

NOTE: Please refer to **Figure 2** for general reference diagrams. Manufacturer sensor specifications indicate the difference between the signal, power, and ground wires based on color. A low pass-filter is a simple circuit that uses a resistor and capacitor to filter out unwanted noise from electrical signals. This type of filter attenuates electrical signals with frequencies higher than the cutoff frequency as determined by the resistance and capacitance. This filter helps to remove or smooth electrical noise from the sensor signal.

1. Using wire strippers, cut a ~2 inch piece of green connector wire; strip 0.25 in of insulation off one end and ~0.5 in from the other end of both pieces.
2. Identify the analog signal output wire on the light sensor. Ensure that at least ~0.25-0.50 inches of metal wire are exposed past the wire insulation.
3. Carefully wrap one leg of the 1,000 Ω resistor around the ~0.5 inch stripped end of the connector wire. Wrap the other leg of the resistor around the exposed section of the light sensor analog signal wire.
4. Use a soldering iron and lead-free solder to solder the resistor legs to the wire. Allow the solder to cool for 2-5 min.
   WARNING: The solder and soldering irons get extremely hot and can be very dangerous if users are not properly trained. Instructional videos can be found online. Safety glasses and other precautions are extremely important. Wires should not be connected to a power supply or other devices during this process.
5. Slip a ~1.5 inch piece of heat-shrink tubing over one end of the connector wire and slide the piece until it covers the soldered wire and resistor. Make sure that all metal pieces are fully covered.
6. Heat-shrink using a heat gun. Make sure the tubing wraps tightly around resistor and wires; no bare wire should be exposed.
7. Attach the ground wire of the light sensor to a free ground (GND) terminal on the data acquisition and control unit using a screwdriver.
8. Secure the free end of the signal connector wire to a free analog input (AIN) terminal using a screwdriver.
9. Secure the positive lead of the 1,000 µF capacitor (*i.e.*, the longer leg) to the same AIN terminal as in step 2.1.8 and the negative lead (*i.e.*, the shorter leg) to the same GND terminal as in step 2.1.7. Make sure that both the capacitor leg and the wire are firmly connected to the terminal.
10. Identify the power input wire for the light sensor and secure this wire to a voltage supply (VS) terminal on the data acquisition and control unit.

2. **Set up and configure the pH electrode with the data acquisition unit using a unity-gain amplifier and a low-pass filter.**
   NOTE: Due to the nature of pH measurements (*i.e.*, high impedance and low voltage), a unity-gain amplifying buffer is often required between the pH probe and the data acquiring device. A low-pass filter is also beneficial for measuring pH, to protect the signal from ambient electrical noise.
   1. Connect the unity-gain amplifier to the pH probe using the transmitter wire.
   2. Connect the co-axial adapter, with positive and negative port terminals, to the other end of the unity-gain amplifier.
   3. Cut two 6-in pieces of green and one ~12 inch piece of black connector wire using wire strippers. Strip ~0.25 inch of insulation off both ends of the black connector wire.
   4. Strip ~0.25 inch and ~0.5 inch of insulation off the ends of the green connector wires using wire strippers.
   5. Carefully wrap one leg of the 1,000 Ω resistor around the ~0.5 inch stripped section of one green connector wire. Wrap the other resistor leg around the ~0.5 inch stripped section of the other green connector wire.
   6. Use a soldering iron and lead-free solder to solder the resistor legs to the wire. Allow the solder to cool for 2-5 min.
   7. Slip a ~1.5 inch piece of heat-shrink tubing over one end of the connector wire and slide the piece until it covers the soldered wire and resistor. Make sure that all metal pieces are fully covered.
   8. Heat-shrink using a heat gun. Make sure that the plastic wraps tightly around the resistor and wires; no bare wire should be exposed.
   9. Secure one end of the black connector wire to the negative (black) terminal post on the co-axial adapter. Insert the other end of this wire into a GND terminal of the data acquisition and control unit and secure using a screwdriver.
   10. Secure one end of the green connector wire (with the resistor in series) to the positive (red) terminal post on the co-axial adapter. Insert the other end of this connector wire into a free AIN terminal on the data acquisition and control unit.
   11. Identify the positive lead of the 1,000 µF capacitor (*i.e.*, the longer leg) and secure this lead to the same AIN terminal as in step 2.2.9; make sure both the capacitor leg and the signal wire are firmly connected to the terminal.
   12. Secure the negative lead of the 1,000 µF capacitor (*i.e.*, the shorter leg) to the same GND terminal as in step 2.2.8.

3. Connect the temperature sensor to the data acquisition and control unit by connecting the signal, ground, and power wires of the probe to free AIN, GND, and VS terminals.

3. Set up the Live Data Acquisition and Experimental File

NOTE: The data acquisition and control software described here communicate with the data acquisition and control unit to monitor and log sensor data at user-specified time intervals. The instructions below explain how to set up a control file in this software to monitor and record pH, temperature, and light. These instructions are specific to the software and data acquisition and control unit listed in the materials section. Further instructions can be found in product user manuals.

1. Connect the data acquisition and control unit to a computer near the experimental setup using a USB cable and download all required drivers.
2. Download and open the data acquisition and control software.
3. Set up 'Conversions' for each sensor in the software.
   NOTE: To convert the physical voltage signal into a meaningful value, some conversion factor, established by calibration, must be applied. Many sensors come with factory calibration factors found within product-specific specification sheets. Conversion equations are specific to the setup and the sensors. Many conversion equation parameters, especially those for electrodes, must be updated regularly via calibration. The lifetime of a sensor and calibration frequency will depend upon product-specific specifications and the working environment.
   NOTE: Users should read and understand these specifications in full. **Table 1** shows conversions for sensors found in the materials list. An example conversion for the temperature probe is shown below.
   1. Navigate to "Conversions" in the software workspace, on the right side of the main homepage.

2. Add a conversion name, such as, "volts_to_celsius" and type in the conversion equation: *(55.56* x *value) + 255.37 - 273.15.*

Channel Name	Conversion Name	Equation	Notes
Temperature	volts_to_celsius	(55.56 x value) + 255.37 - 273.15	Manufacturer conversion equation to convert volts to celsius.
Light	volts_to_PPFD	value x 500	Manufacturer conversion factor to convert volts to photosynthetic photon flux density (μmol $m^{-2}s^{-1}$), manufacturer LED-correction not applied.
pH	volts_to_pH	(-17.05 x value) + 6.93	Calibration-dependent conversion equation (Figure 4b) to convert pH electrode voltage readings into pH values. Only apply conversion to pH channel after calibration.

Table 1: Channel Conversion Table for the Data Acquisition File. Examples of how to input channel and conversion information for the sensors into the data acquisition software.

4. **Set up appropriate *Channels* for each sensor within the software to acquire sensor data.**
NOTE: Each sensor needs its own analog-to-digital channel in the software and a designated analog input terminal within the data acquisition and control unit.
    1. Navigate to the "Channel" page within the software.
    2. Add a sensor channel name. No space characters are allowed.
    3. Select the appropriate device to collect data for the corresponding channel; this device will correspond to the data-acquiring device.
    4. Input the device number used to reference the data acquisition and control unit or other data-acquiring device; if only one unit is being used, the default number is often zero.
    5. Select analog-to-digital, "A to D," for the input-output type ("I/O Type") and input the channel number that corresponds to the AIN terminal number on the data acquisition and control unit
    6. Input the desired sampling "Timing" (s); this value indicates how often the sensor signal will be read. Input 1.0 to acquire a reading every 1 s. To average data over 1-min intervals prior to logging, check the "Avg" box and specify 60 for the averaging length.
    7. Select the appropriate conversion from the dropdown menu, if applicable (see step 3.3 to generate conversions); otherwise, all channel data will be displayed/recorded as a voltage.

5. **Set up the "Logging Set" to log the experimental data.**
    1. Navigate to the "Logging Panel" within the software workspace, add a new logging set, and name the set accordingly. Select the output file type and location; the ASCII file type will provide a comma-separated value file if the extension '.csv' is specified in output file name.
    2. Add all desired channels to log to this set.
    3. Start and stop logging as desired by right-clicking on the logging sequence in the workspace and selecting the appropriate option.
    NOTE: Do not attempt to access the file when actively logging data. This action can disrupt the logging process. The file location for continuously logged files should not be saved/written within a cloud directory.

6. **Set up the "Page" to display the data and graphs.**
    1. Navigate to the "Pages" display within the software workspace. Click on one of the default blank pages.
    2. To display a sensor output reading numerically on page, add a "Variable Value" display to the page.
        1. Right-click anywhere within blank page, select "Displays," and click the "Variable Value" option; a small box will appear on the screen.
        2. Right-click on this newly-created box and select "Properties." Type in the display caption (e.g., "Temperature in Reactor"), the channel reference (e.g., "Temperature[0]"), and the associated units (e.g., "Celsius"). Click "OK" and return to the display page.
    3. To display the sensor data graphically and in real time, add a 2D graph to the display page.
        1. Right-click anywhere within blank page and select "Graphs" and then "2-D graphs;" a small plot will appear on the screen.
        2. Right-click the newly-created graph and select "Properties." Within the "Traces" tab, type in the desired sensor channel name (e.g., "Temperature") in the box for "Y Expression:" and make sure that "Time" is written in the box for "X Expression:." Click "OK" and return to the display page.

4. Calibrate the pH Probe

NOTE: pH calibration should be done before every experiment, at the intended temperature of experiment, and the *pH* channel conversions should be updated accordingly. pH electrode readings can drift during experiments; to determine the extent of this drift, repeat the calibration process after running the experimental setup and compare the readings. pH electrodes should be properly stored in the appropriate storage solution before and after experimentation, as directed by the manufacturer.

1. Connect the pH and temperature sensors, as described in step 2.
2. Insert both the pH electrode and the temperature probe into pH calibration buffer 7.

3. Check the graphical display to ensure the temperature reading of the probe is at the desired temperature for running experiments (step 3.6.2.2).
4. Allow the pH electrode voltage output to stabilize (*i.e.*, the voltage readings no longer change in one direction). Use a graphical display to confirm stabilization.
5. Log both the temperature and pH electrical data to a file (step 3.5) for 30-60 s. During this process, the pH channel should not have any conversions applied or include any averaging.
   Note: Since pH electrodes are sensitive to electrical noise, a lower acquisition timing (i.e. faster sampling) for the pH channel might be preferable (*e.g.* 'Timing' = 0.1 s). Keep in mind, a lower timing will require more computational resources.
6. Repeat the calibration for buffers 4 and 10. Confirm that the response of the sensor is between -57 and -59 mV/pH (**Figure 3a**).
7. Generate a conversion equation by plotting the pH buffer value versus voltage and fitting a line (**Figure 3b**). Update the conversion equation as described in step 3.3 .
8. Apply this conversion to the pH channel and update channel settings to include averaging as desired for logging.

5. Set up the PBR for the Algal Experiment

NOTE: The steps below are specific to *Dunaliella* and the custom-made PBR shown in **Figure 1**. Moreover, these setup instructions are not in accordance with sterile protocols, as this system was not designed in such a way.

1. Prepare the algae inoculum and growth medium, as needed for the experiment and experimental objectives.
2. Connect the pH and temperature wires to the data acquisition and control unit, as described in steps 2.2-2.3.
3. Calibrate and update the conversion equation for the *pH* channel, as described in steps 3.3 and 4.

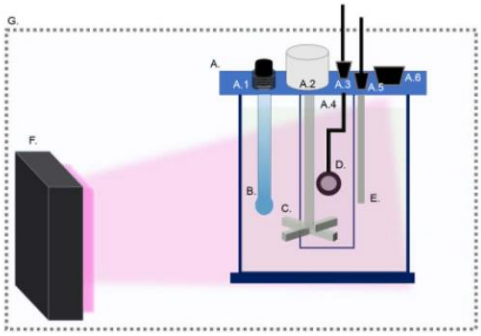

Key	
A. Reactor lid	
A.1	PG-13.5 threaded port for pH sensor
A.2	Motor mounted to lid
A.3	Light sensor port with rubber stopper
A.4	Lid extension for mounting light sensor
A.5	Temperature probe port with rubber stopper
A.6	Sampling port with rubber stopper
B. pH sensor	
C. Mixer impeller and shaft	
D. Light sensor	
E. Temperature sensor	
F. Grow lamp	
G. Temperature-controlled incubator	
**diagram not drawn to scale*	

Figure 4: Wiring Diagram for the Mixer. This diagram shows how to set up a mixing device for a PBR using a mini-gear motor, a power supply, and a 3D-printed impeller and shaft. Please click here to view a larger version of this figure.

4. **Set up the PBR inside a temperature-controlled incubator with accessories and sensors. Refer to Figure 4 for visualization.**
   1. Set up the light sensor within the PBR by threading the light sensor wire through the lid port and then mounting the sensor head onto the lid extension mount using the provided screw. Use a rubber stopper or grommet to keep this port closed to the atmosphere.
   2. Attach and secure the mixer impeller onto the PBR lid by placing the impeller shaft over the DC mini-gear motor shaft inside the PBR lid; secure the shaft with a set screw and an Allen wrench.
   3. Add algae-specific growth medium, place the lid, and secure the lid with screws. Place the PBR inside the incubator (set at 25 °C or the desired temperature).
   4. Insert the temperature probe into its designated port and secure it into the port using a rubber stopper.
   5. Secure the pH probe into the reactor lid port using a PG-13.5 threaded mount.
   6. Connect the light sensor wires to the data acquisition unit , as described in step 2.1.

5. **Power the mixer impeller to the desired speed.**
   1. Set up the variable DC power supply adjacent to the setup. Turn on the power supply and adjust the voltage knob until the voltage value reads 0 volts. Turn off the power supply.
   2. Connect the impeller motor power lines to the positive and negative output terminals of the variable power supply (**Figure 5**).
      WARNING: Never connect or touch live wires or circuits. Make sure that all power supplies are turned off before connecting any wires. Always read manufacturer instructions/specifications to ensure compatibility between the motor, power supply, and wires.
   3. Turn on the power supply and slowly increase the voltage by turning the voltage knob until the desired mixing speed is reached; calculate the mixing speed by measuring the rotations per min.

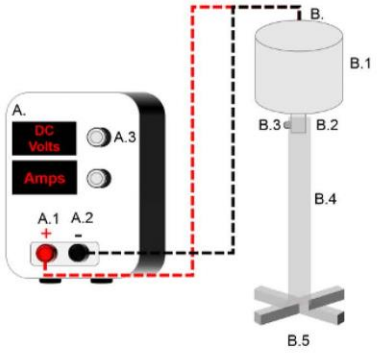

Key	
A. Variable DC Power Supply	
A.1	Positive terminal with connector wire
A.2	Negative terminal with connector wire
A.3	Voltage control knob
B. Mixer with Motor	
B.1	DC mini-gear motor (max 12-V)
B.2	Motor rotor shaft
B.3	Set screw to secure impeller shaft to motor
B.4	Impeller shaft
B.5	Impeller
**diagram not drawn to scale*	

Figure 5: Reactor Experimental Setup Diagram. Visualization of a PBR experimental setup within a temperature-controlled incubator. This setup includes a grow lamp and a PBR, with sensors and a mixer secured within the PBR lid. Please click here to view a larger version of this figure.

6. **Set up the grow lamp to illuminate the PBR.**
   NOTE: A high-powered, LED grow lamp that emits in the blue and red spectrum was chosen to achieve the photosynthetic light intensity levels required for this *Dunaliella*-specific research. The size and shape of the light fixture should be selected such that the light evenly illuminates the incident surface of the PBR. Verify that the incubator can handle an internal heat source. Not doing so could shorten the incubator lifetime and/or could cause damage or excessive heating within the incubator.
   1. Center the grow lamp along the front face of the PBR. Make sure that the light path is directly oriented towards the light sensor mounted on the back of the reactor.
   2. Turn on the light and adjust the light intensity as needed by moving the grow lamp directly toward or away from the reactor. Check the sensor variable display for light readings.

7. Monitor and log the sensor data for 6 - 24 h to ensure that the light, temperature, and pH readings within the PBR are stable and within the desired range. Adjust as needed.
   NOTE: Electrical noise can often be observed by bouncing, unsteady readings, and/or abrupt shifts in values, without apparent changes in the PBR environment.
8. Remove the rubber stopper on the sampling port to add algae inoculum via transfer pipette.
9. **Remove the samples and monitor the conditions to ensure that they stay within the range desired for the experiment.**
   1. Remove the cultures for analysis as needed from the sampling port using a pipette.
      NOTE: The sample volume, frequency, and duration of experiment will depend upon step 1.1.2.
   2. Monitor the water temperature within the PBR by checking the data display in the software and manually adjusting the incubator air temperature set point to keep the water temperature constant.
      NOTE: This adjustment will depend upon the incubator manufacturer instructions.
   3. Monitor and adjust the pH within the PBR, as desired, to ensure that the pH stays within the expected range for the experiments.
      NOTE: Here, the pH was controlled with a 12 V solenoid valve (normally-closed) in line with a compressed CO2 tank (99.99%). The valve was opened as required using the control functionality of the data acquisition and control unit and software. This setup required an accessory relay board and DC modules and was implemented using custom computer programming tailored to specific research goals.

Representative Results

Data from this real-time monitoring system show the dynamic culturing environment for algae within a bench-scale PBR and highlight the need for monitoring and controlling the system. The logged temperature data (**Figure 6**) demonstrates how light illumination, incubator air temperature, and energy dissipation associated with algal growth can change the temperature within the PBR and how the real-time data can be used to adjust incubator temperature controls, as needed.

The measured light over the course of the experiment further emphasizes the dynamic nature of this growing environment. As observed in **Figure 7**, the light sensor reading, measured as photosynthetic photon flux density (PPFD; $\mu E\text{-}m^{-2}s^{-1}$), was ~100 PPFD before algae was added and dropped immediately to 85 PPFD after inoculating the reactor with the algal culture. The light continued to drop to less than 5 PPFD on day 7. This decrease in light intensity is due to increasing biomass and cell counts, and/or to increasing absorption by increased chlorophyll content, showing that algae are active through day 7, despite low light levels. Additional biological measurements are required to make further inferences.

The continuously logged pH data show that, overall, the pH was adequately controlled during this experiment with the implemented pH control algorithm (**Figure 8**). This data, showing both minute-by-minute readings and hour-long averages, demonstrate a few key points about culturing algae and monitoring pH in real time. First, the pH increased above the desired set point of 7.6 immediately after inoculating the PBR with algae. This change was expected, as the culture seed that was added to the PBR had a pH value higher than the set point, since the flask used to grow the inoculum was not pH-controlled. Secondly, this live data highlights how sensitive pH electrodes are to external electrical noise. This sensitivity is noted by a drastic jump in the electrode values between day 1 and day 2. These sudden changes in pH values were likely created by electrical noise from a solenoid valve from an adjacent experimental setup. This electrical disturbance prematurely triggered the pH control algorithm to inject CO_2 into the PBR. Consequently, the pH dropped below the desired set point. The sensitivity of the pH electrodes can lead to extreme outliers and can potentially disrupt control systems.

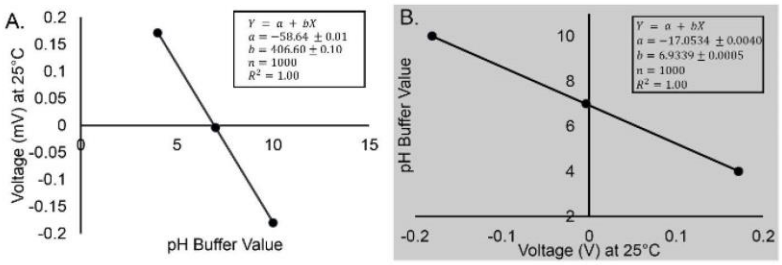

Figure 3: pH Response and Calibration Example Graphs. (**a**) Example response graph of the pH sensor (**b**) Example calibration graph of the pH sensor, with an equation to use for the conversion. Regression analysis shows a 95% confidence interval. Error bars are not visible (standard error less than 0.03%). These graphs show that the pH sensors was connected properly and that its signal was very steady. Please click here to view a larger version of this figure.

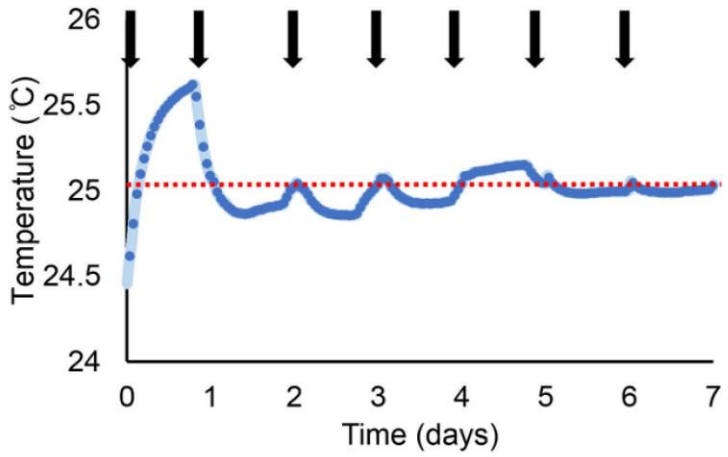

Figure 6: Temperature Measurements Within the PBR During a 7 day Experiment. Dark blue points represent 1-h averages of sensor data, and light blue points represent sensor readings acquired over 1 min (acquisition timing of 1 s, average length of 60) and converted to temperature using manufacturer-supplied conversion factors. Black arrows show when the incubator temperature setting was adjusted to maintain the culture temperature around 25 °C (this desired set point is designated with a red, dotted line). Fluctuations in temperature are due to algal growth and changes in incubator temperature. Please click here to view a larger version of this figure.

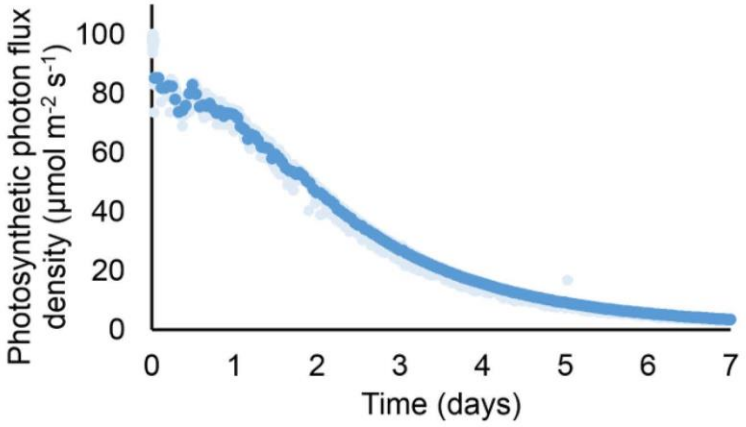

Figure 7: Light Measurements Within the PBR During a 7 day Experiment. Dark blue points represent 1 h averages of sensor data, and light blue points represent sensor readings acquired over 1 min (acquisition timing of 1 s, average length of 60) and converted into PPFD using default light-sensor factory calibration values. Please click here to view a larger version of this figure.

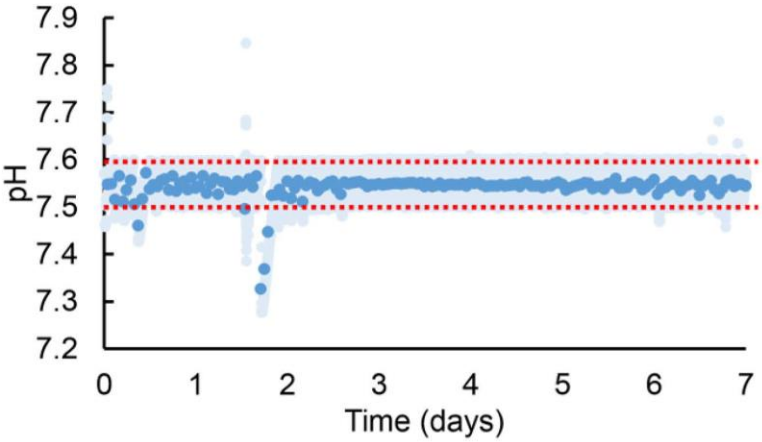

Figure 8: pH Measurements Within the PBR During a 7 day Experiment. Dark blue points represent 1-h averages of sensor data, and light blue points represent sensor readings logged every 1 min (acquisition timing of 0.1 s, average length of 600) and converted into pH using conversion equation established via calibration. The pH was maintained between 7.6 and 7.5 using a 99% CO_2 gas injection. The red, dotted lines indicate the desired pH range. Please click here to view a larger version of this figure.

Discussion

This PBR system offers the ability to monitor and control bench-scale algal kinetic growth experiments, allowing for more repeatable results from experimental assays used to quantify growth. However, an understanding of the limitations and uncertainties of sensor measurements is critical to ensure that the sensor readings accurately reflect reactor conditions. This understanding includes basic knowledge of the measurement principles involved with sensors, the process and frequency of calibration, the measurement uncertainty, and what the sensor can and cannot measure. For example, the electrical response for the light sensor described here is not equally distributed across the visible spectrum range, and certain correction factors may need to be applied to the sensor output, depending upon how this sensor data will be analyzed.

Temperature levels and variations are also extremely important, as changes in temperature can drastically influence the sensor response. Understanding potential interferences that can impact the sensor readings is also critically important; this interference can be ambient electrical noise from the building or could stem from the measurement environment (*e.g.*, sodium ions can drastically impact pH readings at pH values over 10)[12]. Moreover, submerging multiple probes into a solution, especially a highly ionic and conductive salt solution, is also a potential source of interference. Electrodes that measure pH (or ionic strength, dissolved oxygen, dissolved CO_2, *etc.*) are especially sensitive to ambient electrical noise and can be easily perturbed. Signal conditioning used for protecting the electrode signal cannot guarantee that other factors will not interfere with the probe readings. As part of quality control, other laboratory equipment, such as a hand-held pH probe, a hand-held spectrometer, and a thermometer, should be used to verify the sensor readings and to ensure that the system is set up and running properly.

Another limitation that must be addressed is the possible impact of the algae and/or culturing environment on the sensors. For example, if algal debris or bubbles cover the photodiode receptor of the light sensor, the readings will be affected. Similarly, pH electrodes are extremely sensitive and require extra care to ensure accurate readings. These electrodes work by measuring a voltage difference across an internal junction due to the buildup of H^+ ions; a hydrated buffer layer within the probe is required to maintain accurate measurements[12]. Depending upon the conditions within the reactor, this layer will wear off, and the response of the sensor may change over the course of the experiment while the probe is submerged. In preliminary tests, the pH voltage output did not drift by more than ~0.2 pH units over the course of a 20-day experiment, but further assessments should be performed to characterize this change in sensor response and to establish maximum experimental run times, especially if fine pH adjustments/quantifications are needed.

Many current bench-scale PBR systems built to analyze algal growth do not monitor and control the internal culture environment as tightly as needed to discern how different factors impact algal growth, since setting up systems in this way can be challenging. This protocol can help facilitate more controlled experiments by giving step-by-step instructions for constructing a PBR with real-time monitoring. Moreover, this live data can be used not only to better control experimental conditions, but it can potentially be utilized to estimate growth kinetics (*e.g.*, optical density readings as reference for general growth rates).

Controlled experimental systems can help to make algal research more reproducible. Bench-scale PBR setups that are monitored and controlled can increase experimental efficiency by minimizing unintended artifacts in experimental design and can help to advance efforts to make algal biofuels a sustainable, alternative fuel source.

Disclosures

The authors have nothing to disclose.

Acknowledgements

The authors acknowledge the National Science Foundation Emerging Frontiers in Research and Innovation (Award #1332341) for funding this research. The authors would also like to acknowledge Dr. Andrew Grieshop, as well as the LabJack and DAQFactory online support communities for their assistance and help offered throughout this process.

References

1. EPA Office of Transportation and Air Quality. *Renewable Fuel Standard Program.* <http://www.epa.gov/OTAQ/fuels/renewablefuels/>(2013).
2. Liu, X., Clarens, A. F., Colosi, L. M. Algae biodiesel has potential despite inconclusive results to date. *Bioresour. Technol.* **104**, 803-806 (2012).
3. Chisti, Y. Biodiesel from microalgae. *Biotechnol. Adv.* **25**(3), 294-306 (2007).
4. Lardon, L., Hélias, A., Sialve, B., Steyer, J.-P., Bernard, O. Life-cycle assessment of biodiesel production from microalgae. *Environ. Sci. Technol.* **43**(17), 6475-6481 (2009).
5. Henry, W. Experiments on the Quantity of Gases Absorbed by Water, at Different Temperatures, and under Different Pressures. *Philos. Trans. R. Soc. London.* **93**(1), 29-276 (1803).
6. Wang, X., Hao, C., Zhang, F., Feng, C., Yang, Y. Inhibition of the growth of two blue-green algae species (Microsystis aruginosa and Anabaena spiroides) by acidification treatments using carbon dioxide. *Bioresour. Technol.* **102**(10), 5742-5748 (2011).
7. Juneja, A., Ceballos, R. M., Murthy, G. S. Effects of Environmental Factors and Nutrient Availability on the Biochemical Composition of Algae for Biofuels Production: A Review. *Energies.* **6**(9), 4607-4638 (2013).
8. Bernard, O. Hurdles and challenges for modelling and control of microalgae for CO 2 mitigation and biofuel production. *J. Process Control.* **21**(10), 1378-1389 (2011).
9. Guest, J. S., van Loosdrecht, M. C. M., Skerlos, S. J., Love, N. G. Lumped Pathway Metabolic Model of Organic Carbon Accumulation and Mobilization by the Alga Chlamydomonas reinhardtii. *Environ. Sci. Technol.* **47**(7), 3258-3267 (2013).
10. Packer, A., Li, Y., Andersen, T., Hu, Q., Kuang, Y., Sommerfeld, M. Growth and neutral lipid synthesis in green microalgae: A mathematical model. *Bioresour. Technol.* **102**(1), 111-117 (2011).
11. Oren, A. A hundred years of Dunaliella research: 1905-2005. *Saline Systems.* **1**, 2 (2005).
12. Hach Company. *What is pH and How is it Measured?* <http://www.hach.com/asset-get.download.jsa?id=7639984488>. (2010).

CHAPTER 3: CHLOROPHYLL A AND NON-PIGMENTED BIOMASS ARE SUFFICIENT PREDICTORS FOR ESTIMATING LIGHT ATTENUATION DURING CULTIVATION OF DUNALIELLA VIRIDIS.

See the following attached paper published in journal *Algal Research* in 2021.

Algal Research 55 (2021) 102283

Contents lists available at ScienceDirect

Algal Research

journal homepage: www.elsevier.com/locate/algal

Chlorophyll a and non-pigmented biomass are sufficient predictors for estimating light attenuation during cultivation of *Dunaliella viridis*

Amanda L. Karam, Yi-Chun Lai, Francis L. de los Reyes III, Joel J. Ducoste *

Department of Civil, Construction, and Environmental Engineering, North Carolina State University, Raleigh, NC 27695, USA

ARTICLE INFO

Keywords:
Light
Light attenuation
Microalgae
Cultivation
Modeling
Dunaliella viridis

ABSTRACT

Characterizing light in microalgal cultivation vessels is needed for modeling and optimizing microalgal growth for large-scale cultivation. Dynamic changes in light intensity over space due to geometry, refraction/reflection, and the interactive impacts of algal growth and their biocomponents with light make this characterization challenging. Understanding which biocomponents within microalgal cultures are key variables in accurately estimating light attenuation is fundamentally important, yet, inconsistent and wide-ranging applications of the Beer-Lambert law are often used to estimate light attenuation.

This research rigorously evaluated which biocomponents (total biomass, cell count, and chl a, chl b, and total photosynthesizing pigments), or biocomponent combinations, serve as best predictors for light attenuation when modeling with the Beer-Lambert law. Calibration and validation experiments were performed using salt-water species *Dunaliella viridis* microalgal cultures grown in 3-L flat-plate PBRs with continuous light monitoring. Results at the various light and nitrogen levels tested showed Beer-Lambert's law predicted photosynthetic light attenuation well when both biomass and chlorophyll *a* were considered as distinct attenuating components, providing light estimates with less than 6% error on average over validation experiments. If the model included only one component as a predictor for attenuation, pigments were best, with a 20% error in estimating light, as compared to ~70%, 60%, 40% for models that used solely biomass, cells, or chlorophyll *a* as an attenuating component., respectively. These results suggest that when using the Beer-Lambert's law to estimate photosynthetic light attenuation in microalgal cultures, both a chlorophyll *a* and biomass component should be consistently included.

1. Introduction

1.1. Background and motivation

Light energy fuels the growth of microalgae and their valuable products [1–4]. A proper quantitative understanding of light, both in terms of transmission and biological utilization, is therefore critical to develop accurate growth models needed for designing full-scale cultivation facilities. While both aspects of light integration into these growth models are important, the ability to derive the mathematical relations between light and biological growth requires a proper characterization of this variable within microalgal photobioreactors (PBRs).

The complex nature of light (i.e., how it is diffusive, and can be absorbed, scattered, and reflected—the degree of which is dependent on wavelength and medium) has led to a wide variety of approaches for estimating light within a microalgal culture, many of which are dependent on the cultivation setup (PBR geometry, size, lighting, bubbling, among others). These approaches vary from complex models that use radiative transfer and computational fluid dynamics (CFD) to simple 1D models that consider only the attenuation-driven (i.e., forward scatter and absorbance) change in light across depth of the medium [5–8]. Light models that are developed to also capture the impacts of reflection, refraction, bubble scattering, etc. on the light distributions within PBRs will aid in designing unique cultivation chambers that optimize the growth of microalgae. However, when developing the microalgal growth models needed prior to the aforementioned optimization, the primary objective is typically modeling growth mechanisms, not light. Thus, to minimize potential error within a larger growth modeling framework that could be associated with complex light models, many bench-scale experimental setups used for growth model

* Corresponding author at: Department of Civil, Construction, and Environmental Engineering, North Carolina State University, Campus Box 7908, Raleigh, NC 27695-7908, USA.
E-mail addresses: alkaram@ncsu.edu (A.L. Karam), ylai5@ncsu.edu (Y.-C. Lai), fldelosr@ncsu.edu (F.L. de los Reyes), jducoste@ncsu.edu (J.J. Ducoste).

https://doi.org/10.1016/j.algal.2021.102283
Received 24 September 2020; Received in revised form 3 March 2021; Accepted 13 March 2021
Available online 25 March 2021

Table 1
Various approaches used when quantifying light within algal cultures using the Beer-Lambert law. (VSS – Volatile suspended solids.)

Attenuating component(s)	Algal species	Attenuation coefficient, ϵ, info.	Reported coefficient values	Reference
Chlorophyll a only	*Pseudochlorococcum sp.*	Determined with model calibration. Note: light data not used in calibration	4.82 m^2(g chl a) [1]	Packer, 2010 [12]
	Dunaliella tertiolecta	Experimentally measured at steady-state growth under high and low light conditions. Note: cultures were grown optically thin to prevent self-shading	9.345 m^2(g chl a) [1], High Light 3.827 m^2(g chl a) [1], Low Light	Sukenik 1986 [13]
Biomass only	*Scenedesmus obliquus*	Experimentally determined and held constant	0.182 m^2(g biomass) [1]	Castrillo, 2018 [14]
	Chlamydomonas reinhardtii	Experimentally determined and held constant	0.049 m^2(g VSS) [1]	Guest, 2013 [15]
Biomass and total pigments (chlorophylls, carotenoids)	*Isochrysis galbana*	$\epsilon = 0.0199 + 1.7356\ X_p$ X_p: total pigment content Note: equation determined empirically w. *Isochrysis galbana*	0.0325 to 0.08163 m^2(g biomass) [1]	Molina Grima, 1994 [9]
Biomass, chlorophylls, & carotenoids	*Haematococcus pluvialis*	$\epsilon = 0.086 + 0.0065\ X_{chl} - 0.016 X_{carotenoids}$ X_{chl}: chlorophylls dry weight % $X_{carotenoids}$: carotenoid dry weight % Note: equation based on Molina Grima, 1994	~0.086 to 0.109 m^2(g dry weight) [1]	Garcia, 2006 [16]

calibration are constructed such that a simpler 1D light modeling approach can be used, e.g., a flat-plate PBR with a uniform, one-directional light source incident to the surface. This type of configuration minimizes reflection/refraction (as compared to PBRs with curvature and light source(s) that are not incident to the surface) and permits more justification for a simple 1D approach to estimating the primarily attenuation-driven light variation throughout the depth of the PBR.

In these simpler engineered cultivation systems, the Beer-Lambert equation, as generalized in Eq. (1), is often used to estimate light at a depth z, assuming n independent attenuating species in a well-mixed solution,

$$I(t) = I_0 exp\left(-z \sum_{i\ 1}^{n} \epsilon_i\ C_i(t) \right) \quad (1)$$

where $I(t)$ is the cumulative light irradiance at time t, and depth z; I_0 is the irradiance at time $t = 0$, and depth z; ϵ_i is the attenuation or absorbance coefficient, of species i (often averaged over the irradiance spectrum); and C_i is the concentration of species i at time t. This approach can be used to estimate the attenuation driven by both absorbent and forward-scattering properties from the microalgae.

However, the implementation of this Beer-Lambert approach varies widely, especially in how the attenuating components and their associated absorption/attenuation coefficients are defined (Table 1). For example, many light models only consider a singular attenuating component, such as suspended biomass, despite knowledge that changes in the relative concentrations of cellular bioproducts, particularly photosynthetic pigments, will impact the overall attenuation coefficient of the biomass [9,10]. Some models correct for this impact—not by considering biomass and chlorophylls/pigments as distinct attenuating components—but rather by adjusting the bulk biomass attenuation coefficient using an empirically-derived formula based on pigment or chlorophyll content [9,11]. This approach as shown in Table 1, Row 5 is mathematically equivalent to considering biomass and pigments as two unique attenuating components with unique coefficients (i.e. $\epsilon_1 = 0.0190\ m^2(g\ biomass)$ [1] and $\epsilon_2 = 1.7356\ m^2(g\ pigment)$ [1]). However, when framing Beer-Lambert in such a way where the overall attenuation coefficient varies (instead of considering distinct components), the physical meaning of this equation, i.e., that different biocomponent components have distinct attenuation characteristics, is lost. For example, the negative parameter value in the empirical equation in Table 1, Row 6 could represent a unique attenuation coefficient for carotenoids, but a negative value here is physically meaningless. The use of these empirical relationships presents challenges for researchers to compare the relative attenuation of bioproducts across components and different microalgae in the literature.

Table 2
Relevant mathematical symbols, descriptions, and units for the variable and parameters considered in the models considered. (PPFD – Photosynthetic photon flux density).

Symbol	Description	Units
$I(t)$	Light intensity at the PAR sensor at time t	*PPFD*, μmol/m^2-s
I_0	Initial light intensity at PAR sensor	*PPFD*, μmol/m^2-s
z	Depth of PAR sensor	m
$A(t)$	Concentration of chlorophyll a at time t	g/m^3
$B(t)$	Concentration of chlorophyll b at time t	g/m^3
$P(t)$	Concentration of total pigments at time t	g/m^3
$S(t)$	Concentration of the non-pigmented suspended biomass component at time t	g/m^3
$C(t)$	Concentration of cell number at time t	$\#/m^3$ ($x\ 10^{12}$)
ϵ_a	Avg. attenuation coefficient parameter for chlorophyll a	m^2/g
ϵ_b	Avg. attenuation coefficient parameter for chlorophyll b	m^2/g
ϵ_p	Avg. attenuation coefficient parameter for total pigments	m^2/g
ϵ_s	Avg. attenuation coefficient parameter for non-pigmented suspended biomass component	m^2/g
ϵ_c	Avg. attenuation coefficient of cells	$m^2/cell$

1.2. Goals and objectives

A deeper understanding of how microalgae attenuate light is necessary to understand how light impacts microalgal growth, particularly under wide-ranging conditions, including stress conditions that may cause significant changes in specific bioproducts. The Beer-Lambert 1D light modeling strategy is widely used in microalgal growth models. However, relatively little work has rigorously assessed the validity of incorporating selected bioproducts as described above. Some important questions include: Can the Beer-Lambert law be used to reliably predict the light in a microalgal culture under transient conditions? What microalgal culture properties (e.g., culture density, pigments) are sufficient to capture light attenuation in a PBR using Beer-Lambert's Law?

Critical assessment is needed to answer these questions and help validate the Beer-Lambert law in modeling microalgal growth. ***Thus, the overall goal of this research was to rigorously examine the relationship between various microalgal culture properties/biocomponents and light attenuation in microalgal cultures using Beer-Lambert's law.*** The specific objectives of the research were to: (1) use an in-situ method to quantify light attenuation in a PBR grown with marine *Dunaliella viridis* under different transient light and nitrogen conditions; (2) evaluate

Table 3
Model equations and reference numbers for the 11 model variations tested.

	Model reference	Model equation	Attenuation components included
1-parameter models	#1-A	$I(t) = I_0 \exp(-z[\varepsilon_a A(t)])$	Chl. A
	#1-P	$I(t) = I_0 \exp(-z[\varepsilon_p P(t)])$	Total Pigments (Chl. A & B, Carotenoids)
	#1-S	$I(t) = I_0 \exp(-z[\varepsilon_s S(t)])$	Suspended Biomass
	#1-C	$I(t) = I_0 \exp(-z[\varepsilon_c C(t)])$	Cells
2-parameter models	#2-A/B	$I(t) = I_0 \exp(-z[\varepsilon_a A(t) + \varepsilon_b B(t)])$	Chl. A, Chl B
	#2-A/S	$I(t) = I_0 \exp(-z[\varepsilon_a A(t) + \varepsilon_s S(t)])$	Chl. A, 'Non-Chl. A' Suspended Biomass
	#2-P/S	$I(t) = I_0 \exp(-z[\varepsilon_p P(t) + \varepsilon_s S(t)])$	Total Pigments, 'Non-Pigmented' Suspended Biomass
	#2-A/C	$I(t) = I_0 \exp(-z[\varepsilon_a A(t) + \varepsilon_c C(t)])$	Chl. A, Cells
	#2-P/C	$I(t) = I_0 \exp(-z[\varepsilon_p P(t) + \varepsilon_c C(t)])$	Total Pigments, Cells
3-parameter models	#3-A/B/S	$I(t) = I_0 \exp(-z[\varepsilon_a A(t) + \varepsilon_b B(t) + \varepsilon_s S(t)])$	Chl. A, Chl. B, 'Non-Chl. A, B' Suspended Biomass
	#3-A/B/C	$I(t) = I_0 \exp(-z[\varepsilon_a A(t) + \varepsilon_b B(t) + \varepsilon_c C(t)])$	Chl. A, Chl. B, Cells

alternative microalgal attenuating variables that best estimate the photosynthetic light attenuation by calibrating attenuation coefficients for multiple Beer-Lambert model variants and comparing with experimental light data; and (3) evaluate an inverted version of the Beer-Lambert approach to estimate the concentration of the attenuating species given calibrated attenuation coefficients, variables, and in-situ light measurement. Experimentally, eleven Beer-Lambert model variants were calibrated for estimating light under different transient light and nitrogen conditions. These models were then validated by examining their ability to predict light and, when applicable, culture density properties using the inverted form of the equation.

2. Methods

2.1. 1D light modeling

2.1.1. Beer-Lambert model variants

1D light model variants (Tables 2 and 3) based on Beer-Lambert attenuation was used as the base model to estimate the light irradiance within the PBR. A total of eleven models that describe alternative Beer-Lambert's Law relationships were analyzed (Table 3). Four of these models included only one attenuating component; thus, one fitting parameter. Five models included two attenuating components, two parameters, and the remaining two incorporated three attenuating components and three fitted parameters.

The light models and their associated parameters (Table 3) assume that the absorption coefficient parameters (i.e., ε_a, ε_b, ε_p, ε_s ε_c) represent the average value for each material over a range of wavelengths that are photosynthetically relevant since the LED lamp used in this study only has outputs in the blue and red spectrum (*see* Section 2.2.2 *for more detail*). Interest was focused on photosynthetic light since quantifying an average attenuation of white light provides less information about the attenuation of useful light in microalgal cultures, which will impact growth.

2.1.2. Optimization procedure and model evaluation

The optimization was implemented in Python 3.5.1 using the 'Minimize' function (within the Non-Linear Least-Square Minimization and Curve-Fitting package) and the built-in, restrictive-step minimization method 'trust-exact'. The lower limits for the model parameters were set to 0 m^2/g, corresponding to a case where the component would absorb no light. The upper parameter limit for pigment-based parameters (i.e., ε_a, ε_b, ε_p) was set to 30 m^2/g, reflecting a value higher than the upper limit reported in the literature for ε_a, the most commonly estimated pigment absorption coefficient. Likewise, the upper limit for ε_d was set to 1 m^2/g as most researchers have reported bulk biomass absorption coefficients to be in the range of 0.01 to 0.2 (Table 1). A Latin-hypercube sampling matrix was used to randomize 5000 parameter set estimates for initial values to search for the global solution for each model.

2.1.3. Objective function and model fitness criteria

The objective function minimized in this optimization problem (Eq. (2)) was the sum of the normalized squared error (SNSE) between measured and predicted light values,

$$SNSE = \sum_{i\ 0}^{i\ n} \frac{\left(Light_{measured_i} - Light_{predicted_i}\right)^2}{Light_{measured_i}} \quad (2)$$

where n is the total number of data points across all calibration sets. The light error was normalized to the measured light to prevent higher light experiments from carrying more weight during optimization. The Bayesian information criteria (BIC), a criterion that considers both model fitness and the number of parameters [17], k, was also used, as shown in Eq. (3), as a metric for model complexity evaluation,

$$BIC = n\ln(SSNE/n) + k\ ln\ (n) \quad (3)$$

where n is the number of data points used for evaluating the model.

2.1.4. Model calibration and validation experiments

Four different initial light conditions (100, 300, 400, and 600 μmol/m^2-s (PPFD) as measured at the sensor location) and two different initial nitrogen levels (~5 mM nitrate for 'high' condition, ~0.5 mM for 'low' condition) were used for calibrating parameters and validating the most promising model implementations. The model calibration sets include: 600 PPFD, high nitrogen; 100 PPFD, high nitrogen; 400 PPFD, low nitrogen; and 300 PPFD, low nitrogen. The data collected on Day 1 after seeding the PBR was not used for model parameterization due to a high coefficient of variation for many of the culture properties since the cultures were often very diluted.

Three experiments (400 PPFD, high nitrogen; 300 PPFD high nitrogen; and a 600 PPFD, low nitrogen conditions) were used as the validation set to assess the accuracy of the model predictions. In addition to validating the prediction of the light models, the inversion of the Beer-Lambert relationship was used to predict the biomass concentration and cell count, given the fitted light attenuation coefficients, light measurements, and relevant pigment concentration as inputs. When applicable, these estimates were compared to measured values. Eqs. (4) and (5) provide the biomass and cell count output equation prediction based on model #3-A/B/S and #3-A/B/C.

$$S(t) = \frac{\frac{-\ln\left(\frac{I(t)}{I_0}\right)}{z} - a^* A(t) - b^* B(t)}{s^*} + A(t) + B(t) \quad (4)$$

$$C(t) = \frac{\frac{-\ln\left(\frac{I(t)}{I_0}\right)}{z} - a^* A(t) - b^* B(t)}{c^*} \quad (5)$$

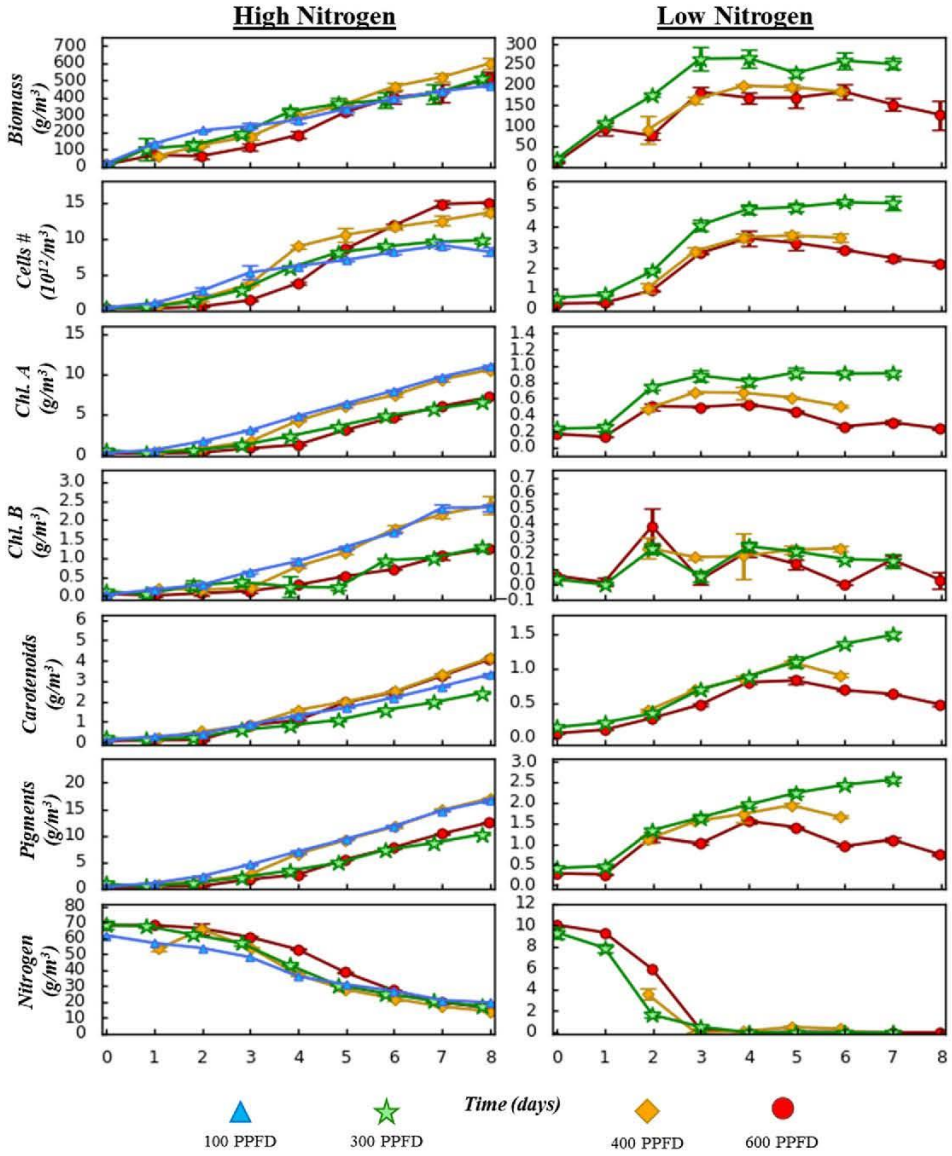

Fig. 1. Overview of measured microalgal culture properties used when calibrating and validating light models. Error bars represent standard deviation for n = 3 measurements.

2.2. Experimental procedure and set-up

2.2.1. Microalgae and experimental PBR setup

Dunaliella viridis, a marine microalga, was used as the model organism for these experiments. Stock cultures, obtained from North Carolina State University's Center for Applied Aquatic Ecology, were maintained in 1 M NaCl artificial media (5 mM nitrate) under continuous light (cool fluorescent light, ambient 1350 lx) and 25 °C. All experiments were performed in a 3.2 L (~21 × 9 × 21-cm) flat-plate photobioreactor (PBR) inside a temperature-controlled incubator. The PBR body and lid were fitted with sensors for real-time light, temperature, and pH monitoring, as well as tubing and diffusers for 99.99% CO_2 gas injection (to maintain pH between 7.5 and 7.6) and an axial impeller for gentle mixing (~60–70 RPM). The temperature was maintained around 25 °C ± 1.5 °C. A more detailed description of the reactor and its setup is provided in Karam et al. [18]

Experiments were initiated by inoculating ~200 mL of stock culture into the PBR with 3-L of appropriate growth media, to achieve a desired starting concentration of ~3 to 5 × 10^5 cells-mL ^{1}. Run times for both calibration and validation sets varied from 5 to 7 days. Triplicate samples were taken daily from the PBR for pigment, nitrogen, and density measurements. Since the stock cultures were maintained under cool fluorescent lighting, samples taken before Day 2 were not used for calibrating the model to ensure adequate adaptation of microalgal cells to the new growth environment.

2.2.2. Light source and light sensor measurements

A high-power LED growth light (SOL1, HydroGrow, Deerfield Beach, FL, 2014) that outputs only photosynthetically relevant light was used as the continuous light source. Red wavelengths (i.e., 600–700 nm)

Table 4
Overview of the results from model calibration including the sum of the normalized squared errors (SNSE), percent error, and the Bayesian information criteria (BIC) in terms of rank for each model, along with how the models comparatively rank with respective to each. The fitted attenuation coefficients for each model variants are shown as e_a, e_b, e_c, e_p, and e_s for chlorophyll *a*, chlorophyll *b*, cells, total pigments, and suspended biomass, respectively.

	Model reference	Performance metrics			Attenuation coefficient (m^2/g, $m^2/cell^*$)				
		SNSE (PPFD) (Rank)	*BIC (Rank)*	*% Error (Rank)*	e_a	e_b	e_c*	e_p	e_s
1-parameter	#1-A	205 (10)	−5.4 (10)	29% (9)	*15.21*	*n/a*	*n/a*	*n/a*	*n/a*
	#1-P	86 (7)	−27.1 (7)	15% (7)	*n/a*	*n/a*	*n/a*	*7.56*	*n/a*
	#1-S	234 (11)	−1.8 (11)	38% (11)	*n/a*	*n/a*	*n/a*	*n/a*	*0.11*
	#1-C	144 (8)	−14.3 (8)	34% (10)	*n/a*	*n/a*	*4.87*	*n/a*	*n/a*
2-parameter	#2-A/B	162 (9)	−8.1 (9)	25% (8)	*7.92*	*32.0*	*n/a*	*n/a*	*n/a*
	#2-A/S	10.1 (2)	−77.3 (1)	4.3% (2)	*6.19*	*n/a*	*n/a*	*n/a*	*0.054*
	#2-A/C	39 (6)	−43.7 (6)	12% (6)	*4.85*	*n/a*	*3.00*	*n/a*	*n/a*
	#2-P/S	17 (3)	−64.7 (3)	6.6% (3)	*n/a*	*n/a*	*n/a*	*4.49*	*0.04*
	#2-P/C	35 (5)	−46.1 (5)	12% (5)	*n/a*	*n/a*	*2.20*	*3.92*	*n/a*
3-parameter	#3-A/B/S	9.9 (1)	−74.7 (2)	3.7% (1)	*5.78*	*2.83*	*n/a*	*n/a*	*0.053*
	#3-A/B/C	26 (4)	−50.2 (4)	9.3% (4)	*1.64*	*17.8*	*2.83*	*n/a*	*n/a*

account for approximately 62% of this light's total spectral power and blue (i.e., 400–500 nm) accounts for ~36%. The spectral output of this light can be found in the Supplemental Information (SI) (Fig. S1). A PAR sensor (SQ-225, Apogee Instruments, Logan, UT) was used to quantify the light inside the PBR (at the approximate center) over the duration of experiments as photosynthetic photon flux density (PPFD), measured in μmol photon m^{-2} s^{-1}).

Light data was recorded continuously at one-minute intervals throughout the duration of experiments. For model calibration purposes, light data across a ~60-minute span at the time of daily sampling was averaged. Any data recorded during the intermittent bubbling from CO_2 injection was removed prior to this analysis.

2.2.3. Chlorophyll a, b and carotenoid quantification

An ethanol-based extraction method was used to measure chlorophyll content. Microalgal samples (1 mL) were centrifuged (16,100 ×*g* at 4 °C) for 10 mins. After decanting the supernatant, 1 mL pure ethanol was added and samples were vortexed until all visible pigments had dissolved into solution, i.e., the microalgal pellet appeared white. The samples were then re-centrifuged, and the supernatant was analyzed in an Eppendorf Spectrometer to quantify absorbance across the visible spectrum in a 1 mL cuvette. Chlorophyll a, chlorophyll *b*, and total carotenoids were calculated according to Eqs. (6) to (8) [19], respectively.

$$Chl\,A\left[\frac{\mu g}{mL}\right] = 13.36\,(Absorbance_{664\,nm}) - 5.19\,(Absorbance_{649\,nm}) \quad (6)$$

$$Chl\,B\left[\frac{\mu g}{mL}\right] = 27.43\,(Absorbance_{649\,nm}) - 8.12\,(Absorbance_{664\,nm}) \quad (7)$$

$$Carotenoids\left[\frac{\mu g}{mL}\right] = \frac{1000\,(Absorbance_{470\,nm}) - 2.13\,Chl\,A - 97.63\,Chl\,B}{209} \quad (8)$$

2.2.4. Cell counts and biomass determination as ash-free dry weight

An automated cell counter (Bio-Rad TC 20, Hercules, CA) was used to estimate cell density using a 10 μL microalgal suspension.

An ash-free dry weight method, adapted from Zhu and Lee (1997), was used to quantify biomass. Ten mL of the microalgal suspension were filtered through pre-combusted (550 °C for 1 h) glass-fiber filters (Whatman GF/F, 47 mm, pore size 0.7 μm). The filtered algal cells were then gently rinsed with 20 mL of 0.5 M ammonium formate to wash the inorganic salts, as described by Zhu et al. 1997 [20] and then baked at 100 °C for 24 h and weighed on a microbalance before baking for another 1 h at 550 °C and reweighing to determine the ash-free dry weight. Non-pigmented biomass was calculated daily by subtracting the relevant pigment concentrations from the ash-free dry weight; these calculations were performed using the averaged component concentrations across replicates.

2.2.5. External nitrogen concentration

mL culture samples were filtered through 25 mm polypropylene syringe filters with a 0.45 μm nylon membrane to remove microalgal. extracellular inorganic nitrogen concentration in the media was quantified using a total inorganic nitrogen test tube kit (Hach method 10021 [21]).

3. Results

3.1. Biocomponent data for calibration and validation experiments

Biomass and pigment concentrations that were used for model calibration and model validation (Fig. 1) show variations in initially recorded biomass and pigments concentration for both the high and low nitrogen conditions. These were likely caused by slight differences in inoculum culture (e.g., concentration, growth phase) and/or subsequent transitional shock. For the low nitrogen conditions, most cultures had halted biomass growth by Day 3 due to the depletion of nitrogen.

3.2. Light modeling

3.2.1. Model calibration and assessment

The calibration results of the eleven light models show that the two models that consider both biomass and chlorophyll(s), i.e. #2-A/S and #3-A/B/S, were the best performing models on the three metrics considered (Table 4). While the three-parameter model #3-A/B/S performed slightly better in terms of percent error, the BIC ranks model #2-A/S, the chlorophyll *a* and suspended biomass model, as the most superior of the models tested since the additional chlorophyll *b* parameter did not significantly improve the model performance. For both these models, the estimated attenuation coefficient for the non-chlorophyll biomass portion remained consistent at around ~0.054 m^2/g. The attenuation coefficient for chlorophyll *a* decreased slightly from 6.26 m^2/g in model #2-A/S to 5.90 m^2/g when chlorophyll *b* is added in model #3-A/B/S.

If only one component is considered for estimating light attenuation in a PBR, the total pigments (#1-P) gave best estimates with 15% error across calibration data sets as compared to 29, 34, and 38% error when cells, chlorophyll *a*, or suspended biomass are used as sole predictor. For the #1-C, #1-A, and #1-S models, respectively. Model #2-A/B, which includes chlorophyll *b* in addition to chlorophyll *a* reduces the SNSE from model #1-A by 20%. However, this value was still almost twice as high as the error observed for #1-P, which included a variable as the sum of chlorophyll *a*, b, and carotenoids. The results clearly show that the model performance significantly increases from the 1-parameter models that include either chlorophyll *a* (#1-A), biomass (#1-S), or cells (#1-C) to a model that includes both chlorophyll *a* and a culture

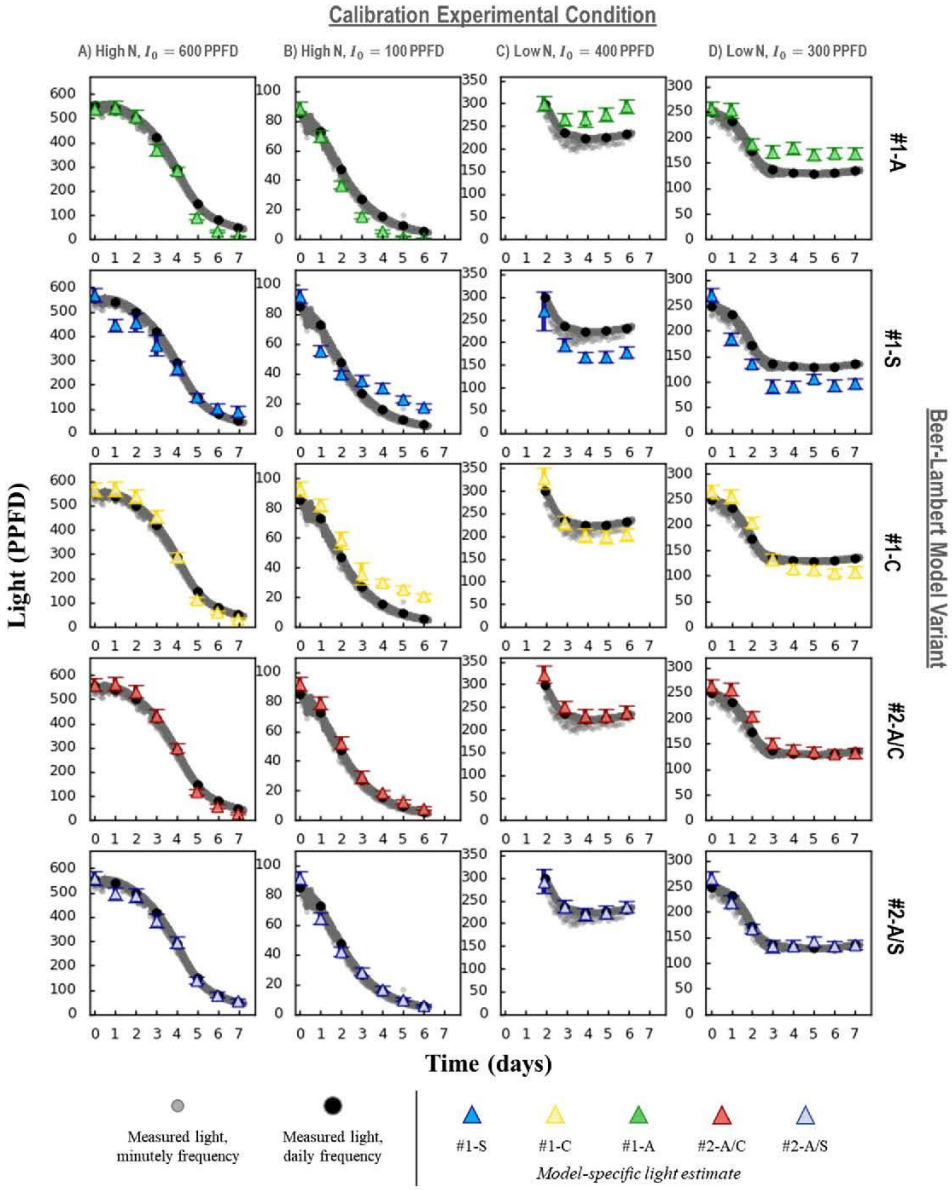

Fig. 2. Calibration results overview comparing measured light data to fitted light model. Rows represent selective Beer-Lambert model variants that consider different absorbing components, i.e. **#1-S** (Biomass), **#1-C** (Cells), **#1-A** (Chl a.), **#2-A/C** (Chl. a and cells), and **#2-A/S** (Chl. a and biomass). Columns represent different experimental conditions. Sub-plots show the base models (rows) for different experimental datasets (columns) and how those results compare to experimentally measured PAR values (grey and black circles). *(PPFD – Photosynthetic photon flux density).*

density metric like biomass or cell count (#2-A/S, #2-A/C). Fig. 2 highlights this improvement of performance by illustrating the light predictions as compared to the in-situ measured light values for these five models across the four calibration experiments.

3.2.2. *Validation results agree with calibration*

The top six models selected based on BIC were further evaluated for performance with validation experiment. Light estimates and culture density estimates (when applicable) as compared to measured values were used to validate the various Beer-Lambert model relationships for these models.

This evaluation was performed by computing the overall average percent error between the predicted and measured values for three additional experimental runs where light and nitrogen conditions varied. The highest-ranking model, #2-A/S, also gave the smallest % error when predicting both light and culture density as biomass: 6% and 12% error, respectively. The next best performing model, both in terms of light and culture density estimates, was #3-A/B/S, which also aligned with the BIC index established during calibration.

After model #2-A/S and #3-A/B/S, model #2-A/C performed best at estimating both light and biomass, despite having a lower BIC index than #2-P/S, #3-A/B/C, and #2-P/C. The light and culture density estimates for model #2-A/S and #2-A/C, as compared to measured values, are shown in Figs. 3 and 4, respectively, along with uncertainty ranges

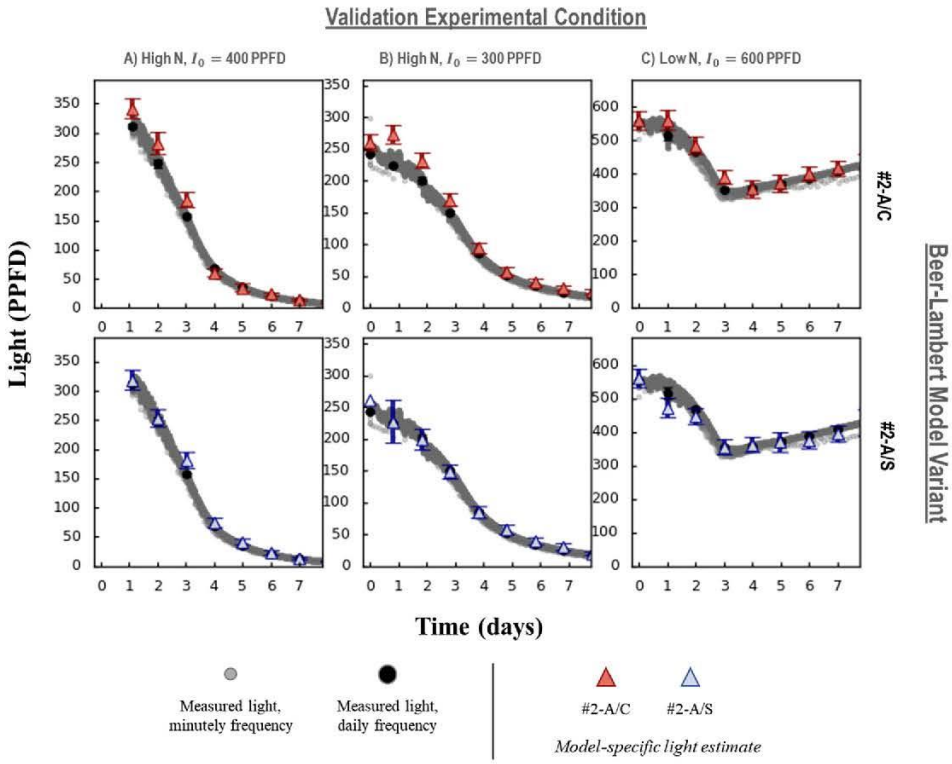

Fig. 3. Validation light model predictions as compared to measured light data for models that include both chlorophyll *a* and either cells (#2-A/C, TOP) or biomass (#2-A/S, BOTTOM). Columns reflect distinct experimental conditions with specified light and nitrogen condition. Sub-plots show the models predictions (TRIANGLES) for the specified condition and how these results compare to experimentally measured light values (CIRCLES). *(PPFD – Photosynthetic photon flux density).*

associated with these values.

4. Discussion

The general estimates for the attenuation coefficients in all evaluated models, even for the poor performing models, is consistent with past work (Table 1, Table 4). More specifically, the attenuation coefficients fitted here for chlorophyll *a* are well within the range of reported values when chlorophyll *a* is the only absorbing species considered (3.8 to 17 m^2/g). Moreover, the fitted biomass attenuation coefficients in all the tested models ranged from 0.04–0.11 m^2/g, aligning with the range reported in literature (0.03–0.20 m^2/g) (Table 1).

Overall, models that considered a separate attenuation factor for both biomass/cells and photosynthesizing pigments produced better estimates for light across the range of calibration and validation conditions tested versus those that only used a combined value for these components. This increase in performance is especially noteworthy under more stressed conditions (i.e., low nitrogen, low light). The error patterns that arise for models that did not consider these two factors can be explained when considering that the relative chlorophyll content of the algal cells is forced to their minimum or maximum cell quota when nitrogen is depleted or when light levels are low, respectively. For example, when compared to the fitted coefficient for biomass in #2-A/S, ϵ_s doubles in magnitude for #1-S model to compensate for the photosynthesizing pigments, which have much higher absorption coefficients, albeit very low relative abundance in the cell. This misallocation of attenuation capability for the biomass leads to the overestimation of the light attenuation for conditions where cells lack adequate chlorophyll content due to nitrogen starvation and underestimation of the attenuation in low light levels. This is because cells will increase chlorophyll content well past normal levels, as was observed for the biomass only model (Fig. 2, #1-S).

In a similar fashion, when the light attenuation is estimated based on chlorophylls without biomass, the coefficient for the chlorophyll species is again forced upwards to compensate for the attenuation and/or scatter caused by a higher quantity of biomass. Thus, a similar yet opposite pattern emerges for the error in light predictions with these models for the low nitrogen conditions, as the measured light irradiance is overestimated (Fig. 2, #1-A). If a single culture property is to be considered to estimate light attenuation in a microalgal PBR, total pigments (#1-P) appeared to provide the best estimates of light across the wide-ranging conditions across both calibration and validation experimental sets (Tables 4,5; SI, Fig. S2, S3). The addition of the carotenoid into the lumped pigment term appears to play an important role in this model's performance as this model offers better light estimates at the sensor than the model that includes both chlorophyll *a*, b (#2-A/B). Carotenoids contain little to no nitrogen and were also found to be correlated with biomass in a similar fashion across the light and nitrogen conditions tested (SI, Fig. S4). Thus, this improvement in predictability could be due to the total pigments capturing some of the attenuation that should be attributed to non-pigmented biomass.

4.1. Significance

The results show that models with both a photosynthesizing pigment component and culture density indicator (i.e., cells or dry weight) performed better than models that included only one of these components. These results are not surprising; researchers have reported absorption/attenuation non-linearities with respect to culture density since cells will vary in their chlorophyll content, biomass, and cell characteristics

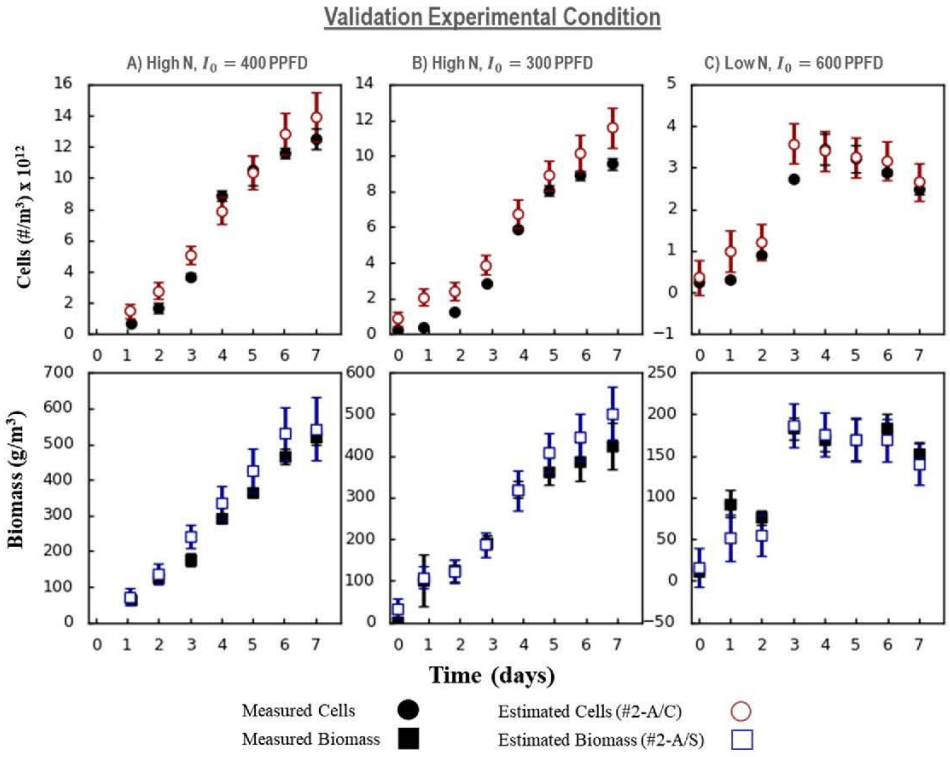

Fig. 4. Measured biomass and cell concentrations as compared to model predictions made with light measurements, fitted absorption coefficients, and measured pigment concentrations. For measured values, the error bars reflect the standard deviation (n 3). For model predictions error bars reflect error propagation, calculating based on the standard deviation of measured values (i.e., chlorophyll *a* and light values) used in the predictive equations (e.g. Eq. (3)). Cell densities shown on top and biomass on bottom.

Table 5
Light and culture density estimates (biomass and cell) average % error from measured values for validation experiments for the various models tested. Model rank in terms of Bayesian information criteria (BIC) is also listed and the rank in term of percent error in shown for each validation effort when comparing models against each other.

		Avg % error across validation experiments	
Model reference	BIC rank based on calibration	Light estimate (rank)	Culture density estimate (rank)
#2-A/S	1	6.3% (1)	12% (1)
#3-A/B/S	2	6.6% (2)	15% (2)
#2-P/S	3	14% (4)	28% (4)
#3-A/B/C	4	14% (5)	29% (5)
#2-P/C	5	15% (6)	34% (6)
#2-A/C	6	13% (3)	23% (3)

depending on culture conditions and resources. These changes in the distribution of non-pigment and pigment related bioproducts will impact the overall absorption coefficient for the microalgae if only one analyte or species is considered. Furthermore, changes in cell size and shape have been documented to impact scatter and absorbing properties [22,23], and these cell variations could explain why models that considered biomass and chlorophyll *a*, and not just cells and chlorophyll *a*, performed better. Even under more ideal conditions (high light and high nitrogen), the models that included chlorophyll *a* and a biomass component proved best at estimating light across calibration and validation data sets and also performed best at estimating biomass from chlorophyll data. These results suggest that these two factors are key in quantifying the relationship between light attenuation and culture properties and are sufficient to produce reliable results across this range of operating conditions for this microalga. Furthermore, while this method focused on the green microalgae *D. viridis*, it has the potential for characterizing cyanobacteria and red algal species. However, experimental validation using this model would be required with any other microalgal species to confirm its accuracy over the range of experimental conditions tested.

Another useful outcome from modeling the in-situ light profile with the Beer-Lambert law using appropriate attenuating species (both biomass and chlorophyll pigments) is highlighted by the biomass predictions in Fig. 4. Even though the parameters used to make these estimates were calibrated to minimize the error associated with the light data, these fitted values within the chlorophyll and biomass models produced relatively good estimates for biomass when the light absorption over time is known. This validation test further suggests that these model equations are providing an accurate mathematical interpretation of the physical light absorbance/attenuation process. Furthermore, estimating cells or biomass from the Beer-Lambert law in this manner can prove important from an experimental standpoint as quantifying these properties, especially biomass as ash-free dry weight, can be very tedious. Experimentalists or engineers monitoring full-scale systems could use a calibration process that includes light sensor measurements and pigment concentrations to determine their associated attenuation coefficients and estimate biomass when a continuous light sensor device is setup within the PBR.

4.2. Limitations

While this study highlights key culture properties that impact light attenuation in a microalgal PBR, there are some important limitations to

consider. First, these experiments were performed under aseptic conditions using a single halotolerant microalgal species where contamination was assumed to be minimal. Other microalgal species could have differing attenuation properties making this Beer-Lambert relation less applicable. For example. *D. viridis* does not have a cell wall like many microalga, and, thus, the impact of scattering could be more pronounced for other species with cell walls [24], which could lead to more error since Beer-Lambert's law does not account for anisotropic scattering. Furthermore, contamination from other light-attenuating microorganism could skew light predictions if their biomass and pigment properties are different from those calibrated with microalgae or not accounted for due to measurement methods (i.e., filtered out and not accounted for in biomass). Other dissolved organics or byproducts from either microalgae or contamination could also muddle accurate light estimates and should be considered. Furthermore, the calibrated attenuation coefficients as determined here are specific to this experimental setup, i.e., light source and light sensor, as they give an overall average attenuation of the light across the spectral output of this grow lamp. A different spectral lamp output, even if still only in blue and red wavelengths, could lead to different coefficients as the chlorophyll/pigments and biomass could attenuate specific wavelengths more or less effectively. An in-situ light sensor that measures spectral irradiance, versus a cumulative, would allow using more wavelength-specific attenuation coefficients, but these are very expensive. Another important consideration is that this method was not tested under highly dense biomass cultures, or with exceptionally low initial light levels. The highest biomass density recorded as part of this research was only 600 g/m^3. As cultures become increasingly dense, the impacts of light scattering or other physiological changes to the cells could limit this Beer-Lambert approach. Additional experimental tests would be needed to confirm the applicability of the approach to these operational or dense culture conditions.

Nonetheless, these results also show that researchers should be able to generally describe light attenuation of *relevant* photosynthesizing pigments under the experimental conditions tested in this 1-D system with chlorophyll a and biomass.

5. Conclusions

The results from this investigation into 1-D modeling strategies show that the Beer-Lambert law can be used to reliably estimate photosynthetic light attenuation in a flat-plate PBR when both chlorophyll and biomass attenuating species are considered with unique attenuation coefficients. This evidence is based on wide-ranging light and nitrogen conditions that were used for both calibration and validation. Understanding this attenuation relationship from a simple 1-D modeling approach is critical as this information can also help improve the accuracy of more sophisticated light models that include more complex reactor geometries and more light distribution mechanisms.

Although these results are specific to *D. viridis* and are limited to attenuation coefficients over a range of wavelengths that are most photosynthetically relevant (i.e., 400–500 nm, 600–700 nm), the general conclusions from this work, as discussed above, highlight possible implications, present an overview, and provide experimental validation for many of the common modeling approaches used to estimate light in algal research. The results from this research could lead to more consensus across modeling approaches for quantifying light, and potentially alternative methods to estimate biomass and better capture the photosynthetic efficiency of algal growth.

CRediT authorship contribution statement

A. Karam, Y.-C. Lai, J. Ducoste, and F. de los Reyes designed this study. Y.-C. Lai and A. Karam conducted the experiment and analyzed the data. A. Karam wrote the paper and others helped make significant edits for its improvement. J. Ducoste, and F. de los Reyes are co-PIs on the NSF grant for this research.

Declaration of competing interest

The authors, as listed below, of the article entitled "Evaluation of light modeling approaches for estimating light attenuation during microalgal cultivation." declare no conflict for submitting paper to Algal Research.

Acknowledgements

The authors would like to thank Dr. Heike Sederoff, Dr. Jacob Dums, and Dr. Colin Murphree for providing *D. viridis* strain and sharing their microalgal knowledge, as well as laboratory space and expertise. This work was supported by the National Science Foundation Emerging Frontiers in Research and Innovation Grant No. 1332341.

No conflicts, informed consent, or human or animal rights are applicable to this study.

Appendix A. Supplementary data

Supplementary data to this article can be found online at https://doi.org/10.1016/j.algal.2021.102283.

References

[1] L. Brennan, P. Owende, Biofuels from microalgae-a review of technologies for production, processing, and extractions of biofuels and co-products, Renew. Sust. Energ. Rev. 14 (2) (2010) 557–577.
[2] M.I. Khan, J.H. Shin, J.D. Kim, The promising future of microalgae: current status, challenges, and optimization of a sustainable and renewable industry for biofuels, feed, and other products, Microb. Cell Factories 17 (1) (2018) 1–21.
[3] M. Gong, A. Bassi, Carotenoids from microalgae: a review of recent developments, Biotechnol. Adv. 34 (8) (2016) 1396–1412.
[4] H. Bin Li, F. Chen, T.Y. Zhang, F.Q. Yang, G.Q. Xu, Preparative isolation and purification of lutein from the microalga Chlorella vulgaris by high-speed counter-current chromatography, J. Chromatogr. A 905 (1–2) (2001) 151–155.
[5] Z.C. Wheaton, G. Krishnamoorthy, Modeling radiative transfer in photobioreactors for algal growth, Comput. Electron. Agric. 87 (2012) 64–73.
[6] D. Fuente, J. Keller, J.A. Conejero, M. Rögner, S. Rexroth, J.F. Urchueguía, Light distribution and spectral composition within cultures of micro-algae: quantitative modeling of the light field in photobioreactors, Algal Res. 23 (2017) 166–177.
[7] J.F. Cornet, C.G. Dussap, J.B. Gros, Conversion of radiant light energy in photobioreactors, AICHE J. 40 (6) (1994) 1055–1066.
[8] F.B. Scheufele, C.L. Hinterholz, M.M. Zaharieva, H.M. Najdenski, A.N. Módenes, D. E.G. Trigueros, C.E. Borba, F.R. Espinoza-Quiñones, A.D. Kroumov, Complex mathematical analysis of photobioreactor system, Eng. Life Sci. 19 (12) (2019) 844–859.
[9] E. Molina Grima, F. Garcia Camacho, J.A. Sanchez Perez, J.M. Fernandez Sevilla, F. G. Acien Fernandez, A. Contreras Gomez, A mathematical model of microalgal growth in light-limited chemostat culture, J. Chem. Technol. Biotechnol. 61 (1994) 167–173.
[10] M.J. Barbosa, J.W. Zijffers, A. Nisworo, W. Vaes, J. Van Schoonhoven, R. H. Wijffels, Optimization of biomass, vitamins, and carotenoid yield on light energy in a flat-panel reactor using the A-Stat Technique, Biotechnol. Bioeng. 89 (2) (2005) 233–242.
[11] M.C. García-Malea, F.G. Acién, J.M. Fernández, M.C. Cerón, E. Molina, Continuous production of green cells of Haematococcus Pluvialis: modeling of the irradiance effect, Enzym. Microb. Technol. 38 (7) (2006) 981–989.
[12] A. Packer, Y. Li, T. Andersen, Q. Hu, Y. Kuang, M. Sommerfeld, Growth and neutral lipid synthesis in green microalgae: a mathematical model, Bioresour. Technol. 102 (1) (2011) 111–117.
[13] A. Sukenik, P.G. Falkowski, J. Bennett, Potential enhancement of photosynthetic energy conversion in algal mass culture, Biotechnol. Bioeng. 30 (8) (1987) 970–977.
[14] M. Castrillo, R. Diez-Montero, I. Tejero, Model-based feasibility assessment of a deep solar photobioreactor for microalgae culturing, Algal Res. 29 (2018) 304–318.
[15] J.S. Guest, M.C.M. van Loosdrecht, S.J. Skerlos, N.G. Love, Lumped pathway metabolic model of organic carbon accumulation and mobilization by the alga Chlamydomonas Reinhardtii, Support Info. Environ. Sci. Technol. 47 (7) (2013) 3258–3267.
[16] C.B. Alías, M.C. García-Malea López, F.G. Acién Fernández, J.M. Fernández Sevilla, J.L. García Sánchez, E. Molina Grima, Influence of power supply in the feasibility of Phaeodactylum Tricornutum cultures, Biotechnol. Bioeng. 87 (6) (2004) 723–733.
[17] G. Schwarz, Estimating the dimension of a model, Ann. Stat. 6 (2) (1978) 461–464.

[18] A.L. Karam, C.C. McMillan, Y. Lai, F.L.I. de los Reyes, H.W. Sederoff, A. M. Grunden, R.S. Ranjithan, J.W. Levis, J.J. Ducoste, Construction and Setup of a Bench-Scale Algal Photosynthetic Bioreactor with Temperature, Light, and PH Monitoring for Kinetic Growth Tests, 2017, pp. 1–11 (No. June).
[19] Sumanta, N.; Haque, C. I.; Nishika, J.; Suprakash, R. Spectrophotometric Analysis of Chlorophylls and Carotenoids From1. N. Sumanta, C. I. Haque, J. Nishika, R. Suprakash, Spectrophotometric analysis of chlorophylls and carotenoids from commonly grown Fern species by using various extracting solvents. Res. J. *Res. J. Chem. Sci. Res. J. Chem. Sci* 2014, 4 (9), 2231–2606.
[20] C.J. Zhu, Y.K. Lee, Determination of biomass dry weight of marine microalgae, J. Appl. Phycol. 9 (1997) 189–194.
[21] Nitrogen, Total Inorganic. Hach Company/Hach Lange GmbH, 2014, pp. 1–8.
[22] C. Rioboo, J.E. O'Connor, R. Prado, C. Herrero, Á. Cid, Cell proliferation alterations in Chlorella cells under stress conditions, Aquat. Toxicol. 94 (3) (2009) 229–237.
[23] A. Solovchenko, I. Khozin-Goldberg, L. Recht, S. Boussiba, Stress-induced changes in optical properties, pigment and fatty acid content of Nannochloropsis sp.: implications for non-destructive assay of total fatty acids, Mar. Biotechnol. 13 (3) (2011) 527–535.
[24] Ø. Svensen, Ø. Frette, S.R. Erga, Scattering properties of microalgae: the effect of cell size and cell wall, Appl. Opt. 46 (23) (2007) 5762–5769.

CHAPTER 4: CONTINUOUS pH CONTROL AND MONITORING AS AN ON-LINE TOOL FOR ASSESSING MARINE MICROALGA DUNALIELLA VIRIDIS CULTIVIATION GROWTH AND CARBON ASSIMILATION.

4.1 Introduction and Overview

4.1.1 Background

As microalgae absorb light for energy, they produce oxygen gas (O_2) and consume carbon dioxide (CO_2). Plant and micro- biologists have long used oxygen sensors as a tool for assessing photosynthetic and respiratory activity in algae. These types of measurements are often performed over relatively short time periods using close-chambered apparatuses that can measure oxygen exchange, light, and absorbance of small sample volumes[15]. Much of the data collected from these types of experiments have formed the basis of many current photosynthetic models used in engineering applications that attempt to model and optimize algal growth[16–19]. Many of these same measurement principles can be applied to monitor microalgal growth over longer time scales in larger bench- and pilot-scale applications.

Measuring gas production or consumption in microalgal cultures over longer time scales and larger volumes, however, is complicated as the mass transfer of O_2 and CO_2 between the gas and liquid phase must be considered, in addition to the chemical and biological processes that can potentially impact these transfer rates. Nonetheless, on-line gas measurements, both dissolved and gaseous, provide invaluable information for those studying and modeling these photosynthetic microbes. Historically, DO measurements have been more commonly utilized in microalgal experiments as compared to gaseous O_2/CO_2 measurements or dissolved CO_2. Estimating the oxygen production rate (OPR) and carbon uptake rate (CUR) of cultures directly via gas sensors requires a sophisticated airtight setup to allow for *quick* and reliable gas exchange measurements. Measuring the dissolved CO_2 has only recently been feasible with newer membrane technology, and still requires special consideration of the chemical reactions involved with carbonate species. While more commonly implemented in experimental setups, DO probes still have limitations. DO electrodes are relatively expensive as compared to pH electrodes, which do not require special membranes. In addition, certain types of electrodes consume oxygen as part of the measuring process, limiting their measurement accuracy, response time, and applicability[27,28,29].

pH electrodes are arguably the most commonly used on-line sensor in bench-scale PBRs. These inexpensive probes are used to monitor and control the pH, which is often done with CO_2 injection. While dissolved oxygen electrodes are still more commonly used to estimate photosynthetic activity and growth with microalgae, there has been an increase interest in implementing pH data into growth models in ways to *help* define the carbon flows within an algal culturing environment[30,31].

As also described in Chapter 1, to fully capture the state of the carbon within a system—including the total dissolved inorganic carbon (DIC) and the distribution of carbon species—more than just the pH must be considered. However, tracking the total carbon is possible using various approaches that combine lab-based measurements with chemical equilibrium models. If the pH and the activity of the dissolved CO_2, i.e. **{**$H_2CO_3^*$**}**, are known, then the DIC concentration, m_{DIC}, can be theoretically calculated using equilibrium constants for carbonic acid K_1, K_2 and knowledge of the relevant activity coefficients γ. These relations are shown by Equations 4-1 through 4-4

where carbonic acid is referred to as $H_2CO_3^*$ since it is difficult to distinguish dissolved CO_2 in solution and are lumped together.

$$\{H^+\} = 10^{-pH} \quad \textit{4-1}$$

$$m_{DIC} = m_{H_2CO_3^*} + m_{HCO_3^-} + m_{CO_3^{2-}} \quad \textit{4-2}$$

$$m_x = \frac{\{x\}}{\gamma_x} \quad \textit{4-3}$$

$$DIC = \{H_2CO_3^*\}\left[\frac{1}{\gamma_{H_2CO_3^*}} + \frac{\frac{K_1}{\{H^+\}}}{\gamma_{HCO_3^-}} + \frac{\frac{K_1K_2}{\{H^+\}^2}}{\gamma_{CO_3^{2-}}}\right] \quad \textit{4-4}$$

Filali et al. (2011) utilized this concept to experimentally measure DIC when performing growth experiments in an air-lift PBR used for modeling *Chlorella vulgaris.* Since *Chlorella* is a freshwater species, the largely salt-dependent activity coefficients are assumed to equal one, thus, simplifying this approach for estimating DIC from dissolved CO_2 measurements. DIC is then tracked as a state variable in this model (Equation 4-5), where it is dependent on 1) the microalgal growth rate μ, 2) microalgal biomass concentration X, 3) a carbon-to-biomass conversion coefficient M_x, and 4) the mass transfer rate of CO_2 into solution N_{CO2}, since CO_2 is continuously bubbled into the PBR.

$$\frac{d[DIC]}{dt} = -\mu\left(\frac{X}{M_x}\right) + N_{CO_2} \quad \textit{4-5}$$

Using a similar concept as shown in Equation 4-5, Titica et al. (2014) formulates a dynamic pH model for autotrophic growth of the microalgae marine *Chlamydomonas reinhardtii*[30]. This approach is different, however, in that an algal growth model is combined with a chemical and thermodynamic model to estimate pH. In this salt-water system, the dissolved CO_2 is not measured, requiring additional constraints involving the mass and charge balance of the chemical system to fully define the DIC.

To our knowledge, pH has not been used in a method for assessing growth directly by relating this property to DIC outside a growth-modeling context, where microalgal growth parameters could affect carbon flow estimates**. While the concepts behind these approaches are similar, the direct approach does not depend on any estimate of the microbial growth rate. This differentiation is key because this new approach allows for many of the built-in assumptions in the previous work when relating pH to DIC to be tested directly and rigorously validated.** Therefore, the new approach places a greater emphasis on directly modeling the inorganic-to-organic carbon flows, and less on modeling microalgal growth with respect to light and nutrients, as has been performed in previous work as part of fitting growth parameters that affect DIC estimates.

4.1.2 Research framework overview

The PBR used herein is equipped with pH control where the increase in pH can be related to the DIC removal rate when combined with a thermochemical equilibrium model. This approach, which assumes a quasi-equilibrium pH state between CO_2 injections, provides a piece-wise carbon estimation approach to determine the DIC *removal rate* from the culture liquid. Given this information and the background loss of carbon into the headspace, and subsequent environment—which can be quantified experimentally and described by a diffusion transport model—the carbon uptake rate of the microalgae can be calculated (Equation 4-6). This biological carbon uptake rate is subsequently used to estimate the total organic carbon within the system. Figure 4-1 displays a workflow diagram the tested methodology.

$$\frac{dDIC}{dt} = \frac{dDIC}{dt}_{microalgae} + \frac{dDIC}{dt}_{diffusion} \qquad 4\text{-}6$$

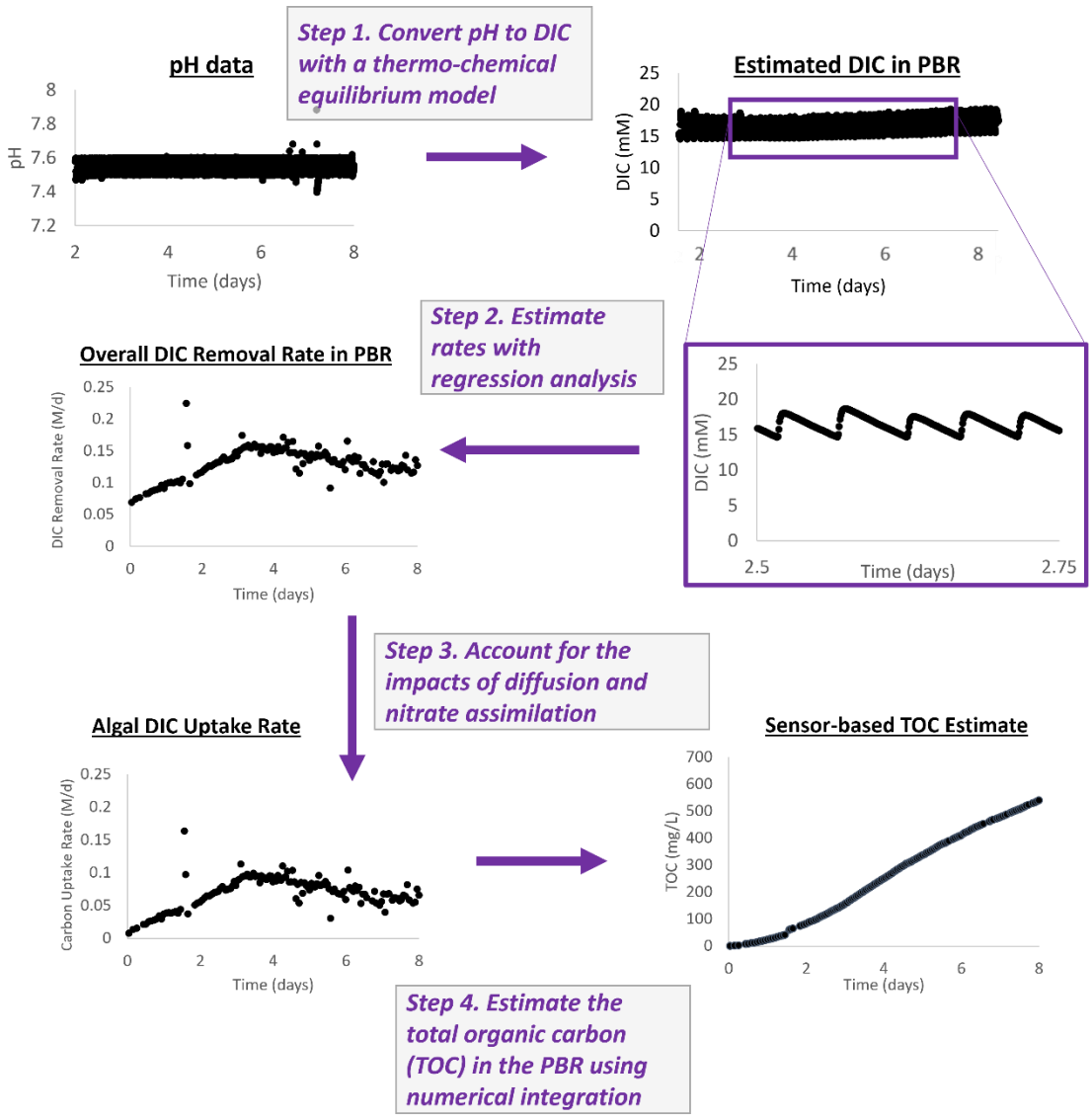

Figure 4-1. Simplified workflow diagram for proposed method for estimating microalgal carbon uptake rates and total inorganic carbon assimilation from continuous pH measurements in a pH-controlled PBR.

This research tests a novel approach for using pH as a tool for tracking carbon flows within a PBR and estimating the total carbon assimilated by microalgae by relating pH to the carbon removed from a marine microalgal culturing system. This method involves developing a model that included both a chemical equilibrium sub-model and a carbon mass transfer by diffusion relationship to relate the pH to total dissolved inorganic carbon during microalgal cultivation within a pH-controlled PBR. This method was validated by performing cultivation experiments with *D. viridis* microalgae over a range of conditions, as described in Table 4-1, and comparing carbon estimates made using this pH-sensor approach with the lab-based carbon estimates and cell counts.

Table 4-1. Overview of experimental conditions under which this pH-to-carbon method was tested using the marine microalgae D. viridis.

Set Name	pH	Init. $NaHCO_3$ (mM)	Init. DIC (mM)	Init. KNO_3 (mM)	Init. Light (PPF)
A-R1	7.5	13.4	13.4	5	175*
A-R2	7.5	10	10	5	175*
B-R1	7.5	5.0	5.0	2.5	200
B-R2	7.5	10	10	2.5	200
C-R2	8.13	38	35	3.5	55*
D-R2	8.13	38	35	5	145

**These experiments had brief cycles where the light was turned off throughout the experiment.*

4.2 Results & Discussion

4.2.1 pH sensor-based TOC estimates agree with other microalgal growth metrics

In Figure 4-2, the pH sensor-based carbon estimates for the assimilated carbon evaluated over the cultivation period show the same overall qualitative growth patterns as seen with the cell counts and the measured TOC of the spun cell portions of the microalgae as shown in Figure 4-2. Cell counts were over 1.0×10^7 four to five days after cells had reached an initial cell concentration of 0.20×10^6 cells/mL, regardless of the nitrogen or bicarbonate concentrations, although a slower cell growth rate for was observed for the lower light condition tested (Figure 4-2, Column C, C-R2).

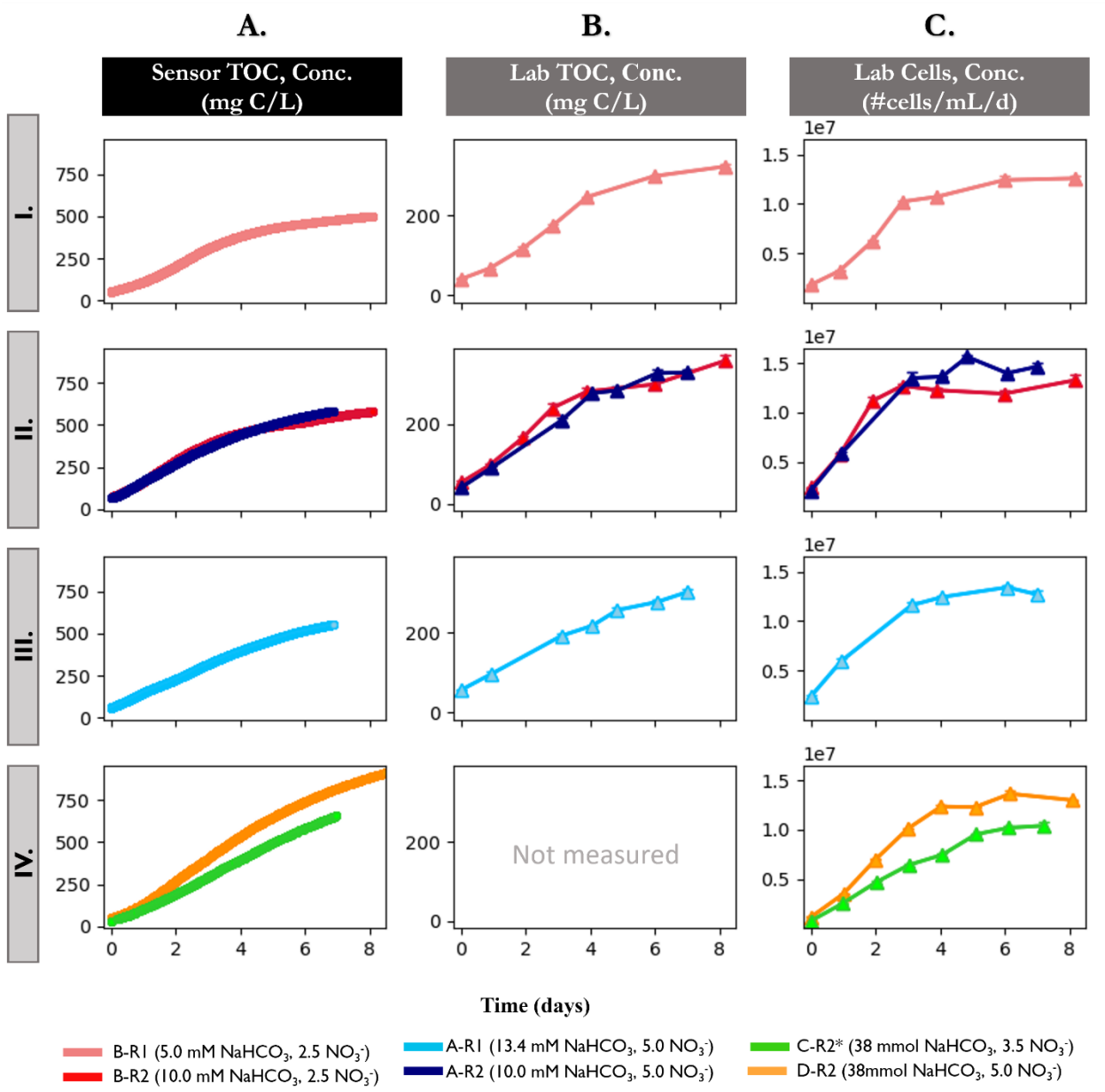

Figure 4-2. Comparison of different growth measurements properties using sensor-based approach for estimating TOC (**A**), lab-based TOC measurements (**B**), and cell counts (**C**) over experimental duration relative to the sampling start time. Units for the y-axis are noted at the top of each column. Rows represent the four bicarbonate concentrations tested, *i.e.*, I.) 5.0 mM $NaHCO_3$; II.) 10.0 mM $NaHCO_3$; III.) 13.4 mM $NaHCO_3$; IV.) 38 mM $NaHCO_3$. Colors represent different experimental sets, with conditions as specified in legend. *The initial light condition for Set C-R2 was ~30% of the initial irradiance as compared to other sets, *i.e.*, 55 PPFD as compared to 150-200 PPFD

A comparison of the lab and sensor-based approach for estimating growth rates show similar trends (Figure 4-3). The carbon uptake rates as shown in Figure 4-3 show 'light on' estimates for carbon uptake rate. While the growth rates are estimated over longer time scales for the lab TOC and cell data (given that these measurements were taken once a day, at most) similar trends are observed

between the lab measurements and sensor-based growth estimates for carbon across the four bicarbonate conditions tested (Figure 4-3).

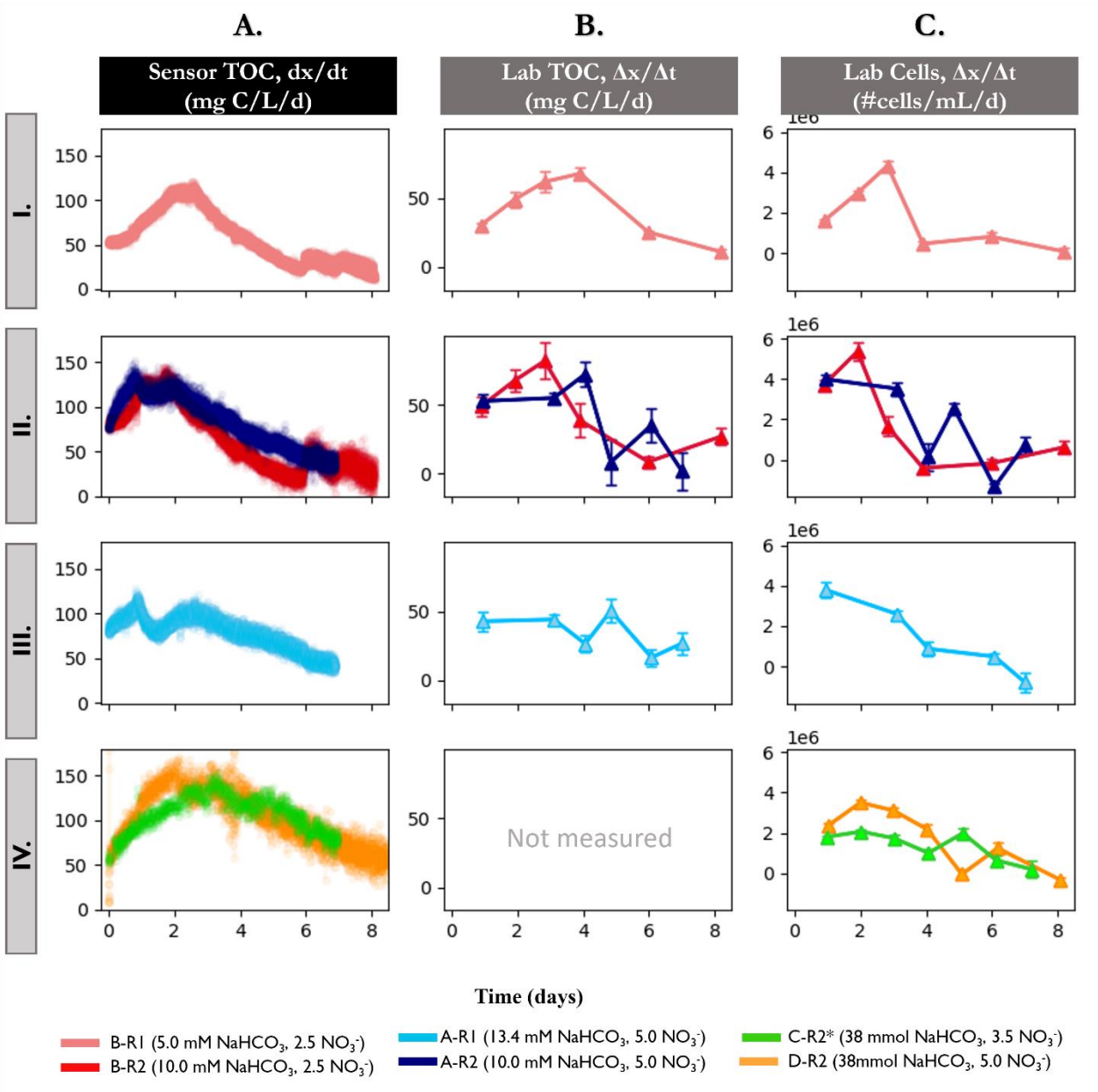

Figure 4-3. Growth rate estimates using the pH-to-carbon sensor approach (**A**), lab-based TOC carbon measurements (**B**), and cell counts (**C**) over the experimental duration. Units for the y-axis are noted at the top of each column. Rows represent the four bicarbonate concentrations tested, *i.e.*, I.) 5.0 mM $NaHCO_3$; II.) 10.0 mM $NaHCO_3$; III.) 13.4 mM $NaHCO_3$; IV.) 38 mM $NaHCO_3$. *The initial light condition for Set C-R2 was ~30% of the initial irradiance as compared to other sets, *i.e.*, 55 PPFD as compared to 150-200 PPFD. Note, carbon uptake rates for sensor estimates show only light ON conditions. 'n/m' indicates not measured. Error bars for lab-based measurements represent standard error.

Comparison of the specific growth rates (Figure 4-4) across these three metrics displays both qualitative agreement in trends and quantitative agreement with respect to specific growth rates between the sensor-based estimates and the lab data.

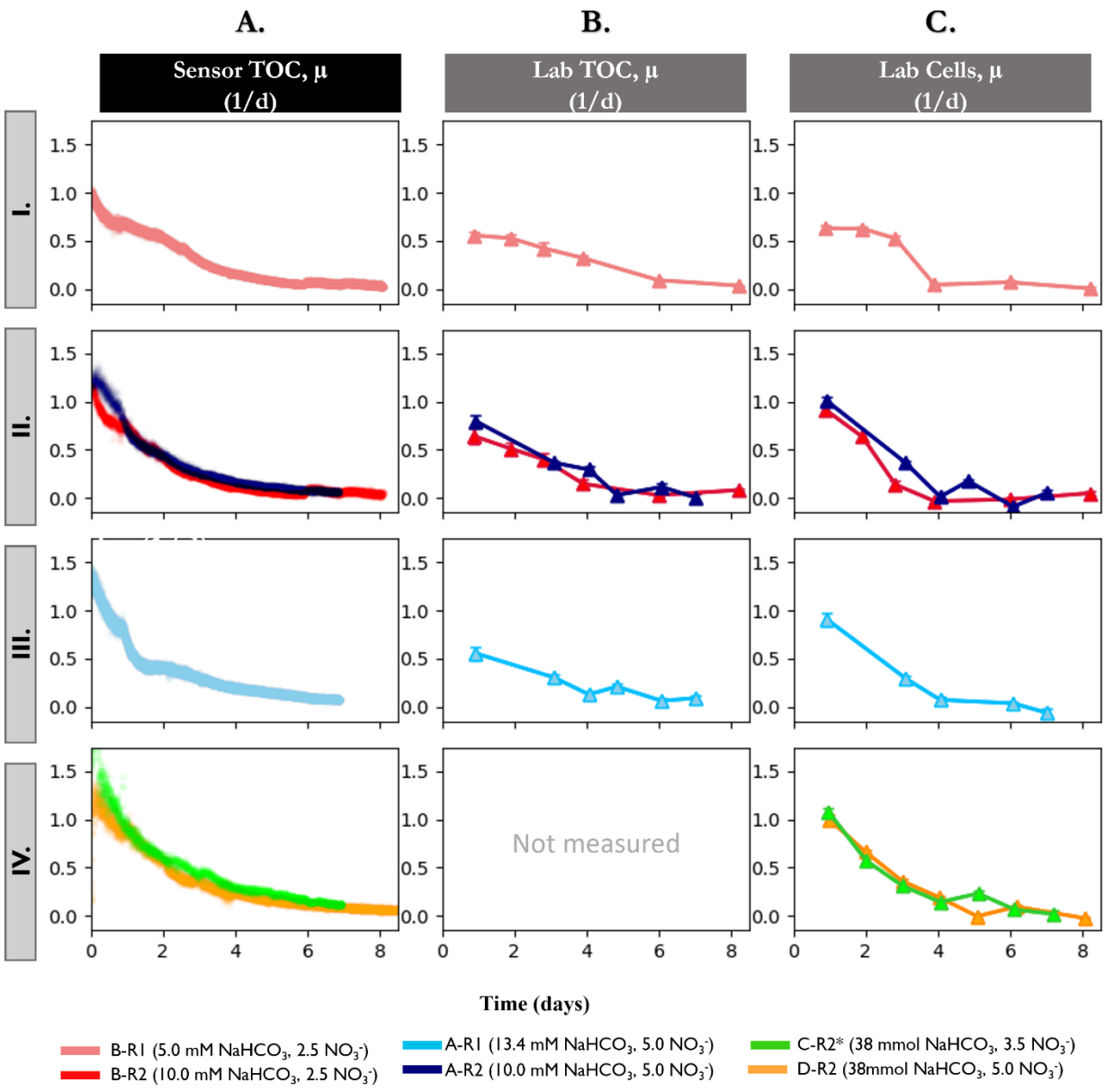

Figure 4-4. Specific growth rate estimates using the pH-to-carbon sensor approach (**A**), lab-based carbon measurements TOC (**B**), and cell counts (**C**) over the experimental duration (time relative to cell cultures reaching specified cell density). Units for the y-axis are noted at the top of each column. Rows represent the four bicarbonate concentrations tested, *i.e.*, I.) 5.0 mM $NaHCO_3$; II.) 10.0 mM $NaHCO_3$; III.) 13.4 mM $NaHCO_3$; IV.) 38 mM $NaHCO_3$. *The initial light condition for Set C-R2 was ~30% of the initial irradiance as compared to others. 'n/m' indicates not measured. Error bars for lab-based measurements represent the propagation of uncertainty based on standard error.

This sensor-based carbon-estimation approach not only shows strong qualitative agreement when comparing trends of this metric to the other two lab-based metrics (Figure 4-2 through Figure 4-4), but also show agreement in magnitude and trends amongst across the experimental sets, despite the wide-ranging conditions under which these experiments were performed. More specifically, the algal carbon uptake rates start and increase at similar rates up until the organic carbon in the system reaches a concentration around 150-200 mg/L, at which point the algal carbon uptake rates begin to decline, at rates which appear dependent on culture conditions (
Figure **4-5**).

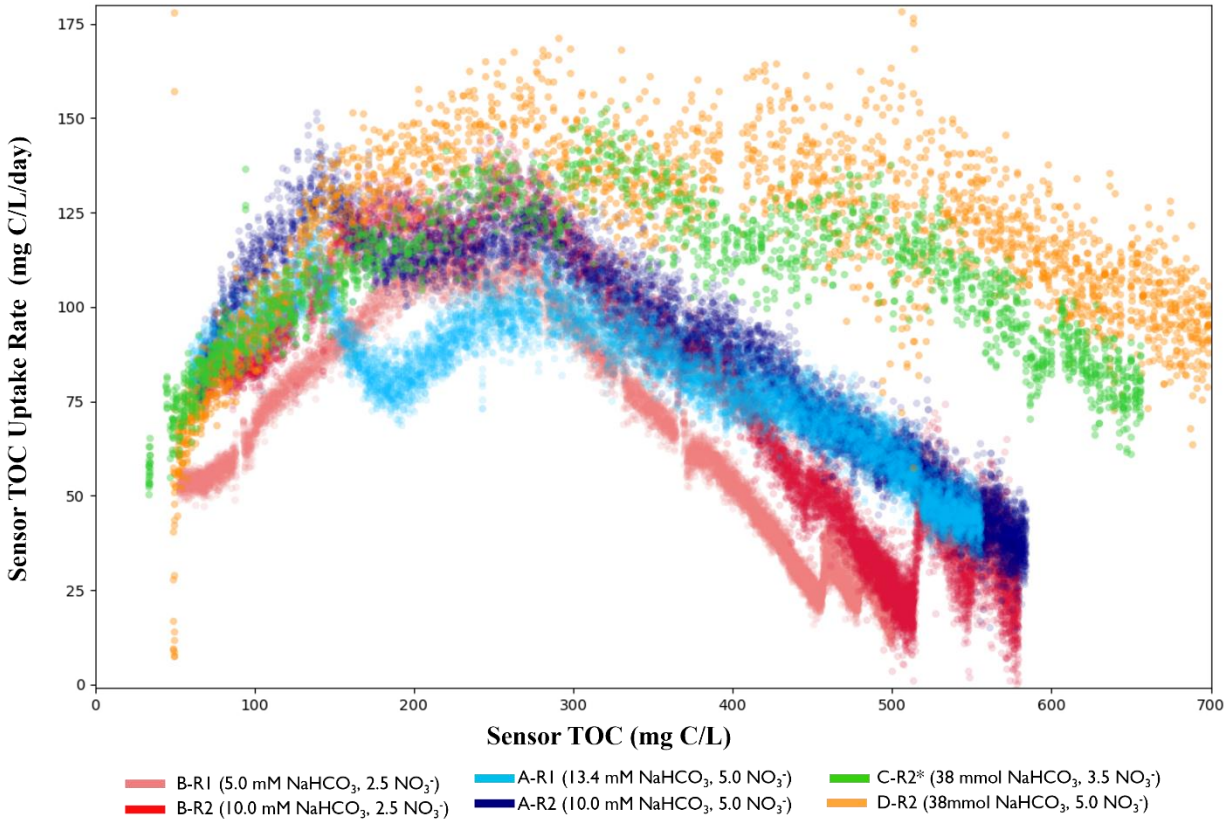

Figure 4-5. Sensor-based carbon uptake rates for all experiments relative to the total organic carbon (TOC) concentration as estimated with sensor. Colors represent experimental set.

The higher resolution of sensor measurement also provides insights into how perturbances, such as sampling, might impact the organisms differently under stressful conditions. For example, the act of mixing the PBR after day five for the two 2.5 mM KNO_3 experimental sets (when nitrogen is depleted) leads to a sudden increase in carbon uptake rates; this phenomenon is not observed for the higher nitrogen sets (Figure 4-3, Column A, Set B vs A). This immediate increase in carbon uptake rate after mixing suggests that these nitrogen-deplete cells can still photosynthesize. Thus, the faster rate of decline in carbon uptake rates, as compared to nitrogen-replete conditions is likely due to cell settling. While these sensors do not provide insight into whether this settling is a willful

behavioral response to stress (*i.e.*, retreating into a palmelloid vegetative state), or due to a loss of flagellar locomotion due to nutrient deprivation, or both, this observed change does give quick insights into the state of the culture under different growth conditions.

4.2.2 Sensor-based TOC estimates show reasonable quantitative agreement with lab-based estimates based on the suspended solid portion of algal cultures

Figure 4-2 through Figure 4-4 highlight how well this method matches qualitatively with other growth assays, they do not provide a complete mass balance-based quantitative assessment of the method's accuracy when tracking inorganic-to-organic carbon. This step is very important, especially if this method is used in combination with growth modeling efforts.

Figure 4-6 shows an overview of the raw results from these validation experiments by comparing the freshly assimilated carbon between sampling points for the two methods. In all experiments, for the first two to three days, the relative difference between the two sets is ~60%. Thereafter this relative difference diverges for each set, becoming more sporadic. Figure 4-6 graphically illustrates how the sensor and lab-based results compare along how the daily difference changes over the course of the experiment, with no markedly different trends observed across different bicarbonate or nitrate conditions. In summary, these two methods show an overall strong linear relationship across sampling time, even when considering the increase in noise in this relationship that occurs at later phases of growth (Figure 4-7).

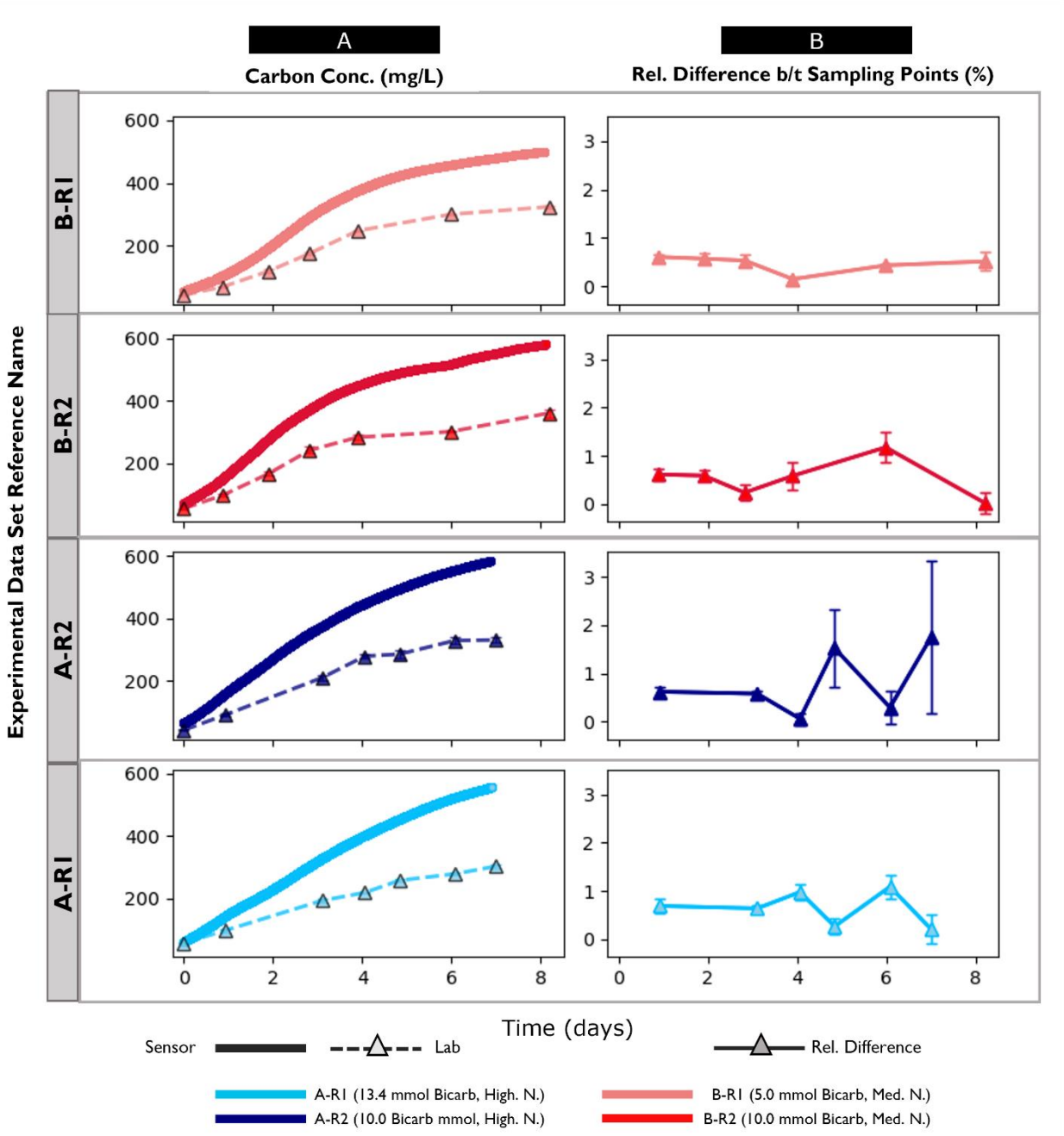

Figure 4-6. Comparison of carbon estimates using pH-sensor approach as compared the lab-based TOC analyzer (**A**) and the relative different between the two methods when considering the newly assimilated carbon between two sequential sampling points (**B**). Error bars show propagated error based on the standard error of lab-based TOC measurements.

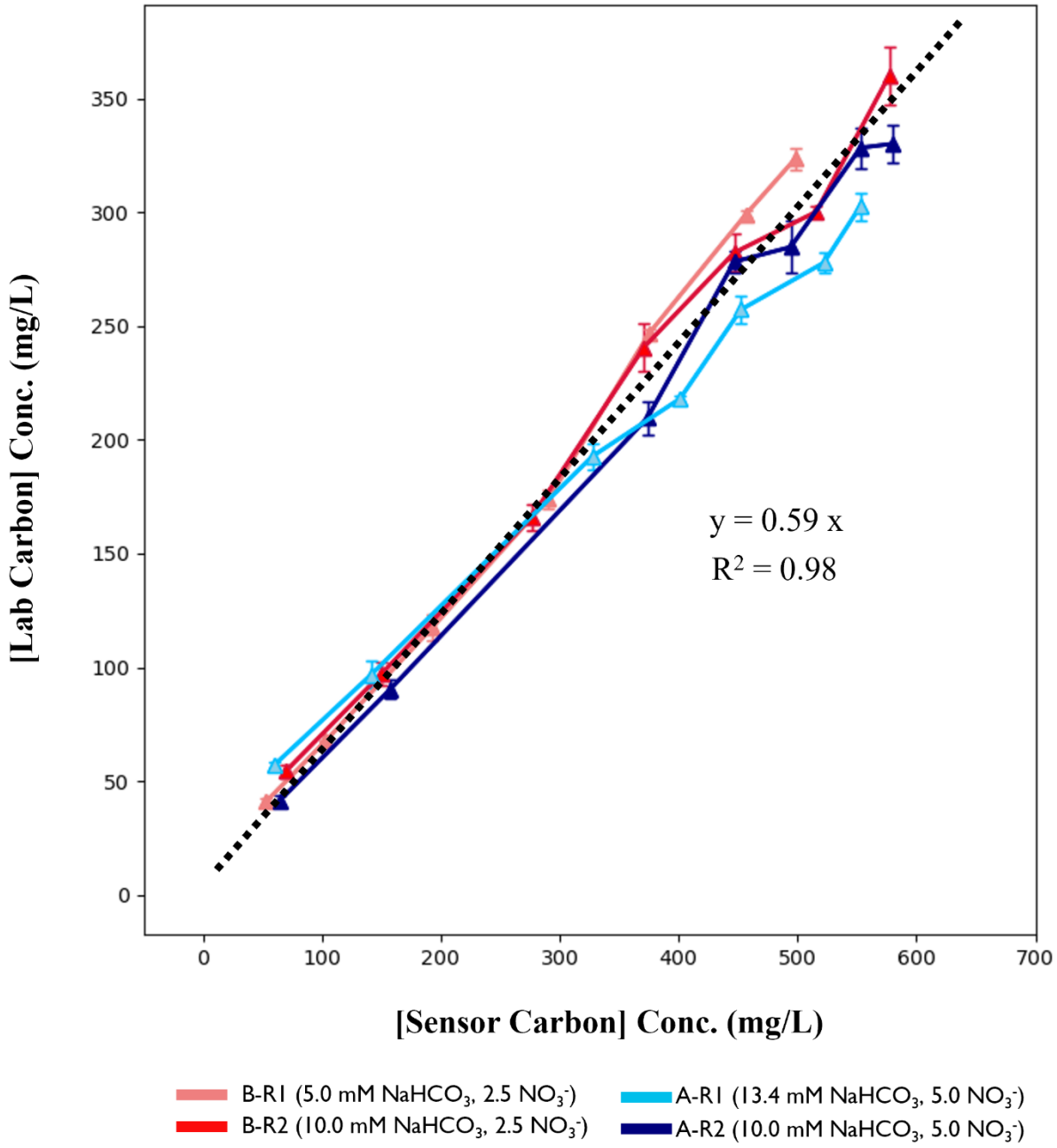

Figure 4-7. Lab-based TOC of spun microalgae biomass versus TOC estimated using the sensor method with cursory regression analysis. Error bars show standard error based for lab TOC estimates only.

4.2.3 Lab-based TOC measurements may underestimate TOC

Dunaliella spp. are known for excreting dissolved organics, such as glycerol, into their surrounding media[32–34], but due to the interferences from salt and high inorganic carbon content, the TOC within the media was not analyzed within the scope of this work. Sets A, B showed an increase in UV_{254nm} absorbance in this range, suggesting an increasing presence of dissolved organic material (Figure 4-8). Interestingly, the 5.0 mM nitrogen conditions show a greater increase rate in UV_{254nm} absorbance relative to 2.5 mM conditions after day three; this divergence in UV_{254nm} roughly corresponds with the decline in carbon uptake rates (Figure 4-3).

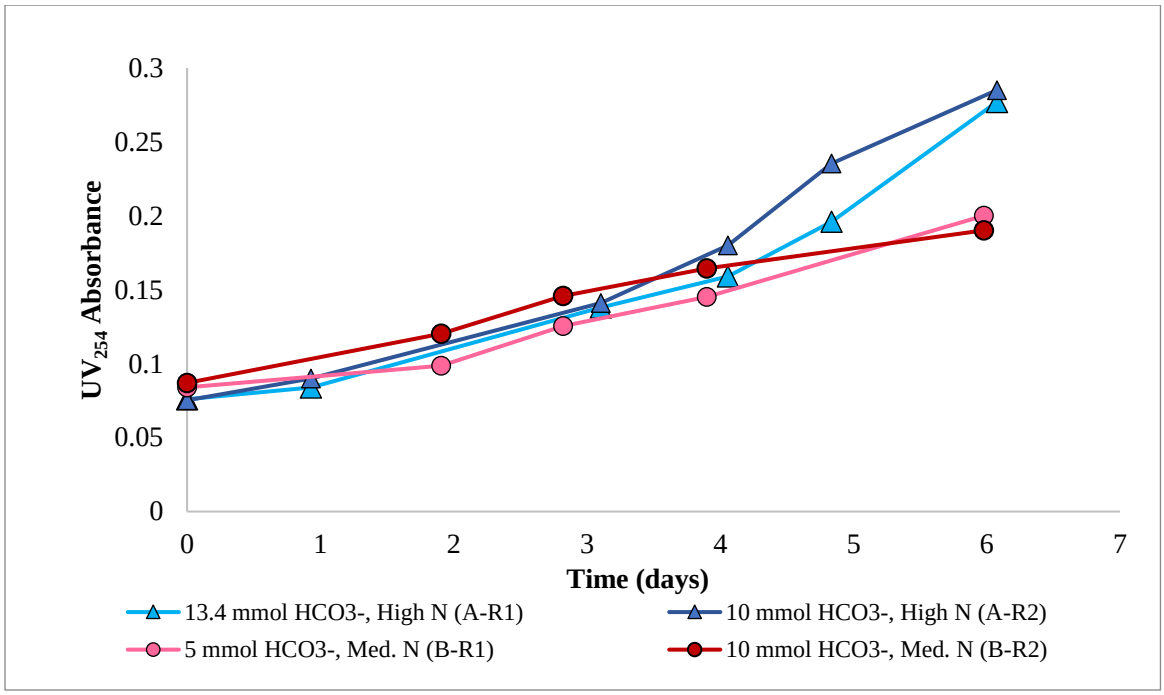

Figure 4-8. UV_{254nm} absorbance of culture media after cell and biomass separation with centrifugation. Time is relative to the start of sampling, which corresponds to around 0.20 x 10^6 cells/mL. **High N** refers to an initial KNO_3 concentration of 5.0 mM. **Med. N** refers to 2.50 mM KNO_3. UV_{254nm} absorbance measurements were not taken for other data sets.

Furthermore, a large portion of the lab-measured TOC from *D. viridis* was easily and quickly purged from the diluted samples within 2-3 minutes. This purgeable fraction, as estimated from analyzing both TOC and non-purgeable organic carbon (NPOC) on the analyzer, also appears to vary with time (Figure 4-9). Given the observed volatility of the organic contents within these cells, lab-based TOC estimates could lead to an overall underestimate of the true carbon produced

by these organisms, especially if these osmotically-sensitive cells are diluted and not quickly placed on the TOC analyzer machine for analysis.

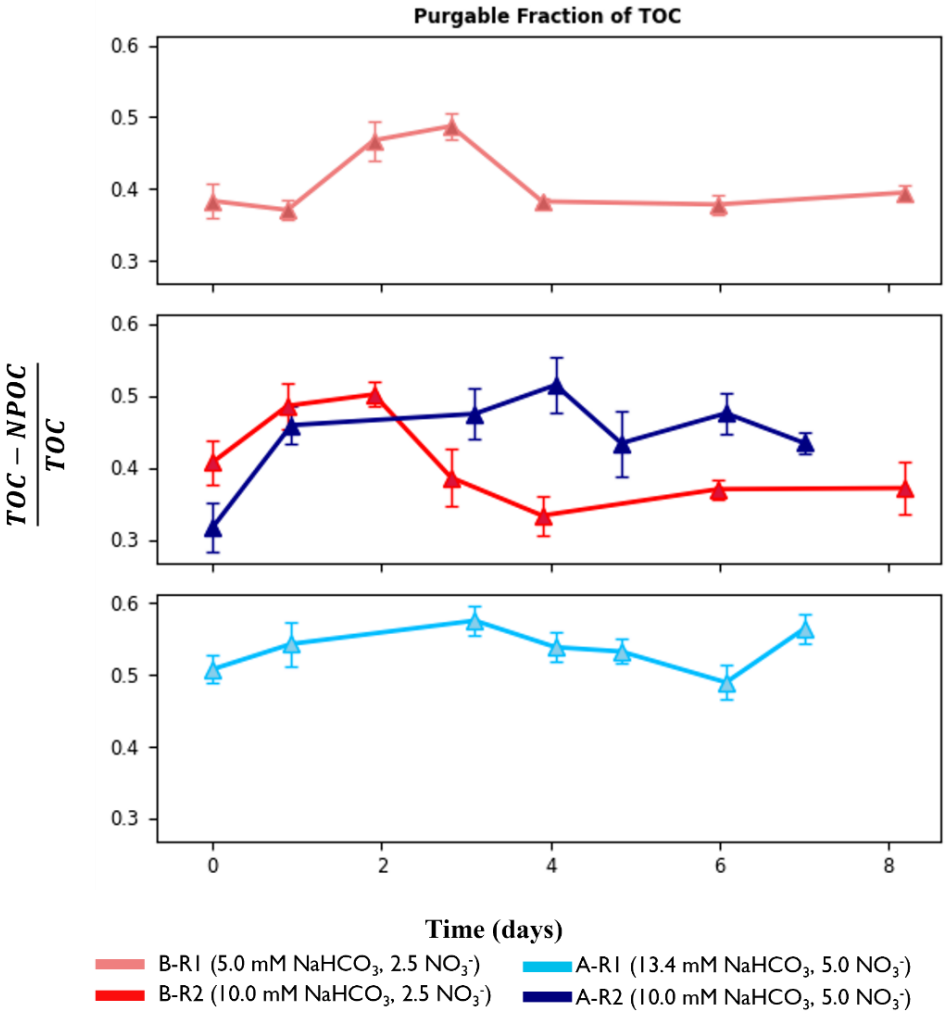

Figure 4-9. Purgeable organic carbon (POC) fraction of TOC as estimated based on measurements from TOC analyzer for validation experiments. Error bars represent propagated uncertainty based on standard error in TOC and NPOC measurements used to estimate the POC fraction. NPOC was measured after purging samples for 3-5 minutes with high purity air after 5% acidification with 2 M HCl.

4.2.4 Sensibility checks

When performing any in-depth analysis and modeling with large datasets and processing, reviewing raw and partially processed data is important for both verifying assumptions and verifying that code used in processing data is performing its intended function. For example, comparing the regression analysis for the raw pH sensor data against the estimated algal carbon

uptake rates provides a simple verification to check that the model outputs seem reasonable. Figure 4-10 (B vs C) shows this comparison for *all* the processed sensor data used to estimate algal TOC, including the two days prior to inoculating the PBRs with algae, and the short periods of when the light was turned off for select experiments. These short 'light off' periods lead to negative carbon uptake rate since photosynthesis has halted as respiration continues with stored cell products (Figure 4-10, Column C gray area).

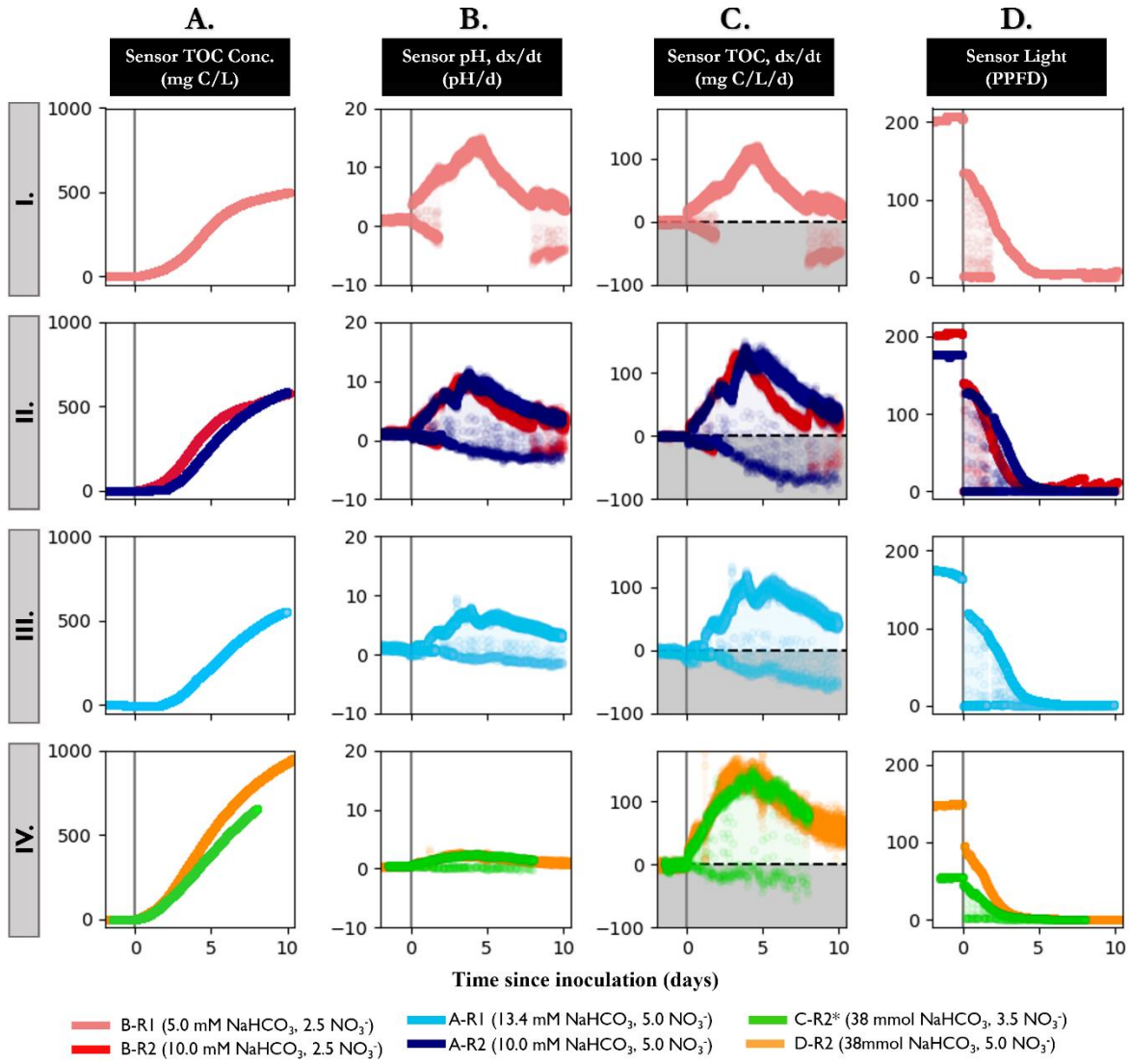

Figure 4-10. Sensibility checks for model verification. **A**) sensor TOC estimates in PBR including two days prior to inoculation, **B**) pH increase rate, **C**) net carbon uptake rate due to microalgae under light and dark conditions, **D**) Light in PBR in photosynthetic photon flux density, µmol/s-m^2. *Time reflects time since inoculation and not time since the start of sampling* and is represented by a SOLID GRAY LINE. This figure shows all data used to estimate carbon assimilation, including two days prior to inoculation and the brief cycles of time when the light was temporarily turned off. GRAY AREA for subplot C shows a negative rate value for algal carbon uptake that occurred when the light was briefly turned OFF.

The lack of organic carbon accumulation in the PBRs before inoculation suggest that the K_L coefficient combined with the diffusion model accurately estimated the carbon flows before microalgal addition (Figure 4-10, Column A, C). Furthermore, overall, the pH increase rates follow the same trends as the algal carbon uptake rates, with slight perturbations noted around sampling times for both the raw pH rate data and model-based carbon uptake rates (Figure 4-10, B, C).

Aside from helping to verify that the model is performing reasonably, Figure 4-10, highlights how the buffering capacity (*i.e.*, $NaHCO_3$ concentration) of the different media conditions impact the model's pH-to-DIC sensitivity. More specifically, the peak rate of pH increase is around five times higher for the 5.0 mM $NaHCO_3$ system as compared to the 38 mM experiments (~15 pH/day as compared to 3 pH/day, respectively), despite the relatively similar maximum algal carbon uptake rate between these two conditions (~120 mg/L/d to ~150 mg/L/d, respectively). This pH-to-DIC relationship is important when considering this model's sensitivity to pH measurement error.

The raw data output showing the pH, temperature, CO_2 headspace readings, and light conditions in the PBRs over the course of experiments and for four days prior to inoculation can also be found in the SI, Figure 6-1.

4.2.5 Model sensitivity to pH depends on media and operating conditions

A cursory sensitivity analysis for this method showed that the model sensitivity to ±0.05 pH error increases at higher bicarbonate conditions (Figure 4-11). This result is not unexpected, as the media solutions with different buffering capacity may have different pH-to-carbon relationships. While this simple analysis assumes that constant offset, *i.e.*, the magnitude of pH error does not change with time, using the K_L parameters calibrated from the base-case during this sensitivity analysis indicates the potential error in pH measurements that may occur after calibration. Overall, this cursory analysis shows that this method, when used in a neutral pH and low bicarbonate conditions, produces reliable estimates with at most 5% error if the pH shifts by 0.05 units; this low error is important for applicability since pH electrodes are known to drift over time.

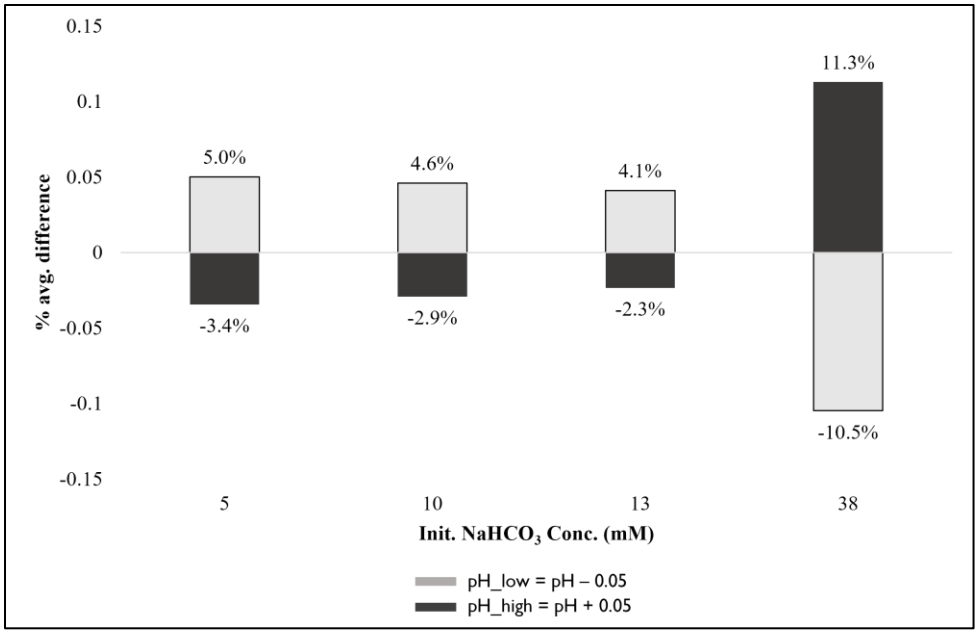

Figure 4-11. Cursory sensitivity analysis showing the percent difference in carbon assimilation estimates when pH is shifted up and down before processing reactor data in model as compared to the base-case (i.e., pH measurement used for primary analysis). These comparisons were done for each sampling time and averaged across time points and replicates. Note, this sensitivity analysis uses the calibrated K_L parameters from the base case (no pH shift) across all sets.

4.2.6 The apparent mass transfer coefficient, K_L, varies logarithmically with DIC concentration.

Analyzing the background rate carbon loss in the PBRs due to diffusion under various media conditions and PBR setups showed that, for this modeling approach, the K_L varies with respect to DIC concentration (Figure 4-12). Note, the large variation seen for each DIC condition, especially in less buffered systems, is likely due to the inherent sensor noise combined with the decision to estimate rates in a piecewise fashion across CO_2 injection intervals rather than performing a regression across each CO_2-injection interval. This decision was made to as a tradeoff for reducing error that could emerge from non-linear changes in pH/carbon between CO_2 injection points, and because the observed variability should be similar between diffusion and algal rates since are estimated from the pH sensor.

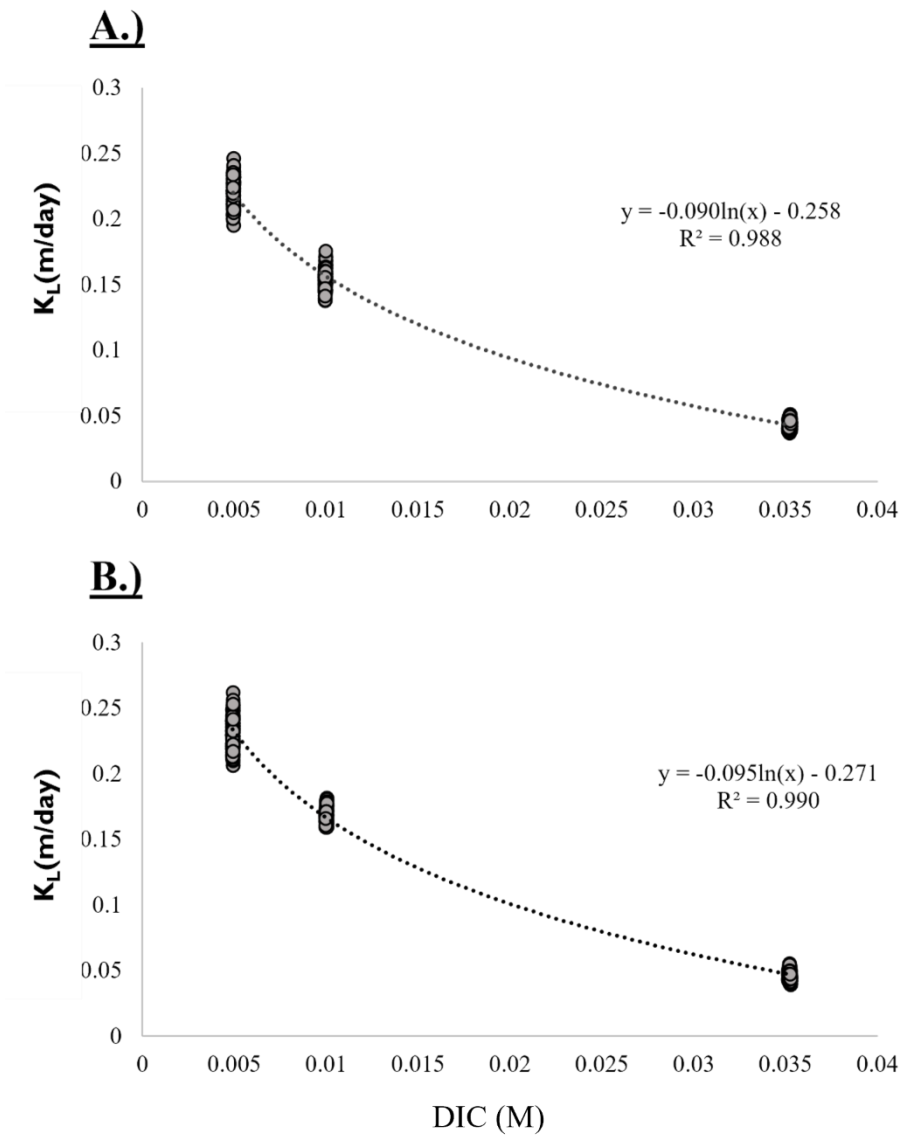

Figure 4-12. The apparent mass transfer K_L coefficient estimate for Reactor #1 (A) and #2 (B) across 5, 10, and 35 mM DIC conditions. Conditions for background tests can be found in the SI, Table 6-2.

4.3 Methods and Modeling Approach

4.3.1 Modeling framework for using pH to estimate carbon uptake rates and total organic carbon

4.3.1.1 A Pitzer thermo-chemical equilibrium model will relate the pH to total dissolved inorganic carbon.

A Pitzer approach for estimating activity was used to solve the chemical equilibrium states for this system. This approach, along with the specific ion interaction theory (SIT) are both commonly utilized methods for determining the chemical equilibrium of solutions with high ionic strengths. The Pitzer model involves a rigorous thermodynamic derivation based on the virial expansion of excess Gibbs free energy and considers all potential ion-ion interactions while the SIT model assumes that only that only chemical species with opposing signs interact with each other[35]. Due to the high ionic strength of the media used with *D. viridis*, the Pitzer approached was selected to estimate the chemical state of the system with respect to the most prominent chemical species in the marine media.

Furthermore, if nitrate (NO_3^-) is used as a nitrogen source, protons are consumed during the assimilation process, impacting the overall pH-to-carbon relation. Thus, the inputs to the chemical equilibrium model should include this proton loss by nitrogen assimilation. This incorporation by adjusting the chemical inputs based on the Redfield ratio[36] (Equation 4-7).

$$CO_2 + H_2O + 0.15\,NO_3^- + 0.15\,H^+ \rightarrow CH_2O(NH_3)_{0.15} + 1.22\,O_2 \qquad 4\text{-}7$$

This approach for relating ‘pH-increase rates’ to ‘carbon-removal rates involved first solving multiple chemical equilibrium conditions across the range of chemical states of the PBR system throughout the duration of an experiment using chemical equilibrium software. The implementation of this chemical equilibrium model into the larger modeling framework is described in more depth in subsequent sections.

4.3.1.2 Diffusion model

Without microalgae present, the change in the total dissolved inorganic carbon within a culture media, assuming no solid formation or biological activity is entirely due to the transfer of CO_2 between the air and water interphase. This transfer assumption is valid if the DIC concentration in the liquid solution is not at the equilibrium concentration. DIC^*, for a given CO_2 partial pressure. Due to the complex nature of the carbonate system, and the multiple interacting concentration gradients that drive this system, an additional assumption is made to track the CO_2 loss from the PBR. Specifically, the mass transfer rate of the DIC out of a solution with a given pH and bicarbonate concentration is driven by the gradient between the total DIC in the solution at those conditions and the DIC concentration of the solution at a pH that has equilibrated with the headspace CO_2 partial pressure, *i.e.*, DIC.

Without algae present, this relationship is defined in Equation 4-8:

$$\frac{dDIC}{dt} = K_L \frac{A}{V(t)}[DIC^*(t) - DIC(t)] = K_L \frac{1}{D(t)}[DIC^*(t) - DIC(t)] \quad \text{4-8}$$

where K_L *is an apparent mass transfer coefficient for the overall DIC*; ***A*** is a constant that represents the area of the surface of the liquid in the PBR exposed to the headspace concentration in square meters; **V** is the volume of the reactor in cubic meters and **D** is the depth. **V** and **D** are both a step-wise function of time based on sample removal during experimental process. **DIC*** refers to the **DIC** in the system at equilibrium with the ambient CO_2 partial pressure.

After relating pH data to DIC using the chemical equilibrium model, the K_L coefficient is estimated using the on-line data and Equation 4-8. More specifically, the K_L apparent mass transfer coefficient is estimated by using Equation 4-9.

$$K_L = \frac{\frac{dDIC}{dt} D(t)}{DIC^*(t) - DIC(t)} \quad \text{4-9}$$

Background tests in the PBR were conducted over the range of test conditions under which validation tests will be performed to establish K_L estimates. *Furthermore, due to the multiple reactions involved with the carbonate chemical species, the K_L was estimated over a range of DIC conditions to account for differences in this CO_2 mass transfer velocity that might arise due to differences in the chemical state of the system.*

4.3.2 Experimental setup & procedure

4.3.2.1 Photobioreactor (PBR)

A 3-L photobioreactor (PBR) was constructed and fitted with sensors for pH, temperature, and light monitoring as described in Karam et al.[37]. The PBR setup was further modified to include pH control via CO_2 injection as well as headspace monitoring of the CO_2 concentration. Figure 4-13 displays a schematic overview of the setup.

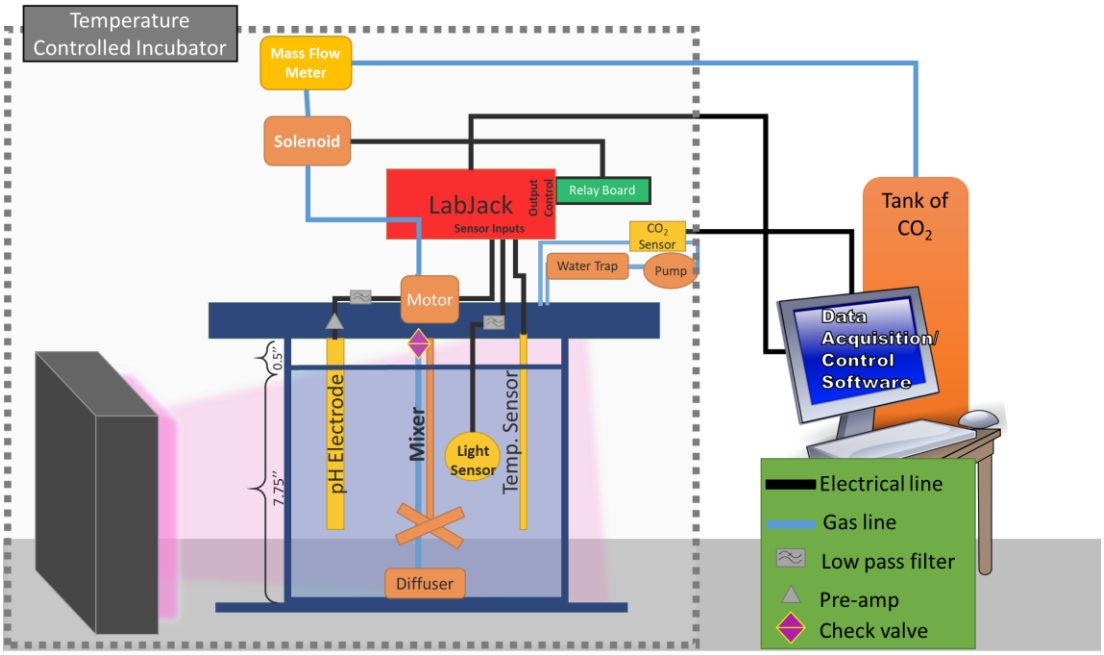

Figure 4-13 Schematic overview of experimental setup showing overview.

A few key differences between this setup and the setup as explained in Chapter 2 and previously published work[37]:

- A LumiGrow Pro 325 (LumiGrow, USA, 2016) grow lamp, adjusted to output approximately 40% blue and 60% red light was used as the light source.

- The photosynthetic active radiation (PAR) light sensor (SQ-212, Apogee Instruments, USA, 2016,) was located on the back side of the PBR and not within the highly ionic salt-water media since there was suspected voltage leakage from this aging sensor that disrupted pH readings. Light measurements were estimated in terms of photosynthetically active photon flux density (PPFD).

- pH electrodes were differentially connected to the analog inputs of the LabJack U6 microcontroller (LabJack, USA, 2014) using a 5-volt amplifier (2.2 V gain) to increase the signal and ensure that the electrodes worked properly despite the high impedance of

the microcontroller. This signal processing device had an inherent 1.2 V offset and was powered with a DC power supply connected to power on a circuit line without any other devices. Instead of a low-pass filter, the pH electrodes were isolated using a 10 K-Ohm resistor between one of the differential analog connectors and ground terminal.

Two dual setups, as shown in Figure 4-14 (A, B), were constructed for these validation tests, which were constructed within a temperature-controlled incubator. However, given the multiple heat sources within the incubator from the grow lamps, and the large fluctuations in temperature observed when opening the door to sample, the incubator temperature control was not used. Instead, the temperature within PBR's were maintained by balancing the heat from light sources with the ambient room temperature air using a fan and black curtain (Figure 4-14 B, C).

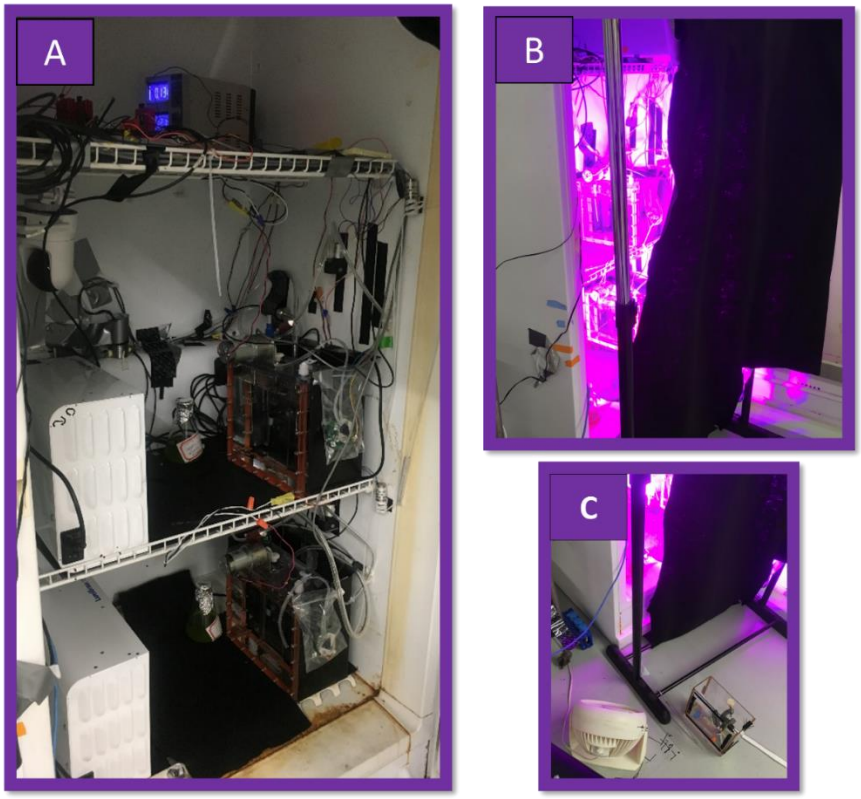

Figure 4-14. Dual experimental setup showing two reactors setup inside incubator. Reactor #1 refers to the reactor configuration on the upper shelf, and Reactor #2 is on the lower shelf.

The nature of this setup was such that certain components could not be easily randomized throughout experiments (*i.e.*, 1.0-liter per minute (lpm) air circulation pump, mixing power supply, solenoids/gas lines, etc.). Thus, 'Reactor #1' refers to the upper most setup configuration and 'Reactor#2' refers to the lower configuration. Temperature, light, pH, and the CO_2 headspace concentrations were measured continuously for all experiments. Further details on sensors and logging can be found in the Supplemental Information (SI) (Table 6-1,Table 6-2).

4.3.2.2 pH control

pH control was implemented in the setup above using DAQFactory data acquisition and control software (DQ, Lite Release 5.91) along with a relay board, a 12-V normally closed solenoid valve (McMaster, Part#5077T134, 2014, USA), a mass flow meter (TopTrex® 822/824, Sierra Instruments, USA, 2014), and 99.99% CO_2 gas, injected into the PBR with a nylon diffuser.

The pH control software algorithm implemented within DQ was a custom script that worked by setting an upper and lower pH setpoint limits. Once the pH probe measured past the specified high setpoint for a given time, the solenoid valve opens until a pre-specified setpoint CO_2 flows into the reactor, as specified by the mass flow meter to drop the pH to the lower setpoint. This initial pre-specific CO_2 input estimate is based on a simple thermochemical model which relates pH to DIC. Thereafter, by comparing the amount of CO_2 that was injected into the PBR with the theoretical amount of CO_2 needed to obtain the pH reduction observed after giving the reactor time to mix (e.g., ~two minutes after an injection), a correctional 'mass transfer injection efficiency factor' is estimated. This efficiency factor, which was observed to depend on the gas flow rate, bubble size of diffuser, and the working liquid volume, was used as feedback to adjust the CO_2 input setpoint amount and help ensure that the pH was consistently maintained between the pre-set range. Note, to minimize oscillations in CO_2 injection setpoints, the newly projected CO_2 input setpoint value was averaged with the previous three estimated setpoints.

4.3.2.3 Experimental procedure

Dunaliella viridis strain *dumsii* microalgae were grown from sterile 1M NaCl agar plates. PBRs were thoroughly bleached and set up with clean diffusers and tubing prior to each experiment. pH probes were soaked overnight in 3M KCl solutions between experiments to hydrate them. The probes were calibrated before and/or after experiments at close to 25ºC. Calibration data can be found in the SI. For each experiment, the mixing impeller mixed at a speed of ~80-100 rotations per minute (RPM). This relatively low rate was selected to prevent shear and was found to provide adequate mixing in this PBR system with respect to pH control, having a characteristic bulk mixing time of approximately two minutes. Before algal inoculation, filter-sterilized culture media was added to the reactors and pH control was started. Data was logged for multiple days to obtain background data and ensure system stability.

After inoculation with microalgae, samples were removed daily once the microalgae cell concentration reached ~0.2 to 0.5 x 10^6 #/mL. Approximately 12 to 20 mL of culture volume was removed from the PBR after opening the vessel and thoroughly mixing with a handheld stirrer since the gentle mixing from impeller did not prevent algae from settling to the bottom under stressful conditions. Samples were taken for an additional 5 to 7 days after cells reached sampling concentration levels.

Cells concentrations were measured using an automated cell counter (TC20^{TM}, BioRad, USA, 2016) immediately after sampling. This cell data, in combination with past work by Lai et al., 2018[38] , provided estimates for nitrogen removal from the media. For the experiments that included lab-based TOC analysis, samples were processed and stored as explained below.

4.3.2.4 Experimental conditions

Table 4-2 shows an overview of the experimental conditions for this validation tests, followed by a brief description and justification for the tested conditions.

Table 4-2. Overview of experimental conditions under which this pH-to-carbon method was tested. Experiments highlighted indicate primary validation (i.e., validation with TOC-based lab measurements). Experimental set letter values reflect temporal association.

Set Name	Reactor #	NaCl (M)	pH setpoints	Init. $NaHCO_3$ (mM)	Init. DIC (mM)	Init. KNO_3 (mM)	Init. Light (PPF)
A-R1	1	0.75	7.45-7.55	13.4	13.4	5	175*[A]
A-R2	2	0.75	7.45-7.55	10	10	5	175*[A]
B-R1	1	0.75	7.40-7.50	5.0	5.0	2.5	200[*B]
B-R2	2	0.75	7.40-7.50	10	10	2.5	200[*B]
C-R2	2	0.75	8.10-8.15	38	35	3.5	55*[A]
D-R2	2	0.75	8.10-8.15	38	35	5	145*[C]

**Three different light schemes were used during these experiments. See note in section below.*

Salt concentration (0.75M) - *D. viridis* and other *Dunaliella spp*. are known for their wide-ranging salt tolerance. This salt concentration was selected as it is within an ideal range for this species and because many of the empirically determined Pitzer model parameters that gauge ion-ion interactions were calibrated within this range.

pH and Sodium bicarbonate ($NaHCO_3$) Concentration– $NaHCO_3$ and pH both determine the overall DIC and CO_2 within a system. These conditions shown in Table 4-2 reflect different pH-bicarbonate combinations that result in a system with comparable H_2CO_3* concentrations (Figure 4-15). Furthermore, these DIC/pH levels represents conditions that should not cause carbon limitation[39,40] and could be realistic $NaHCO_3$ concentration for scale-up (*i.e.*, closer to that of seawater).

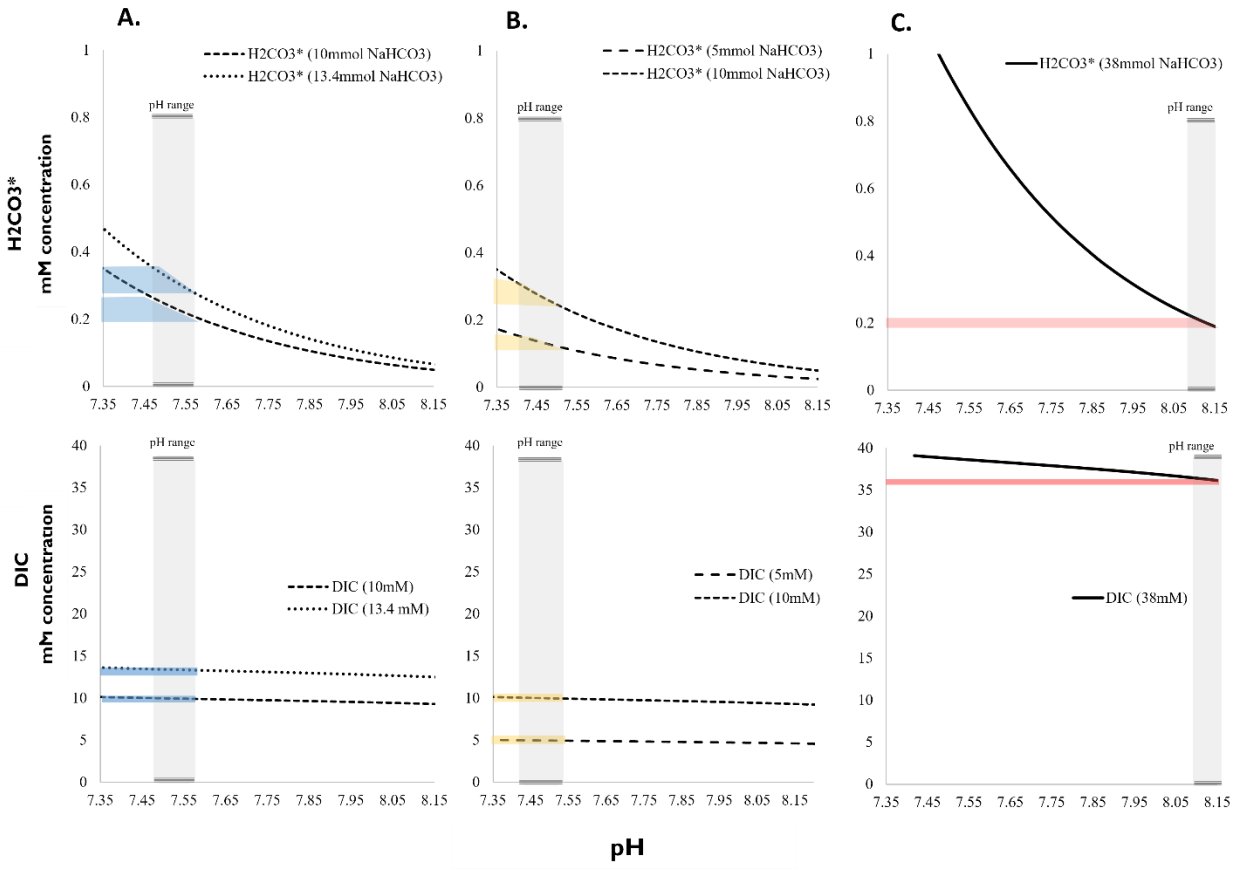

Figure 4-15. Graphical illustration showing the chemical state for the different media conditions tested as estimated by the Pitzer equilibrium model.

Light: The light intensities selected for the primary validation experiments reflect intensities that, based on prior work, should not be limiting nor inhibitory. Furthermore, to test that this method can be used over wide-ranging light conditions, three different light schemes were used as part of this validation approach, two of which had brief periods of turning the light off using a custom script in DAQ Factory, voice-recordings, and Alexa Echo (Amazon.com Inc., 2019). The light-off cycles were meant to 1) reduce light shock and stress to cultures immediately after inoculation, and 2) ensure rigorous validation conditions since algal cultivation systems may not have continuous lighting. Furthermore, by turning off the light for short time increments, a 'light' respiration rate can be estimated. *This technique is discussed and presented briefly in Chapter 5 since the scope of Chapter 4 is focused on validation and not method applications.*

> ***Light scheme A*** → For this light scheme, in order to reduce shock between inoculation and the start of sampling, the light was switched off for 15-30 minute during each injection interval, resulting in the light being off for approximately 40-50% of the time before the algal reached sampling conditions (*i.e.*, cell counts of 0.2×10^6 #/mL). Thereafter, the light was switched off for ~5 minutes in the middle of every 3-4 injection intervals. This scheme resulted in 'light off' conditions for approximately 5% of the total experimental duration.

Light scheme B → For this light scheme, in order to reduce shock between inoculation and the start of sampling, the light was switched off for 10-20 minute every other injection interval, resulting in the light being off for approximately 15% of the time before the algal reached sampling conditions (*i.e.*, cell counts of $0.2x10^6$ #/mL). Thereafter, the light was continuously kept on until sampling day 6, at which point the light was again cycled on and off. This scheme was done to compare the 'dark' respiration rate at the beginning and end of cultivation cycle.

Light scheme C → The light was continuously on from inoculation until the end of the experiment.

4.3.2.5 TOC analysis for primary validation

After samples were removed from the PBR during ongoing experiments, algal cells were separated from their media via centrifugal separation by adding 3.5 mL of culture into 15 mL centrifuge tubes and spinning for 30 minutes at 2500 relative centrifugal force and 4ºC. The algal pellet was frozen at -20ºC. These algal pellets were thawed immediately prior to TOC analysis, re-suspended in 3.5 mL ultrapure deionized water. This suspension was further diluted (1:40 to 1:80) before placing on the TOC analyzer. To minimize fluctuations caused by settling/separation, all samples were analyzed within one to three hours after placement on the analyzer's automatic sampler in 40-mL amber vials. These vials were cleaned thoroughly before baking at 400ºC for four hours and acid washed with 1% hydrochloric acid, rinsed with DI water, and dried prior to preparing samples.

Total organic carbon was measured using a TOC analyzer (TOC-V_{CSN}, Shimadzu Scientific). Preliminary method analysis with *D. viridis* showed that a large part of the TOC in the spun-and-then-diluted microalgae was purged out within 2-3 minutes, and thus estimating TOC via non-purgeable organic carbon (NPOC) would not suffice for providing reasonable estimates for the TOC. Therefore, TOC was estimated by analyzing the total carbon (TC) and subtracting the inorganic carbon (IC) content, which was estimated with either DI water controls (Set A) or using the IC analyzer on the TOC-V_{CSN} instrument (Set B). The spun algal biomass samples were analyzed both for total carbon TOC and non-purgeable organic carbon (NPOC) after 5% acidification with 2 M hydrochloric acid and 3-5 minutes of purging with high purity air to remove all inorganic carbon.

Potassium hydrogen phthalate (KHP) was used to generate three calibration curves across the range of expected concentrations (1-10 mg/L after dilution). Glucose was used as a secondary standard and 1,4 Benzoquinone was used as a tertiary standard to ensure that even difficult-to-combust carbon was combusted. Quality control samples were performed throughout experiments using KHP and glucose.

4.3.3 Model implementation and diffusion model calibration

4.3.3.1 Chemical equilibrium model integration

Since this Pitzer based approach considers multiple interactions, only the most prominent chemical species in the media are tracked (Table 4-3). Furthermore, since computationally solving the state of equilibrium for each pH data point is not computationally efficient, equilibrium equations were solved over a range of pH and NO_3- conditions using the chemical equilibrium software package *PyEquIon* (2021) in Python (v3.8) with the Pitzer-based activity estimation approach. Nitrogen assimilation estimates were added to each sensor-based data points based on cell counts and previously established relationships between cells and nitrogen. The DIC concentration for each data point was then estimated with a two-phase interpolation based on pH and NO_3^- assimilation.

Table 4-3. Media recipe for cultivating D. viridis for experiments. Bolded and highlighted chemical species were those considered when solving for equilibrium.

Chemical Species	Media Conc.	H^+	OH^-	Na^+	Cl	CO_3^{2-}	K^+	PO_4^{3-}	NO_3^-
NaCl	**0.75 M**	**0**	**0**	**1**	**1**	**0**	**0**	**0**	**0**
$NaHCO_3$	**10* mM**	**1**	**0**	**1**	**0**	**1**	**0**	**0**	**0**
KNO_3	**5# mM**	**0**	**0**	**0**	**0**	**0**	**1**	**0**	**1**
KH_2PO_4	**0.12 mM**	**2**	**0**	**0**	**0**	**0**	**1**	**1**	**0**
$MgSO_4$	5 mM	--	--	--	--	--	--	--	--
$CaCl_2$	0.12 mM	--	--	--	--	--	--	--	--
EDTA	6 µM	--	--	--	--	--	--	--	--
$FeCl_3$	2 µM	--	--	--	--	--	--	--	--
$MnCl_2$	7 µM	--	--	--	--	--	--	--	--
$ZnSO_4$.	1 µM	--	--	--	--	--	--	--	--
$Co(NO_3)_2$.	1 µM	--	--	--	--	--	--	--	--
$CuSO_4$.	1 µM	--	--	--	--	--	--	--	--
$(NH_4)_6Mo_7O_{24}$.	1 µM	--	--	--	--	--	--	--	--

* In addition to 5 mM, 10, and 13.4 mM NaHCO3 conditions were also tested.
\# In addition to 2.5 mM, 5.0 mM KNO3 conditions were also tested

4.3.3.2 The DIC transfer rate in the PBR, $\boldsymbol{r_{DIC_{overall}}}$, is estimated from pH-data with a stepwise regression approach

Before estimating any rates, the raw sensor data was processed to remove known experimental perturbations and to ensure the system was in a quasi-equilibrium state after a CO_2 injection into the system. The post-processing script implemented in Python (v3.8) removes data based on three constraints: 1) known noise (e.g., sampling time, light switching on/off, etc.), 2) system stability based on the time since last CO_2 injection and the pH value relative to the setpoint, and 3) interpolation range; any reactor data that fell outside the range of interpolation was removed from the dataset before analysis.

The remaining data was analyzed for DIC removal rate, r_{DIC}. Each injection interval (i.e., data in between CO_2 injections) was analyzed with a piecewise approach to estimate mass transfer rates. Since electrode data is known for its electrical noise, directly extracting differential rates can be challenging. While there are numerical differentiation approaches for noisy and non-smooth data that are suitable for continuous electrode data[41], adopting such an approach is not appropriate here

given the frequency of the perturbation of pH in the system due to the continuous pH injection. Thus, the DIC removal rate in the PBR, $r_{DIC_{overall}}$, was estimated from the processed data using a piecewise linear regression analysis for the x_n discrete pH measurement over the course of an injection interval. This regression analysis was done for k=4 sampling points $[x_i: x_{i+k}]$ from $i = 0\ to\ i = n - k$. This piecewise approach was intended to balance noise within the data with instantaneous rate estimates.

For the sensor logging frequency—which corresponded to two measurements per minute for most experiments (SI, Table 6-2)—this analysis interval equates a time span of approximately two minutes under ideal circumstances. Note, due to prior data processing and removal of certain data points associated with known noise as described above, a maximum 'interval time span' is specified for the rate data to 'pass' quality control and move along to the next phase of the analysis. This step is performed to ensure that the regression analysis does not occur over data points that are adjacent in the data frame space, but not in time due to the previous removal of noisy points during the data processing phase of analysis.

4.3.3.3 Diffusion model calibration

Table 4-4 provides an overview of the background conditions tested that were used for estimating K_L. Previous work using this experimental setup warranted that a K_L estimate should be performed with each reactor.

Table 4-4. Overview of the background conditions tested for evaluating the K_L coefficient over a range of experimental conditions.

Reactor Setup	pH	$NaHCO_3$ (mM)	$H_2CO_3^*$(mM)	~DIC (mM)	Volumes (L)
Reactor 1	7.45	5	0.13	5	2.85, 2.55, 2.7
Reactor 1	7.50	10	0.24	10	2.80, 2.70
Reactor 1	8.125	38	0.20	35	2.9, 2.85
Reactor 2	7.50	5	0.12	5	2.80, 2.70
Reactor 2	7.45	10	0.27	10	2.85, 2.55, 2.7
Reactor 2	8.125	38	0.20	35	2.9, 2.85

Due to difficulty in maintaining reliable CO_2 headspace measurements over the course of all experiments, DIC* was assumed to be the DIC concentration in the media if media was at equilibrium with baseline CO_2 concentration in the headspace, which was found to be ~750 ppm during background tests.

4.3.3.4 Estimating algal carbon uptake and net carbon assimilation in PBR.

After establishing the relationship for the bulk DIC mass transfer coefficient, K_L, under the experimental conditions, this coefficient was estimated at every point along the sensor dataset based on the relevant system conditions (*i.e.*, volume, DIC). The diffusion model was then applied to estimate the background diffusion rate and provide a net carbon assimilation rate for the microalgae, $\boldsymbol{r_{algae}}$, (Equation 4-10). The impact of nitrogen assimilation on DIC was also considered at this time.

$$r_{algae} = r_{DIC_{overall}} - k_L \left(\frac{1}{D(t)}\right)[DIC^* - DIC(t)] - r_{DIC_{NO3\ assim}} \qquad 4\text{-}10$$

To estimate the total organic carbon in the PBR, the computed algal carbon uptake rates, r_{algae}, were integrated over time using Python SciPy Integration Method using the composite trapezoidal rule. An overview of the implementation of this modeling approach is shown in Figure 4-16.

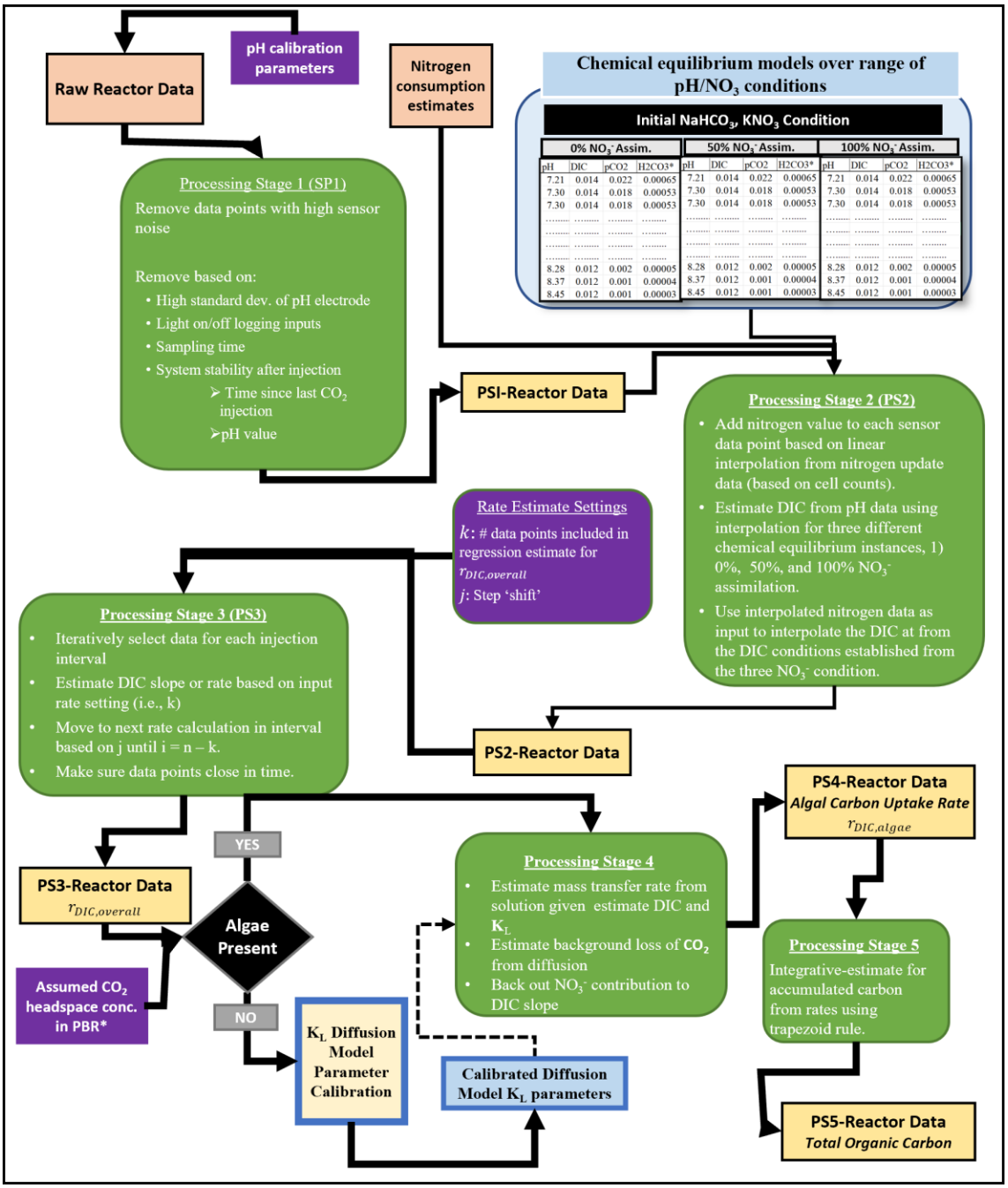

Figure 4-16. Overview of pH sensor model implemented to estimate algal carbon update and net organic carbon accumulation.

4.3.4 Model assessment & assumptions

There were two different approaches used to assess how well the adopted method captures growth. The first compared general trends, growth rates and specific growth rates between sensor-based carbon growth as compared to cellular growth and carbon growth measured with TOC analysis for suspended solids. These comparisons were performed to determine if this pH-sensor method for

estimating carbon satisfies the following: 1) captures similar growth trends and 2) provide similar carbon concentration estimates as compared to those made with a TOC analyzer.

Growth rates for lab-based cell counts and TOC measurements for sample measurement i were estimated by Equation 4-11.

$$\left(\frac{\Delta x}{\Delta t}\right)_i = \frac{x_i - x_{i-1}}{t_i - t_{i-1}} \qquad 4\text{-}11$$

The specific growth rates the microalgae at sampling time, t_i were estimated with Equation 4-12:

$$\mu_i = \frac{\left(\frac{\Delta x}{\Delta t}\right)_i}{(x_i + x_{i-1})/2} \qquad 4\text{-}12$$

The second approach for assessing model predictability quantified the relative error between the carbon assimilation estimates from model as compared to those measured with the TOC analyzer. The relative error was calculated by Equation 4-13,

$$\boldsymbol{d_i(x_i, y_i)} = \mathbf{2}\frac{\boldsymbol{x_i - y_i}}{\boldsymbol{|x_i| + |y_i|}} \qquad 4\text{-}13$$

where x_i, y_i are the newly assimilated carbon values between sampling points as defined in Table 4-5.

Table 4-5. Overview of the how the error measurements for each experiment will be obtained.

Sample Point, n	Sensor Carbon (Model)	Carbon (Lab)	Newly Added Carbon (Model), x	Newly Added Carbon (Lab), y	Relative Error, d_i
0	MC_0	LC_0	n/a	n/a	n/a
1	MC_1	LC_1	$x_1 = MC_1 - MC_0$	$y_1 = LC_1 - LC_0$	d_1
…	…	…	…	…	…
n	MC_n	LC_n	$x_n = MC_n - MC_{n-1}$	$y_5 = LC_n - LC_{n-1}$	d_n

4.3.4.1 Sensitivity analysis & key modeling assumptions

Since this model is driven almost entirely by pH measurements, a sensitivity analysis was done to gauge the model output given possible error in pH measurements. This assessment was performed by shifting raw pH data by ± 0.05 and re-running the model. The total carbon assimilation was compared with the base case, and the percent difference is compared for all experiments across the different pH and bicarbonate conditions at points corresponding to sampling times. This sensitivity analysis was performed after calibrating the DIC diffusion model for the base case (*i.e.*, no pH shift).

Furthermore, Table 4-6 outlines an overview of key assumptions made for each stage of this method, along with method decisions associated with these assumptions.

Table 4-6. Overview of key modeling assumptions.

Data Collection & Processing:	The pH sensor probe does not drift over the course of the experiments and if it does, the magnitude of drift has negligible impacts on the overall model outcome.
	The CO_2 in headspace does not accumulate in the PBR over time. The CO_2 headspace concentration will increase and fall close to a baseline value after CO_2 injection. The data before the CO_2 reaches this baseline will not be analyzed to ensure appropriate background rate estimates.
Chemical Model & Diffusion Model	The main components, as highlighted in Table 4-3, are most important to consider for estimating the DIC in the system.
	Solid formation does not occur.
	The temperature is assumed to be maintained around 25ºC.
	Evaporation does not occur at a scale to impact chemical compositions.
	The error associated with the pH-to-DIC interpolation is negligible.
	Organics or other biological components released into the media will not alter the pH over time.
	The baseline CO_2 headspace value will sufficiently capture the DIC*, such that the gradient in DIC is accurately applied to diffusion model.
	K_L does not change with the change in mixing intensity within PBR due to the volume removal over course of experiment.
	Biofilm formation or other biological material on the air-liquid interface of the culture does not impact the mass transfer over time.
	The main components, as highlighted in Table 4-3, are most important to consider for estimating the DIC in the system.
	Bacterial contamination or growth will minimal and captured with this method, *i.e.*, contamination will be indirectly accounted for by a reduction of the net carbon uptake rate via respiration.

4.4 Conclusions, future work, & limitations

Overall, these pH-sensor based measurements gave qualitatively comparable growth trends as compared to both the TOC analyzer estimates and cell counts (Figure 4-2 - Figure 4-4). Furthermore, this sensor-based TOC estimates were consistently around 1.5x higher than TOC analyzer estimates based on the suspended portions of the four algal cultures grown at pH ~7.5 and 5-14 mM HCO_3^-. The strong linear relationship that persisted throughout cultivation process (Figure 4-7)—despite the metabolic differences in the cultures that likely arose due to different initial nitrogen concentrations (2.5 vs 5.0 mM NO_3^-)—suggests that even with the complex biological and chemical reactions involved during microalgal growth, pH electrodes can be used as powerful tool for advancing our understanding of microalgae.

The direction of future work for this method is largely based on the scope of the intended applications. For example, if attempting to estimate the TOC contained in the algal biomass, the linearity between the two methods (Figure 4-7) shows that this sensor approach could be calibrated with the analyzer-based TOC measurements to estimate the carbon content of the suspended microalgae. However, this lab-to-sensor calibration approach will underestimate the true carbon assimilated during photosynthesis if the dissolved organic carbon of the media is not included. Additionally, since this particular microalga showed high volatility of its assimilated carbon products (Figure 4-9), investigations into the volatility of the excreted dissolved products would allow for better comparisons between these measurements. Using a TOC analyzer capable of analyzing highly ionic samples would improve the accuracy of lab-based method since the bulk samples (*i.e.*, cells and media) could be analyzed together. This approach would 1) account for dissolved organics in the media and 2) potentially reduce the loss of internal volatile components that are released from the cells during the centrifugation and/or freshwater dilution processes.

Furthermore, continued validation of this method at higher pH and bicarbonate concentrations would allow for more impactful studies when attempting to understand the impact of inorganic carbon concentrations on growth. While the results from the experiments here showed relatively similar TOC rates and concentrations estimates for the two experiments conducted at higher pH, HCO_3^- concentrations as compared to the other four (Figure 4-2, Figure 4-5), the changes in chemical equilibrium associated with higher pH and bicarbonate concentrations (*e.g.*, an increased potential for carbonate solid formation) merit more validation with the lab-based TOC analyzer approach.

A more thorough sensitivity assessment of this approach involving the chemical equilibrium and diffusion equations—as well as the numerical implementation of these equations—would give strategic insights into the implementation of this method and a better understanding into which application its suitable. For example, under ideal conditions, microalgae should primarily drive changes in DIC within the system; if the rate of CO_2 loss from diffusion is high relative to the impacts of the microalgae, the error in TOC estimates could become high, especially if the uncertainty around the diffusion rates is also high or not well defined. This type of analysis, combined with knowledge of other system parameters, can inform whether the implementation of this approach outside the described PBR conditions is feasible, *e.g.*, an open raceway pond or other full-scale cultivation systems. Real-time knowledge of the health of the cultures would help inform cultivation and harvesting decisions, such as nutrient addition or harvesting frequency, and improve efficiencies involved with full-scale production.

Regardless of future improvements, the results from this pH-sensor approach warrant excitement for future applications. This approach provides more resolution and flexibility than lab-based metrics, which can elucidate potential shifts in metabolic behavior, and allows for more targeted experiments. Through these rigorous validation efforts, this research suggests that—despite the multiple physical and chemical relationships that govern the relationships between pH and carbon flows—pH measurements in a continuously pH-controlled system provide a relatively inexpensive tool to gain high-resolution insight into the carbon flows within an algal culturing environment. This tool, when used appropriately, can be used to both study and manipulate microalgal growth for full-scale biorefinery applications.

CHAPTER 5: CLOSING REMARKS & A COMMENT ON SIGNIFICANCE

To our knowledge, this research is the first to use pH data as a means for directly estimating microalgal growth based on carbon-induced changes to pH. On-line methods such as these could prove critical to unraveling some of the complex behavior observed in microalgae that has made studying and modeling their growth so challenging. This approach has wide range applications, from a new tool for studying, understanding, and modeling algal growth at the bench scale to integration into cultivation monitoring systems at larger scales. Below briefly showcases how this approach can be combined with light system controls and monitoring to better understand the photosynthetic and metabolic activity of a microalgal culture.

5.1 An overview of potential future applications

The design of this approach also offers unique advantages. The algal carbon uptake rate that is estimated in an illuminated PBR reflects the net carbon uptake rate, $\boldsymbol{r_{algae,net}}$, since the microalgal cells respire and will release a portion of the carbon fixed during photosynthesis as CO_2 (Equation 5-1).

$$r_{algae,net} = r_{photo} - r_{resp} \qquad 5\text{-}1$$

By turning the light off for brief periods of time in between CO_2 injections, the respiration rates of the culture, $\boldsymbol{r_{resp}}$, can be estimated since the photosynthetic uptake rate, $\boldsymbol{r_{photo}}$, halts under dark conditions, *i.e.*, $r_{photo} = 0$. Combining carbon uptake rates in a light-illuminated PBR (*i.e.*, $r_{algae,net}$) with rates estimated from a dark PBR (*i.e.*, r_{resp}) provides an opportunity to estimate r_{photo} using Equation 5-1.

Figure 5-1 below gives ***an illustrative example*** of how this approach can be used to estimate respiration rates and photosynthetic rates by analyzing inorganic carbon flows in the PBR under different illumination conditions as described in Chapter 4.

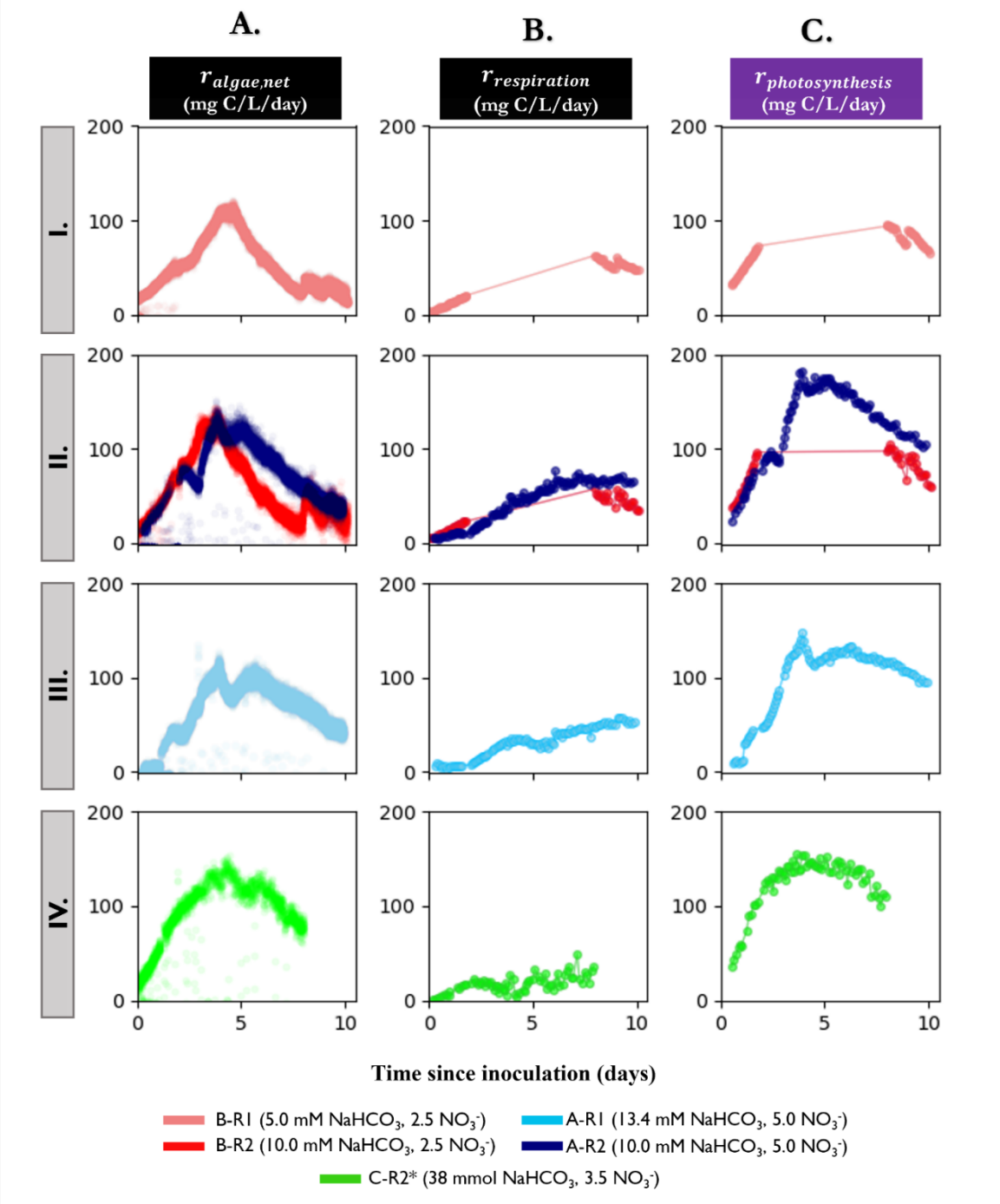

Figure 5-1. Illustrative example highlighting the various carbon flows that can be estimated with this pH sensor method, *i.e.*, net algal carbon uptake estimated under PBR illumination (**A**), algal respiration rates estimated from brief periods of darkness (**B**), and gross photosynthetic rates estimated by combining net and dark measurements (**C**). Rows represent bicarbonate concentrations, *i.e.*, I.) 5.0 mM $NaHCO_3$; II.) 10.0 mM $NaHCO_3$; III.) 13.4 mM $NaHCO_3$; IV.) 38 mM $NaHCO_3$. Colors represent different experimental sets. *The initial light condition for Set C-R2 was ~30% of the initial irradiance as compared to other sets. Black column headers represent estimates made under either light on OR light off conditions. Purple column header represents an estimate made using both these data sets from around same experimental time. Data gaps for B-R1, B-R2 coincides with a constantly-illuminated PBR (*i.e.*, times with no 'light off' cycling).

These sensor-based estimates for photosynthesis and respiration can be used to study more in-depth carbon flows within the cells. Simplified growth models that only track certain cell properties, such as simple sugars, lipids, and functional biomass (e.g., proteins, DNA/RNA), can vastly benefit from tracking two of the arguably most important properties within an algal culture: carbon and light. A simple visual model as shown Figure 5-2 intends to highlight how multiple internal reaction will ultimately dictate the net carbon flows as microalgae grow.

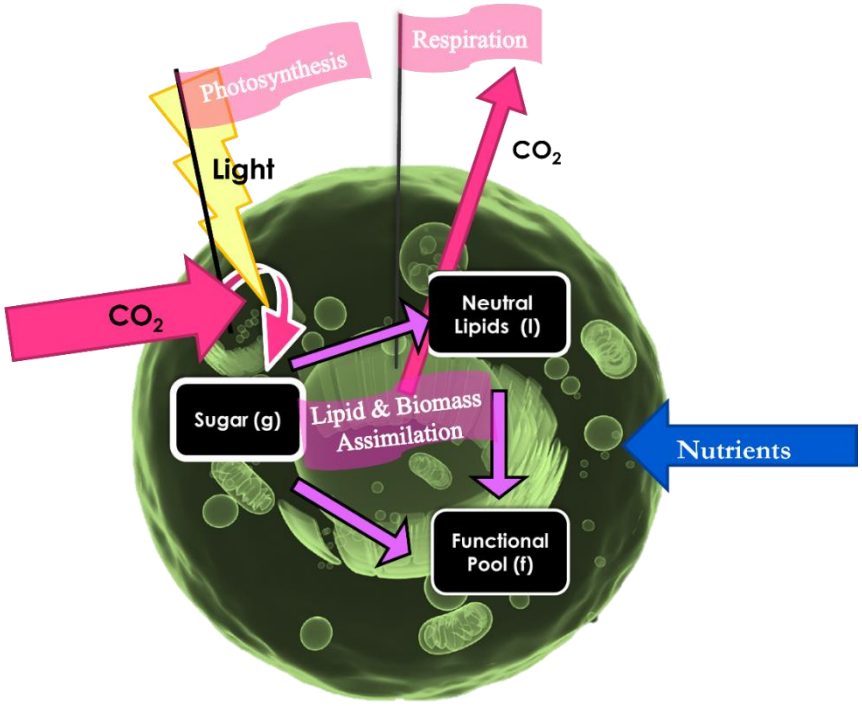

Figure 5-2. Simple graphical illustration showing the multiple processes within a cell that influence carbon flows, and how these processes are interconnected.

While there are multiple sub-processes that will lead to a release of CO_2 from the cell via respiration, photosynthesis is the primary driving force behind inorganic-to-carbon fixation. Understanding how efficiently microalgae are able to capture and utilize light to produce carbon is a critical step in understanding the maximum potential of these microorganisms. Furthermore, quantifying the total fraction of fixed carbon being utilized for respiration can aid in developing and calibrating models that consider multiple subprocesses. Figure 5-3 (Column B) shows the carbon flows allocated to respiration relative to photosynthetic activity.

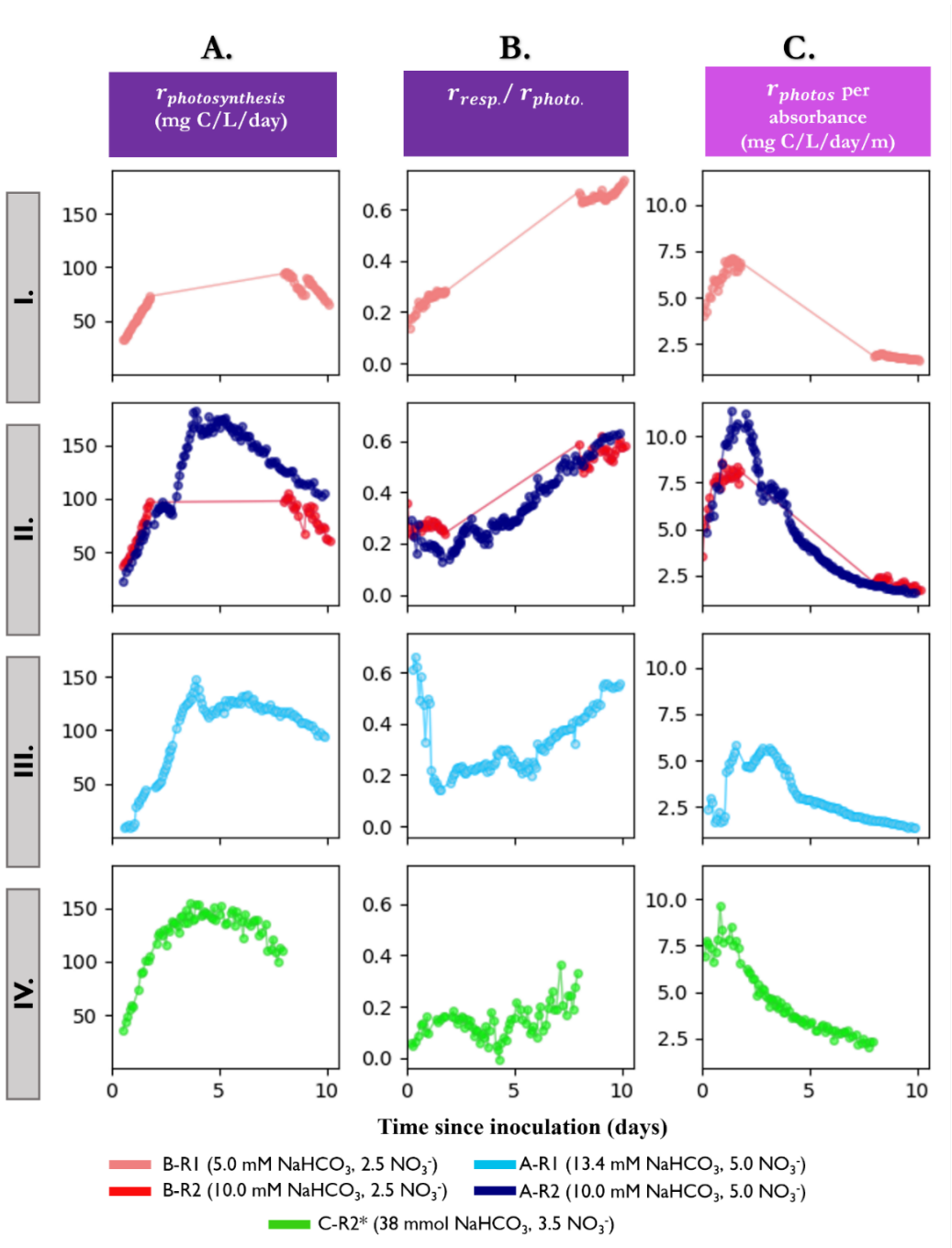

Figure 5-3. Illustrative example highlighting metabolic relations that can be estimated using this on-line approach, *i.e.*, gross photosynthetic carbon assimilation rate (**A**), respiration relative to gross photosynthetic rate (**B**), and gross photosynthetic carbon uptake rate per absorbance (**C**). Rows represent bicarbonate concentrations, *i.e.*, I.) 5.0 mM $NaHCO_3$; II.) 10.0 mM $NaHCO_3$; III.) 13.4 mM $NaHCO_3$; IV.) 38 mM $NaHCO_3$. Colors represent different experimental sets. *The initial light condition for Set C-R2 was ~30% of the initial irradiance as compared to other sets. Purple column header represents an estimate made using both these data sets from around same experimental time. Pink column header represents estimates made using a combination of sensor data under light and dark conditions AND online light data under illumination conditions. Data gaps for B-R1, B-R2 coincides with a constantly-illuminated PBR (*i.e.*, times with no 'light off' cycling).

By combining light absorption as described in Chapter 3 with this pH-to-carbon approach, researchers can gain more insight into how light interacts with the carbon fixation process during photosynthesis (Figure 5-3, Column C). Combining absorbance data with photosynthetic carbon uptake rates in a more rigorous fashion can allow for the parameterization of key photosynthetic parameters and delicate light studies.

5.2 Conclusions and closing remarks

On-line technology for monitoring algal growth in cultivation systems should be encouraged, as should research that focuses on properly validating and the appropriate use of these methods. Better techniques for monitoring algal growth provides the opportunity for more creative and intricately designed experiments that can quickly identify points of interest where further lab-based techniques, including proteomic and genetic analysis, can be applied to gain deeper insights into the metabolic processes that drive these truly incredible microorganisms

New sensor-based technology brings a new level of excitement and responsibility to researchers utilizing their applications. Theoretical principles and equations in biology and chemistry are relatively easy to apply, but real-world systems rarely behave ideally. ***Thorough validation and the characterization of novel methods such as those developed in this research should be celebrated as much as the discoveries they may bring***.

SUPPLMENTAL INFORMATION

Table 6-1. List of PBR sensors and components used in experimental setup.

Name	Source (with weblinks)
Data Acquisition Unit	LabJack U6 (2014)
Control Switch Board	LabJack Terminal Board
Data Acquisition Software	DAQFactory & GasLab
pH sensor	Hamilton EasyFerm120 pH Electrode
CO_2 Mass Flow Meter	TopTrak® 822/824 CO2 Mass Flow Meters
NDIR Sensor 10%*	CO2meter.com
Temperature probe	LabJack 1034-temperature-probe (2014, 2016)
Stainless Steel Solenoid Valve for CO_2 input	McMaster
1-lpm air pump	Ebay
Relay Board	http://labjack.com/support/rb12/datasheet
DC Switching Modules	Digi-Key (DC GH3040-ND 5VDC)
pH sensor signal conditioning	http://www.omega.com/pptst/PHTX21.html
CO_2 Bone Dry 200 CGA 320	AirGas

Table 6-2. pH calibration information and logging frequency for experiments. For A, B, C, D experiments, more heavily buffered seed cultures were added to PBR media that resulted in shifts in overall NaHCO3 concentrations.

Experiment Name	pH Probes Calibration	Phase	HCO_3^- (mmol)	Exp. Logging Frequency (#/min)	Notes
A-R1	Post	Background	10	1	
		Algae	13.4	2	
A-R2	Post	Background	5	1	
		Algae	10	2	
B-R1	Pre/Post	Background	5	2	
		Algae	5	2	
B-R2	Pre/Post	Background	10	2	
		Algae	10	2	
C-R1	Pre/Post	Background	37.55	1	Set not included in analysis due to light failure
		Algae	38.55	1	
C-R2	Pre/Post	Background	37.55	1	
		Algae	38.55	1	
D-R1	Pre/Post	Background	37.55	1	Set not included in analysis due to contamination
		Algae	38.55	1	
D-R2	Pre/Post	Background	37.55	1	
		Algae	38.55	1	

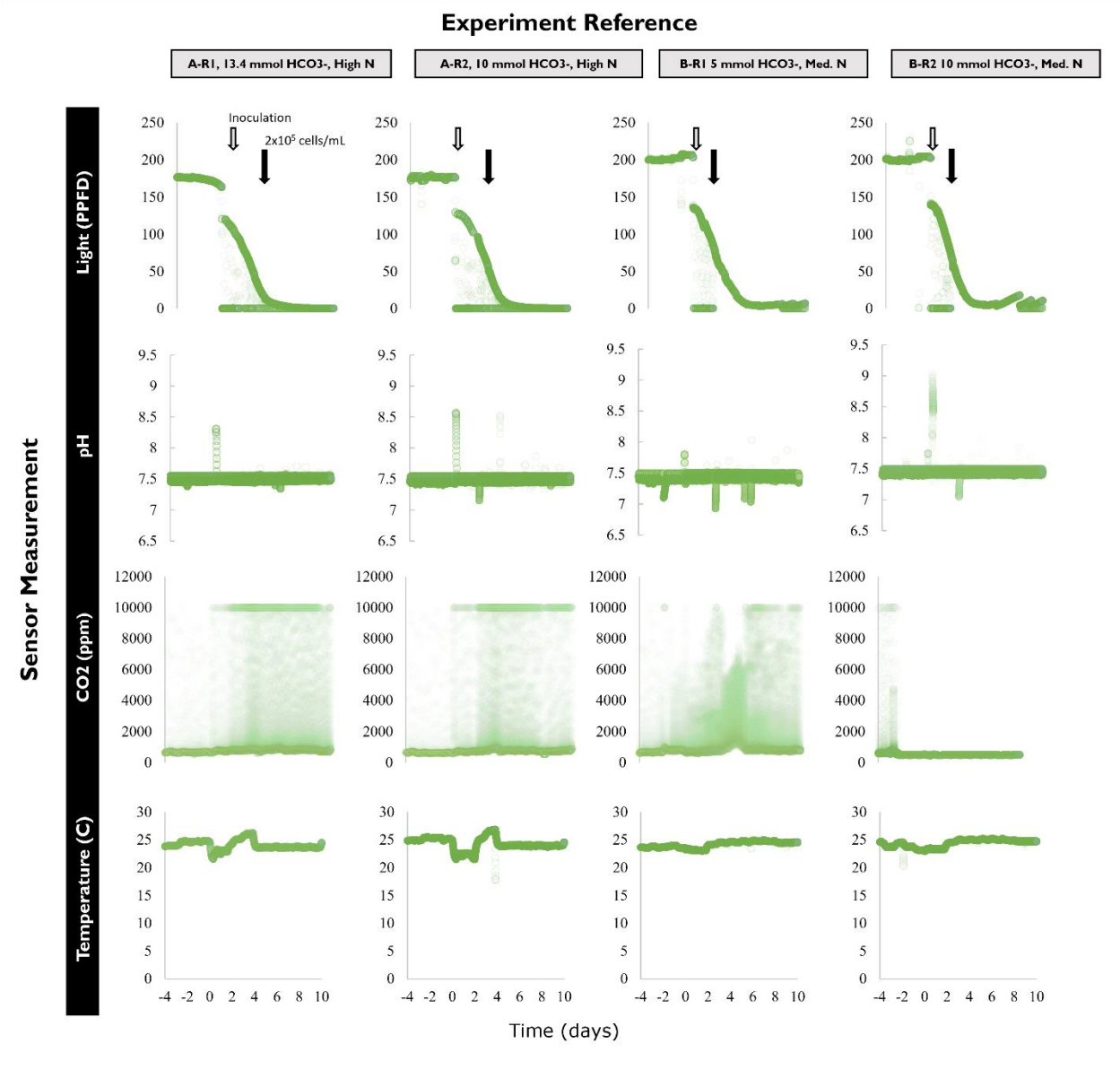

Figure 6-1. Raw sensor output from the four primary validation experiments (Sets A, B). **The time on these axes represent time since inoculation and NOT the time since sampling as reflected in earlier graphs.** The white arrows represent point of inoculation and black is start of sampling. Columns show the four different experimental sets and rows shows the light, pH, CO_2 in headspace, and temperature within the PBRs throughout experiments. Darker shade represents higher frequency of samples fell within that x-y coordinate range. Note, the darker green shades noted near zero for the light data indicate then the light was turned off based on the light schemes described in section 2.2.3.

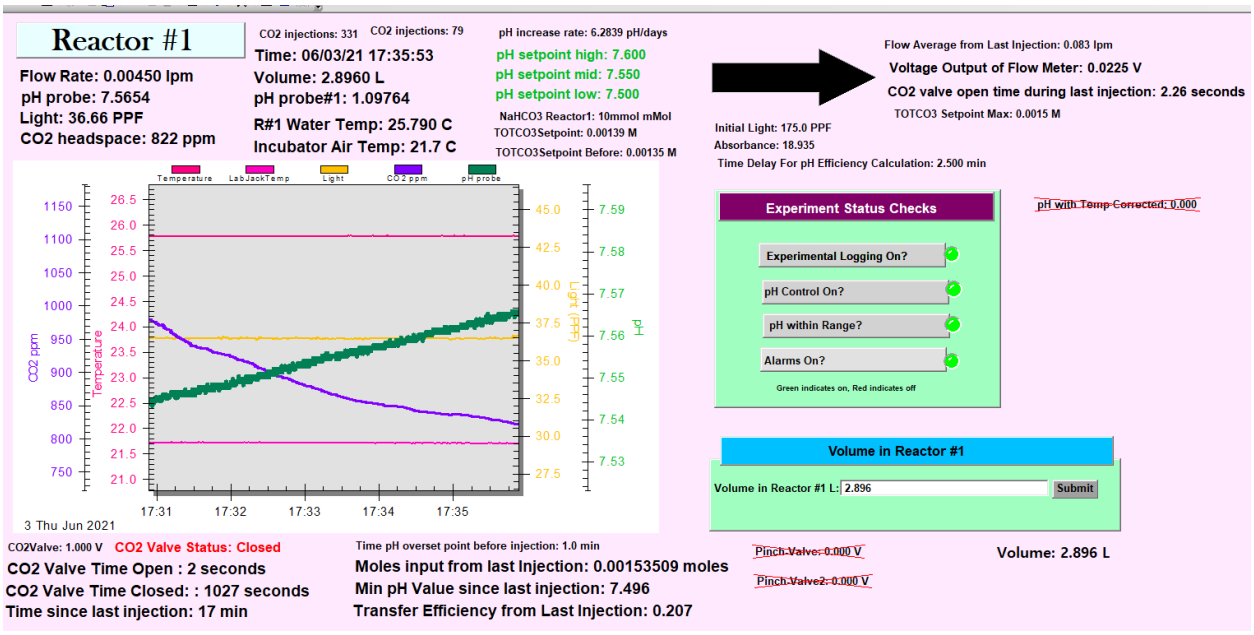

Figure 6-2. Example of the DAQFactory software page built for monitoring experiments.

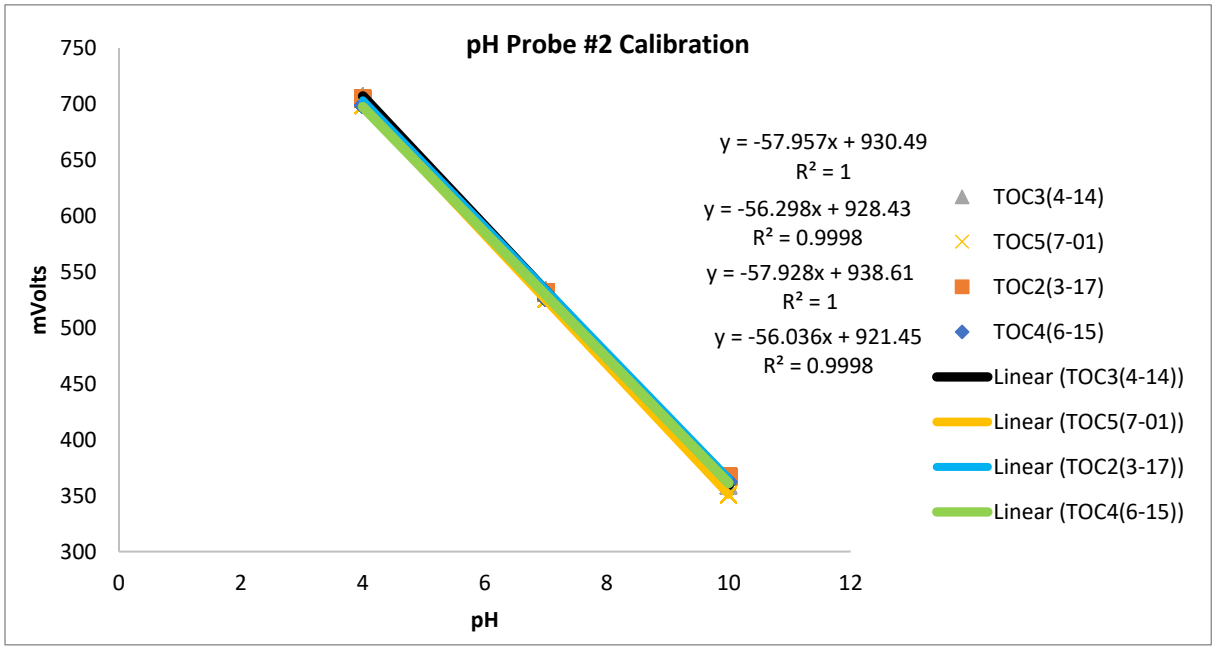

Figure 6-3. Example of pH calibration over various time periods, showing stability of pH probes over course of experiments.

REFERENCES

(1) ATLAS Collaboration. A Look Back at the U.S. Department of Energy's Aquatic Species. *Eur. Phys. J. C* **2012**, *72* (6), 14.

(2) Lardon, L.; Hélias, A.; Sialve, B.; Steyer, J.-P.; Bernard, O. Life-Cycle Assessment of Biodiesel Production from Microalgae. *Environ. Sci. Technol.* **2009**, *43* (17), 6475–6481.

(3) Schenk, P. M.; Thomas-Hall, S. R.; Stephens, E.; Marx, U. C.; Mussgnug, J. H.; Posten, C.; Kruse, O.; Hankamer, B. Second Generation Biofuels: High-Efficiency Microalgae for Biodiesel Production. *BioEnergy Res.* **2008**, *1* (1), 20–43.

(4) Khan, M. I.; Shin, J. H.; Kim, J. D. The Promising Future of Microalgae: Current Status, Challenges, and Optimization of a Sustainable and Renewable Industry for Biofuels, Feed, and Other Products. *Microb. Cell Fact.* **2018**, *17* (1), 1–21.

(5) Stephenson, A. L.; Kazamia, E.; Dennis, J. S.; Howe, C. J.; Scott, S. A.; Smith, A. G. Life-Cycle Assessment of Potential Algal Biodiesel Production in the United Kingdom: A Comparison of Raceways and Air-Lift Tubular Bioreactors. *Energy and Fuels* **2010**, *24* (7), 4062–4077.

(6) Chisti, Y. Biodiesel from Microalgae. *Biotechnol. Adv.* **2007**, *25* (3), 294–306.

(7) Ketzer, F.; Skarka, J.; Rösch, C. Critical Review of Microalgae LCA Studies for Bioenergy Production. *Bioenergy Res.* **2018**, *11* (1), 95–105.

(8) Mulders, K. J. M.; Lamers, P. P.; Wijffels, R. H.; Martens, D. E. Dynamics of Biomass Composition and Growth during Recovery of Nitrogen-Starved Chromochloris Zofingiensis. *Appl. Microbiol. Biotechnol.* **2015**, *99* (4), 1873–1884.

(9) Le, E.; Park, C.; Hiibel, S. Investigation of the Effect of Growth From Low to High Biomass Concentration Inside a Photobioreactor on Hydrodynamic Properties of Scenedesmus Obliquus. *J. Energy Resour. Technol.* **2012**, *134* (March 2012), 011801.

(10) Oren, A. A Hundred Years of Dunaliella Research: 1905-2005. *Saline Systems* **2005**, *1*, 2.

(11) Mixson Byrd, S.; Burkholder, J. A. M. Environmental Stressors and Lipid Production in Dunaliella Spp. II. Nutrients, PH, and Light under Optimal or Low Salinity. *J. Exp. Mar. Bio. Ecol.* **2017**, *487*, 33–44.

(12) Salih, F. M. Microalgae Tolerance to High Concentrations of Carbon Dioxide: A Review. *J. Environ. Prot. (Irvine,. Calif).* **2011**, *02* (05), 648–654.

(13) Lee, E.; Jalalizadeh, M.; Zhang, Q. Growth Kinetic Models for Microalgae Cultivation: A Review. *Algal Res.* **2015**, *12*, 497–512.

(14) Darvehei, P.; Bahri, P. A.; Moheimani, N. R. Model Development for the Growth of Microalgae: A Review. *Renew. Sustain. Energy Rev.* **2018**, *97* (August), 233–258.

(15) Hunt, S. Measurements of Photosynthesis and Respiration in Plants. *Physiol. Plant.* **2003**,

117 (3), 314–325.

(16) Molina Grima, E.; Garcia Camacho, F.; Sanchez Perez, J. A.; Fernandez Sevilla, J. M.; Acien Fernandez, F. G.; Contreras Gomez, A. A Mathematical Model of Microalgal Growth in Light-Limited Chemostat Culture. *J. Chem. Technol. Biotechnol.* **1994**, *61*, 167–173.

(17) Eilers, P. H. C.; Peeters, J. C. H. Dynamic Behaviour of a Model for Photosynthesis and Photoinhibition. *Ecol. Modell.* **1993**, *69* (1–2), 113–133.

(18) Yao, S.; Lu, J.; Sárossy, Z.; Baggesen, C.; Brandt, A.; An, Y. Neutral Lipid Production in Dunaliella Salina during Osmotic Stress and Adaptation. *J. Appl. Phycol.* **2016**, *28* (4), 2167–2175.

(19) Han, B.-P. Effect of Photoinhibition on Algal Photosynthesis: A Dynamic Model. *J. Plankton Res.* **2000**, *22* (5), 865–885.

(20) Grobbelaar, J. U.; Soeder, C. J.; Groeneweg, J.; Stengel, E.; Hartig, P. Rates of Biogenic Oxygen Production in Mass Cultures of Microalgae, Absorption of Atmospheric Oxygen and Oxygen Availability for Wastewater Treatment. *Water Res.* **1988**, *22* (11), 1459–1464.

(21) Guterman, H.; Ben-Yaakov, S.; Vonshak, A. Automatic On-line Growth Estimation Method for Outdoor Algal Biomass Production. *Biotechnology and Bioengineering*. 1989, pp 143–152.

(22) Decostere, B.; Janssens, N.; Alvarado, A.; Maere, T.; Goethals, P.; Van Hulle, S. W. H.; Nopens, I. A Combined Respirometer-Titrimeter for the Determination of Microalgae Kinetics: Experimental Data Collection and Modelling. *Chem. Eng. J.* **2013**, *222*, 85–93.

(23) Li, J.; Xu, N. S.; Su, W. W. Online Estimation of Stirred-Tank Microalgal Photobioreactor Cultures Based on Dissolved Oxygen Measurement. *Biochem. Eng. J.* **2003**, *14* (1), 51–65.

(24) Cabello, J.; Morales, M.; Revah, S. Dynamic Photosynthetic Response of the Microalga Scenedesmus Obtusiusculus to Light Intensity Perturbations. *Chem. Eng. J.* **2014**, *252*, 104–111.

(25) Kliphuis, A. M. J.; Janssen, M.; van den End, E. J.; Martens, D. E.; Wijffels, R. H. Light Respiration in Chlorella Sorokiniana. *J. Appl. Phycol.* **2011**, *23* (6), 935–947.

(26) Bate, G. C.; Sültemeyer, D. F.; Fock, H. P. 16O2/18O2 Analysis of Oxygen Exchange in Dunaliella Tertiolecta. Evidence for the Inhibition of Mitochondrial Respiration in the Light. *Photosynth. Res.* **1988**, *16* (3), 219–231.

(27) Miniaev, M. V.; Belyakova, M. B.; Kostiuk, N. V.; Leshchenko, D. V.; Fedotova, T. A. Non-Obvious Problems in Clark Electrode Application at Elevated Temperature and Ways of Their Elimination. *J. Anal. Methods Chem.* **2013**, *2013*.

(28) Kliphuis, A. M. J.; de Winter, L.; Vejrazka, C.; Martens, D. E.; Janssen, M.; Wijffels, R. H. Photosynthetic Efficiency of Chlorella Sorokiniana in a Turbulently Mixed Short Light-Path Photobioreactor. *Biotechnol. Prog.* **2010**, *26* (3), 687–696.

(29) Eriksen, N. T.; Riisgård, F. K.; Gunther, W. S.; Lønsmann Iversen, J. J. On-Line Estimation of O2 Production, CO2 Uptake, and Growth Kinetics of Microalgal Cultures in a Gas-Tight Photobioreactor. *J. Appl. Phycol.* **2007**, *19* (2), 161–174.

(30) Ifrim, G. A.; Titica, M.; Cogne, G.; Boillereaux, L.; Legrand, J.; Caraman, S. Dynamic PH Model for Autotrophic Growth of Microalgae in Photobioreactor: A Tool for Monitoring and Control Purposes. *AIChE J.* **2014**, *60* (2), 585–599.

(31) Filali, R.; Tebbani, S.; Dumur, D.; Isambert, A.; Pareau, D.; Lopes, F. *Growth Modeling of the Green Microalga Chlorella Vulgaris in an Air-Lift Photobioreactor*; IFAC, 2011; Vol. 44.

(32) Ben-Amotz, A.; Avron, M. The Role of Glycerol in the Osmotic Regulation of the Halophilic Alga Dunaliella Parva . *Plant Physiol.* **1973**, *51* (5), 875–878.

(33) Goyal, A. Osmoregulation in Dunaliella, Part II: Photosynthesis and Starch Contribute Carbon for Glycerol Synthesis during a Salt Stress in Dunaliella Tertiolecta. *Plant Physiol. Biochem.* **2007**, *45* (9), 705–710.

(34) Chow, Y. Y. S.; Goh, S. J. M.; Su, Z.; Ng, D. H. P.; Lim, C. Y.; Lim, N. Y. N.; Lin, H.; Fang, L.; Lee, Y. K. Continual Production of Glycerol from Carbon Dioxide by Dunaliella Tertiolecta. *Bioresour. Technol.* **2013**, *136*, 550–555.

(35) Pitzer, K. S. Activity Coefficients in Electrolyte Solutions. *Act. Coefficients Electrolyte Solut.* **2018**.

(36) Geider, R. J.; La Roche, J. Redfield Revisited: Variability of C:N:P in Marine Microalgae and Its Biochemical Basis. *Eur. J. Phycol.* **2002**, *37* (1), 1–17.

(37) Karam, A. L.; McMillan, C. C.; Lai, Y.; de los Reyes, F. L. I.; Sederoff, H. W.; Grunden, A. M.; Ranjithan, R. S.; Levis, J. W.; Ducoste, J. J. Construction and Setup of a Bench-Scale Algal Photosynthetic Bioreactor with Temperature, Light, and PH Monitoring for Kinetic Growth Tests. **2017**.

(38) Lai, Y. C.; Karam, A. L.; Sederoff, H. W.; Ducoste, J. J.; de los Reyes, F. L. Relating Nitrogen Concentration and Light Intensity to the Growth and Lipid Accumulation of Dunaliella Viridis in a Photobioreactor. *J. Appl. Phycol.* **2019**, *31* (6), 3397–3409.

(39) Gordillo, F. J. L.; Jiménez, C.; Figueroa, F. L.; Niell, F. X. Influence of Elevated CO2 and Nitrogen Supply on the Carbon Assimilation Performance and Cell Composition of the Unicellular Alga Dunaliella Viridis. *Physiol. Plant.* **2003**, *119* (4), 513–518.

(40) Gordillo, F. J. L.; Goutx, M.; Figueroa, F. L.; Niell, F. X. Effects of Light Intensity, CO2 and Nitrogen Supply on Lipid Class Composition of Dunaliella Viridis. *J. Appl. Phycol.* **1998**, *10* (2), 135–144.

(41) Chartrand, R. Numerical Differentiation of Noisy, Nonsmooth Data. *ISRN Appl. Math.* **2011**, *2011*, 1–11.